2011

Enabling Technology and Algorithm Design for Location-Aware Communications

Jiaxin Yang

Enabling Technology and Algorithm Design for Location-Aware Communications

(Spine title: Location-Aware Communications)

(Thesis format: Monograph)

by

Jiaxin Yang

Graduate Program
in
Engineering Science
Electrical and Computer Engineering

A thesis submitted in partial fulfillment
of the requirements for the degree of
Master of Engineering Science

School of Graduate and Postdoctoral Studies
The University of Western Ontario
London, Ontario, Canada

THE UNIVERSITY OF WESTERN ONTARIO
SCHOOL OF GRADUATE AND POSTDOCTORAL STUDIES

CERTIFICATE OF EXAMINATION

Chief Advisor:

Dr. Xianbin Wang

Advisory Committee:

Examining Board:

Dr. Lin Cai

Dr. Anestis Dounavis

Dr. Robert Sobot

The thesis by

Jiaxin Yang

entitled:

Enabling Technology and Algorithm Design for Location-Aware Communications

is accepted in partial fulfillment of the
requirements for the degree of
Master of Engineering Science

Date: _____

Chair of Examining Board
Dr. Serguei L. Primak

Abstract

Location-awareness is emerging as a promising technique for future-generation wireless network to adaptively enhance and optimize its overall performance through location-enabled technologies such as location-assisted transceiver reconfiguration and routing. The availability of accurate location information of mobile users becomes the essential prerequisite for the design of such location-aware networks. Motivated by the low locationing accuracy of the Global Positioning System (GPS) in dense multipath environments, which is commonly used for acquiring location information in most of the existing wireless networks, wireless communication system-based positioning systems have been investigated as alternatives to fill the gap of the GPS in coverage. Distance-based location techniques using time-of-arrival (TOA) measurements are commonly preferred by broadband wireless communications where the arrival time of the signal component of the *First Arriving Path* (FAP) can be converted to the distance between the receiver and the transmitter with known location. With at least three transmitters, the location of the receiver can be determined via trilateration method. However, identification of the FAP's signal component in dense multipath scenarios is quite challenging due to the significantly weaker power of the FAP as compared with the *Later Arriving Paths* (LAPs) from scattering, reflection and refraction, and the superposition of these random arrival LAPs' signal components will become large interference to detect the FAP. In this thesis, a robust FAP detection scheme based on multipath interference cancellation is proposed to improve the accuracy of location estimation in dense multipath environments. In the proposed algorithm, the signal components of LAPs is reconstructed based on the estimated channel and data with the assist of the communication receiver, and subsequently removed from the received signal. Accurate FAP detection results are then achieved with the cross-correlation between the interference-suppressed signal and an *augmented preamble* which is the combination of the original preamble for communications and the demodulated data sequences. Therefore, more precise distance estimation (hence location estimation) can be obtained with the proposed algorithm for further reliable network optimization strategy design.

On the other hand, multicell cooperative communication is another emerging technique to substantially improve the coverage and throughput of traditional cellular networks. Location-awareness also plays an important role in the design and implementation of multicell cooperation technique. With accurate location information of mobile users, the complexity of multicell cooperation algorithm design can be dramatically reduced by location-assisted applications, e.g., automatic cooperative base station (BS) determination and signal synchronization. Therefore, potential latency aroused by cooperative processing will be minimized. Furthermore, the cooperative BSs require the sharing of certain information, e.g., channel state information (CSI), user data and transmission parameters to perform coordination in their signaling strategies. The BSs need to have the capabilities to exchange available information with each other to follow up with the time-varying communication environment. As most of broadband wireless communication systems are already orthogonal frequency division multiplexing (OFDM)-based, a *Multi-Layered OFDM System*, which is specially tailored for multicell cooperation is investigated to provide parallel robust, efficient and flexible signaling links for BS coordination purposes. These layers are overlaid with data-carrying OFDM signals in both time and frequency domains and therefore, no dedicated radio resources are required for multicell cooperative networks.

In the final aspect of this thesis, an enhanced channel estimation through *iterative decision-directed* method is investigated for OFDM system, which aims to provide more accurate estimation results with the aid of the demodulated OFDM data. The performance of traditional training sequence-based channel estimation is often limited by the length of the training. To achieve acceptable estimation performance, a long sequence has to be used which dramatically reduces the transmission efficiency of data communication. In this proposed method, the restriction of the training sequence length can be removed and high channel estimation accuracy can be achieved with high transmission efficiency, and therefore it particular fits in multicell cooperative networks. On the other hand, as the performance of the proposed FAP detection scheme also relies on the accuracy of channel estimation and data detection results, the proposed method can be combined with the FAP detection scheme to further optimize the accuracy of multipath interference cancellation and FAP detection.

Acknowledgements

I would like to express my sincere gratitude to all those who made this thesis possible.

Foremost, I want to thank my supervisor, Dr. Xianbin Wang, for his continuous support of my research, for his patience, stimulating suggestions and encouragement. His guidance helped me to develop a solid understanding of this subject. It has been a true fortune and privilege working with him. I could not have imagined having a better advisor and mentor for my Master's study.

I would also like to thank the examination committee chair Dr. Serguei L. Primak, and the examination committee members, including Dr. Lin Cai, Dr. Anestis Dounavis, and Dr. Robert Sobot. Their insightful comments helped a lot on the final version of this thesis, and also gave great assistants on the future work.

I also owe my deepest gratitude to Dr. Xianbin Wang, Dr. Serguei L. Primak, and Dr. Hanif Ladak for those courses greatly improved my work in theoretical analysis, understanding of communication systems and digital image processing techniques, and simulation works.

It's a honor for me to thank my fellows in my research group for their help and support. These thanks are also for my other friends, roommates, and those friends in China, who have helped me a lot remotely.

I am indebted to my parents. Even far away, they have been present and supportive through every step of my study, providing help in my difficult time, and enjoying every single accomplishment during my study.

Lastly, I would like to give my special thanks to my wife Yanwen whose patient love enabled me to complete this work.

Table of Contents

List of Tables

List of Figures

Acronyms

AOA	*Angle of Arrival*
AWGN	*Additive White Gaussian Noise*
BL	*Base Layer*
BS	*Base Station*
CIR	*Channel Impulse Response*
CoMP	*Coordinated Multi-Point*
CP	*Cyclic Prefix*
CSI	*Channel State Information*
DAB	*Digital Audio Broadcasting*
DTV	*Digital Television*
DVB	*Digital Video Broadcasting*
E-911	*Emergency 911*
EL	*Enhanced Layer*
EM	*Expectation Maximized*
EPA	*Extended Pedestrian A*
EUTRA	*Evolved Universal Terrestrial Radio Access*
FAP	*First Arriving Path*
FCC	*Federal Communications Commission*
FDD	*Frequency-Division Duplex*
FDM	*Frequency Domain Multiplexing*
GI	*Guard Interval*
GPS	*Global Positioning System*
ICI	*Intercell Interference*
IDDCE	*Iterative Decision-Directed Channel Estimation*
IDFT	*Inverse Discrete Fourier Transform*
ISI	*Inter Symbol Interference*
LAP	*Later Arriving Path*
LMMSE	*Linear Minimum Mean Square Error*

LOS	*Line of Sight*
LS	*Least Square*
LTE	*Long Term Evolution*
MAC	*Media Access Control*
ML	*Maximum Likelihood*
ML-OFDM	*Multi-Layered Orthogonal Frequency Divison Multiplexing*
MS	*Mobile Station*
MSE	*Mean Square Error*
NLOS	*None Line of Sight*
NPNR	*Normalized Peak-to-Noise Ratio*
OFDM	*Orthogonal Frequency Division Multiplexing*
OP	*Observation Period*
PACE	*Pilot Aided Channel Estimation*
PDF	*Probability Density Function*
PHY	*Physical*
PNR	*Peak-to-Noise Ratio*
PRACH	*Random Access Preamble*
PSS	*Primary Synchronization Signal*
QoS	*Quality of Service*
RMSE	*Root Mean Square Error*
RSS	*Received Signal's Strength*
RX	*Receiver*
SCP	*Single Cell Processing*
SFN	*Single Frequency Network*
SNR	*Signal-to-Noise Ratio*
SINR	*Signal-to-Noise-and-Interference Ratio*
TDD	*Time-Division Duplex*
TDM	*Time Domain Multiplexing*
TOA	*Time of Arrival*
TX	*Transmitter*
ULA	*Uniform Linear Antenna*
WLAN	*Wireless Local Area Network*

Chapter 1
Introduction

1.1 Motivation

The ever-increasing demand for broadband mobile communications along with the tremendous growth in the number of mobile users drives the rapid evolution of future-generation cellular networks. One of the most prominent feature of next-generation wireless network is its location-awareness. Incorporation of this capability brings significant opportunities in various location-based network optimization schemes, which aim to enhance the performance of the entire network.

The ability for mobile users to determine their positions through automatic means is recognized as the fundamental requirement for location-awareness. Based on the accurate location estimation, adaptive transmission techniques, i.e., link adaptation and channel environment identification as well as location-aware routing protocols can be efficiently designed to achieve reliable and efficient transmission with diverse Quality of Service (QoS) to the large number of mobile users. The most popular "location awareness engine", the Global Positioning System (GPS) is widely used in the existing wireless networks, where the mobile users obtain their location information through the embedded GPS chips. Despite the GPS chip-induced cost, size and battery consumption for mobile handsets, the biggest challenge of the GPS is that the accuracy dramatically degrades in dense multipath environments (dense urban and indoor) due to the severe multipath propagation effects.

For these reasons, future wireless networks cannot fully rely on the GPS as the sole location technology. As a result, some wireless network-based location techniques using existing networks (either cellular or wireless local area networks (WLAN)) have been investigated as alternatives for locationing purposes in dense multipath environments. For broadband wireless communication systems, time-of-arrival (TOA)-based location technique is commonly used, which uses geometric relationships based on multiple distance measurements between the mobile user and a number of fixed transmitters (reference stations) to determine the location coordinates of the mobile user. Each distance measurement can be derived from the signal propagation time by multiplication by the speed of propagation. By assuming the time when the signal leaves the transmitter is known, the distance can be easily obtained by measuring the arrival time of the signal at the receiver. However, in dense multipath environments, signal components arrive at the receiver along multiple paths including the *First Arriving Path* (FAP) corresponding to the direct signal propagation path and the *Later Arriving Paths* (LAPs) caused by scattering, reflection and refraction. Furthermore, the direct signal propagation path is often blocked by various obstacle such as buildings, pedestrians and vehicles in these scenarios such that the power of the FAP's signal component is significantly weaker than those of the LAPs' components. The superposition of these LAPs' signal components becomes large interference for the detection of the FAP. Reliable detection of the FAP is challenging with large LAPs interference and therefore, large location estimation error is inevitable if the FAP is erroneously identified. Therefore, a robust FAP detection scheme in the presence of large LAPs interference needs to be developed to provide accurate location estimation and based on which, high quality location-assisted applications can be successfully realized in next-generation wireless networks for potential performance enhancement.

In the meantime, multicell cooperation, which has the capability of exploiting

inter-cell interference (ICI) cooperatively by enabling joint signal processing among several interfering base stations (BSs), is emerging as a revolutionary technology to remarkably enhance throughput and coverage of traditional cellular networks. The intelligent wireless system prescribes coordinated signaling strategies such as power allocation, beamforming directions, user scheduling and joint encoding/decoding of signals through BS coordination.

Potential improvement can be obtained in both performance and efficiency of multicell cooperation with the location-awareness capability. For instance, utilizing the location information of the target mobile users, the group of BSs which will be involved in coordination can be automatically determined, and therefore reducing the latency caused by BS searching process. Moreover, efficient synchronization scheme can also be designed based on the location of the target mobile users to allow the signals transmitted from different BSs to arrive synchronously at the mobile user for coherent combing.

Current multicell cooperation entails sharing the information via a backhaul network with unlimited capacity and free delay connecting the BSs with each other. In practice, however, the situation is quite unrealistic for large scale networks due to the prohibitive costs involved in establishing high-capacity links. This will restrict the quality of the exchanged information, which in turn affects the performance gain obtained. Therefore, a dedicated signaling with reliable, fast and flexible transmission capabilities for sharing the required information among BSs needs to be established to support multicell cooperation. Meanwhile, the network latency and BS synchronization issues will also lead to dramatic performance degradation of the existing design of multicell cooperation. Motivated by the scarcity of available radio resources, the proposed signaling is expected to share the same radio resource (frequency band and time slot) with the user data carrying information. To support these requirements of

multicell cooperation technique, new signal transmission scheme and its corresponding transceiver have to be designed. Due to the overlap of different signaling links, interference cancellation algorithm is also a necessary part of the desired system.

In addition, since most of the broadband wireless communication systems are already Orthogonal Frequency Division Multiplexing (OFDM)-based due to its high spectral efficiency and robustness to multipath distortion, accurate channel estimation is a fundamental requirement not only indispensable for OFDM receiver to perform coherent data detection but also important for location estimation using the proposed FAP detection. As the proposed FAP detection algorithm relies on multipath interference cancellation, where the multipath interference is reconstructed based on the channel estimation and data detection results. Given the limited length of the training sequence, the performance of channel estimation can be improved by utilizing *Decision-Directed* method. However, this algorithm can only provide limited performance gain under frequency selective channel because a large portion of data decision feedback is unreliable. Therefore, *Decision-Directed* method with reliable data decision feedback selection needs to be developed to optimize the estimation accuracy which successively lead to more accurate location estimation and data demodulation. The proposed channel estimation also fits in multicell cooperative cellular networks where large overhead of training sequences have to be assigned to acquire the channel state information (CSI) of each BS-user link for BS coordination purposes by reducing the length of the training sequence with the aid of the decisioned data.

1.2 Thesis Objective

Conventional TOA-based positioning systems detect the FAP based on the cross-correlation between the received signal and a local preamble signal. In dense multi-

path environments, the correlation detector may suffer from a low correlation peak corresponding to the FAP, and the peak is also significantly distorted by the signal components of the LAPs. Large location estimation error is more likely to occur with the utilization of correlation detector in dense multipath environments. The first objective of the thesis is to develop a weak FAP detection algorithm based on multipath interference cancellation for positioning systems operating in dense multipath environments. To reconstruct the LAPs' interference components, an iterative estimator for joint channel estimation and data detection needs to be developed, and the impact of LAPs on the performance of FAP detection can subsequently be removed. Considering the low correlation peak resulting from the weak power of the FAP, an *augmented preamble* is constructed to provide an enhanced correlation peak such that the FAP detection performance can be substantially improved.

On the other hand, multicell cooperation is a new communication paradigm promising significant system capacity by targeting intercell interference (ICI) elimination. BSs need to have the capability of coordination by sharing transmission-related information with each other. In addition, the location information of the target mobile users also plays an important role in the design of such multicell cooperation. Due to the practical challenges in establishing high-capacity and low-latency backhaul networks, a new *Multi-Layered* transmission scheme is proposed to simultaneously support both data communication and BS coordination. This way, the restriction of backhaul networks on the multicell cooperation strategy design can be removed. Other functionalities such as BS synchronization or location information sharing can also be achieved with the proposed transmission scheme.

The last objective of this thesis is to design a robust channel estimation scheme for practical OFDM system with a short training sequence. In this case, *Decision-Directed* channel estimation (DDCE) can be applied to improve the accuracy with the

aid of the demodulated OFDM data. However, the data decisions may consist of large portion of decision errors in severe frequency selective channels. Therefore, dedicated research effort is given to derive an optimal iterative DDCE (IDDCE) where unreliable data decision feedback can be eliminated on the subcarriers with enhanced noise effects. With this technique, the accuracy of the proposed FAP detection algorithm can also be enhanced.

1.3 Thesis Contributions

The main contributions of this thesis can be summarized as follows:

1. Robust FAP detection for location estimation:

   - A new FAP detection using multipath interference cancellation is proposed for wireless communication-based positioning system. With the FAP detection algorithm, location estimation accuracy is significantly improved as compared with the traditional correlation detector while there is no requirement for special preamble design or hardware modification.
   - An iterative estimator for joint channel and data estimation is proposed to determine the interfering LAPs for the proposed FAP detection algorithm. Semi-analytical expression describing the behavior of the iterative estimator is derived and based on which, an automatic stopping criterion is proposed to avoid unnecessary computation while assuring the acceptable performance.
   - An optimal threshold to select dominant LAPs is derived. LAPs interference cancellation and preamble extension techniques are proposed to make the correlation peak of the FAP more distinctive to identify.

2. Transmission scheme design for multicell cooperative networks:

   - A new multi-layered OFDM (ML-OFDM) system with flexible parallel transmission feature is proposed for multicell cooperative networks. With the transmission scheme, BS cooperation can be easily achieved without the utilization of backhaul network or additional control channels.
   - The transceiver structure and the corresponding signal processing algorithms for the proposed ML-OFDM system are designed and validated through computer simulations.

3. Optimal iterative decision directed channel estimation for OFDM system:

   - An optimal IDDCE is proposed to improve the accuracy of conventional training-based channel estimation in practical OFDM system where the length of the training sequence is limited by the transmission efficiency requirement.
   - An optimal threshold is derived to select reliable data decision feedback by eliminating the data decision errors on the subcarriers where noise components are enhanced due to the impact of frequency selective channel.

1.4 Thesis Organization

The rest of the thesis is organized as follows:

Chapter 2 describes the overall technical backgrounds related to the thesis including the brief introduction of positioning systems, different location techniques, multicell cooperation and channel estimation for OFDM system. Their corresponding technical challenges are also discussed in this chapter.

In Chapter 3, the proposed FAP detection algorithm using multipath interference cancellation is discussed in detail. Different modules including joint channel and data estimation, LAPs selection, LAPs interference cancellation and FAP detection are developed. Performance comparison between the proposed algorithm and the conventional method is analyzed and verified by computer simulations.

In Chapter 4, a ML-OFDM system is depicted in detail. The corresponding transmitter and receiver structures for the proposed ML-OFDM are presented. Later in this chapter, a power distribution scheme is proposed for different layers to optimize the overall system performance. Analysis on the data detection error probability and link capacity is given followed by the simulation results for the evaluation of the system performance.

In Chapter 5, an optimal IDDCE is investigated. The performance of this technique is analyzed in terms of the variance of channel estimation error and based on which, an optimal threshold for reliable data decision feedback selection is derived. Computer simulations are also conducted for performance evaluation.

Finally, in Chapter 6, conclusions are drawn based on the presented studies and some important future works are also discussed.

Chapter 2

Background

In this chapter, the technical background related to the three major research topics in this thesis including positioning techniques, multicell cooperation techniques for cellular networks and channel estimation schemes for OFDM systems is introduced for better understanding of the thesis.

2.1 Positioning Systems

Traditionally, the location estimation of the mobile users in a cellular network relies on the GPS, which is a popular satellite-based positioning system. However, in some circumstances the GPS signal is extremely weak and the resultant location estimation is inaccurate. Based on the unreliable location information, the performance of network optimization including adaptive power control, transceiver algorithm reconfiguration and location-aware routing will be dramatically degraded. Therefore, positioning systems based on existing wireless communication systems have been studied to provide alternative location estimation methods. In this section, the two main types of positioning systems are introduced. The challenges of satellite-based positioning systems are analyzed and a few examples of wireless communication system-based positioning systems are also discussed.

2.1.1 Satellite-Based Positioning System

The most popular satellite-based positioning system, the GPS, provides global location information of mobile receivers with the aid of at least 4 satellites of the total 24 satellites orbiting the earth at altitudes of approximately 11,000 [1, 2, 3]. In Europe, a satellite navigation system named Galileo was deployed by European Commission and Space Agency based on a 30 satellite constellation to provide positioning and timing services in 2008 [4]. Uncorrected positions determined from GPS satellite signals produce accuracies in the range of 50 to 100 meters. When using a technique called differential correction, users can get positions accurate to within 5 meters or less. Although the mobile users equipped with GPS chip may have a relatively high degree accuracy outdoors, there are still some factors making GPS technically challenging:

1. The biggest challenges of GPS is that the precision of GPS measurements dramatically degrades in dense multipath environments, such as in dense urban areas as well as inside buildings, due to the extremely weak strength of GPS signal and severe multipath propagation.

2. GPS is vulnerable to jamming and other disruptions from manmade or natural causes. Without a functional backup, widespread disruption the GPS would be catastrophic for commercial applications, as well as domestic and international security.

3. Embedding a GPS chip into mobile devices may lead to increased cost, size and battery consumption of the mobile devices.

For these reasons, wireless service providers may be unwilling to embrace GPS fully as the sole location technology for the cellular networks, and therefore, alterna-

tive solutions are needed to fill the gaps of the GPS in coverage and provide reliable location information.

2.1.2 Wireless Communications-Based Positioning System

New wireless communication system-based positioning systems have been investigated as alternatives to obtain location estimation of the mobile users in the scenarios where the GPS signal is unavailable. An order issued by the U.S. Federal Communications Commission (FCC) in July 1996 requires all wireless service providers, including cellular and broadband wireless communication systems, to provide location information of the mobile users to Emergency 911 (E-911) public safety services [5]. These FCC E-911 safety requirements, along with the other location-based techniques have boosted research in wireless location techniques.

Cellular networks can be used to provide location services, where the mobile users are located and tracked by measuring the signals' attributes (e.g. signal's arrival time, angle and strength) transmitted from/to a set of fixed cellular BSs [6, 7, 8]. However, due to the low power of each transmitter, narrow bandwidth, as well as the limited time resolution caused by the long symbol duration of cellular wireless signals, the cellular-based positioning system can only achieve very limited accuracy and the positioning error is often larger than several hundred meters [6, 7].

With the deployment of broadband wireless networks, the increasing level of interest drives the rapid evolution of geolocation technique using OFDM-based WLAN [9]. Location estimation based on WLAN positioning system is more accurate within its service area of network. However, its application is limited by the network coverage and outdoor location information is often unavailable, e.g., dense urban areas.

Recently, another kind of positioning system using Digital Television (DTV) networks was proposed in [10]. The major advantage of the DTV locationing includes the low RF frequency, wide band, high transmission power and the broad coverage of DTV transmitting stations. However, the performance may be significantly degraded due to the large cochannel interference in Single Frequency Networks (SFNs).

2.2 Location Techniques

There are several different approaches that can be adopted by wireless communication system-based positioning systems to determine the location of the mobile users in the wireless network, ranging from calculation of the received signal's strength to detection of the arrival time of the received signal. In this section, we introduce different location techniques and compare the advantages and disadvantages of them. Taking the location estimation accuracy and real-implementation complexity into consideration, the most suitable technique for broadband wireless communication systems is also determined.

2.2.1 Received Signal's Strength (RSS)

As the energy of a signal changes with the distance between the mobile user and the reference station, the RSS at the mobile user carries information about the distance between the reference station and the mobile user [11, 12]. In order to convert the RSS information to range estimation, the relation between the signal energy and the distance is required. One important factor called *path loss* determines the attenuation of signal's power/energy along its propagation path. One common model for path loss is given by

$$\overline{P}(d) = P_0 - 10n\log_{10}(d/d_0), \tag{2.1}$$

where n is the *path-loss exponent*, $\overline{P}(d)$ is the average received power at distance d, and P_0 is the received power at a reference distance d_0. (2.1) specifies the relation between the power loss and distance through the path-loss exponent. However, the relation cannot accurately reflect the relation between the received power and the distance in the practical wireless environment as the propagation mechanisms such as reflection, scattering and diffraction, or the obstruction of the direct path may cause dramatic fluctuations in RSS even over short distance and/or small time intervals.

Therefore, in real applications the signal power is commonly obtained by

$$P(d) = \frac{1}{T}\int_0^T |r(t,d)|^2 dt \tag{2.2}$$

where $r(t,d)$ is the received signal at distance d and T is the time measuring interval. Although the averaging operation can mitigate the short-term fluctuations, the RSS still significantly varies about its local mean, due to the obstacles in the environments. Furthermore, the *pathloss* factor n also changes dramatically from place to place and it is difficult to estimate the actual value of n. Therefore, the accuracy of RSS-based method is usually not good enough and can only be used as initial location estimation.

2.2.2 Angle of Arrival (AOA)

Another position related parameter is AOA, which refers to the angle between the mobile user and the reference station. The estimation of location using AOA measurements usually requires the employment of multiple antennas in the form of an antenna array, e.g., uniform linear array (ULA) at the mobile devices [13, 14].

The principle of AOA measurement is that the direction of arrival of the received signal can be calculated by measuring the phase difference between the antenna array

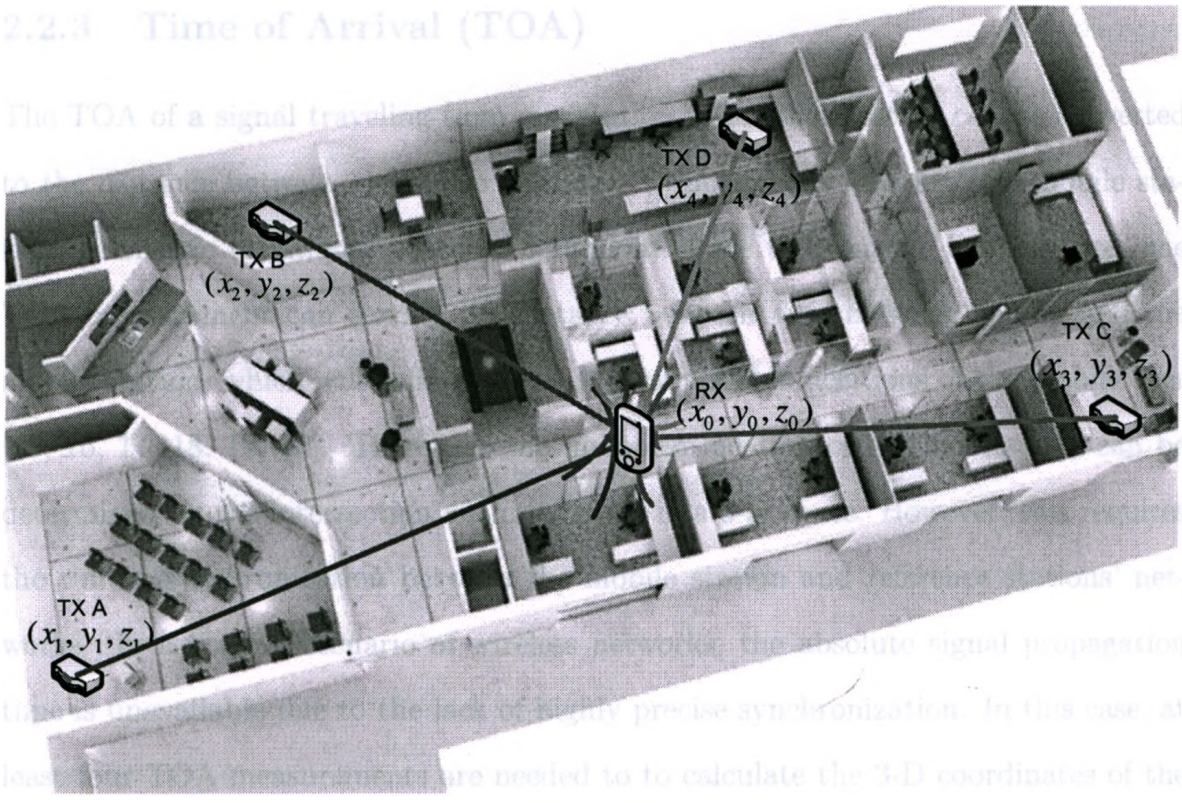

Figure 2.1: TOA-based positioning system using four synchronized transmitters in typical indoor office environment.

elements or by measuring the power spectral density across the antenna array. It is reported in that the accuracy of AOA estimation is related to signal-to-noise ratio (SNR), effective bandwidth of the system, the number of antenna elements and their inter-element spacing. The precision of AOA estimation improves with an increase in the above related parameters. Therefore, for broadband wireless communication systems, high-precision AOA estimation can be facilitated. However, the extremely high implementation cost including the size and complexity of the antenna array makes it challenging for real applications, especially for the mobile stations.

2.2.3 Time of Arrival (TOA)

The TOA of a signal traveling from one station to another station can be converted to the distance between those two stations. To obtain the location of a mobile station, geometric techniques based on *trilateration* are to be used. For instance, one TOA measurement can specify the distance between one reference station and the mobile station, which will define a circle for the possible positions of the mobile user [15, 16, 17, 18, 19, 20]. Therefore, the unknown location of the mobile user can be determined by the intersection of three circles in a 3-D space. However, this requires the timing synchronization between the mobile station and reference stations' networks. In a general scenario of wireless networks, the absolute signal propagation time is unavailable due to the lack of highly precise synchronization. In this case, at least four TOA measurements are needed to to calculate the 3-D coordinates of the mobile station by solving and optimizing the following equations:

$$\begin{cases} (t_1 - \Delta t)\, c &= \sqrt{(x_0 - x_1)^2 + (y_0 - y_1)^2 + (z_0 - z_1)^2} \\ (t_2 - \Delta t)\, c &= \sqrt{(x_0 - x_2)^2 + (y_0 - y_2)^2 + (z_0 - z_2)^2} \\ (t_3 - \Delta t)\, c &= \sqrt{(x_0 - x_3)^2 + (y_0 - y_3)^2 + (z_0 - z_3)^2} \\ (t_4 - \Delta t)\, c &= \sqrt{(x_0 - x_4)^2 + (y_0 - y_4)^2 + (z_0 - z_4)^2}, \end{cases} \tag{2.3}$$

where t_i is the relative signal propagation time from the ith reference station to the mobile station to be measured, Δt is the timing difference between the unknown reference stations' network time and the mobile station's local clock, c is the speed of light, (x_0, y_0, z_0) are the unknown coordinates of the mobile user, and (x_i, y_i, z_i) are the coordinates of the ith reference station which are assumed to be known in the network.

The relative propagation time t_i can be determined by detecting the time index of the FAP from the received signals. However, the unique characteristics of dense multipath scenarios make it challenging for accurate FAP detection as the FAP is often associated with significantly low power and large interference from the LAPs. We will analyze the challenges of traditional FAP detection scheme in dense multipath environments later in this section.

2.2.4 Comparison of different location techniques

The advantages and disadvantages of different location techniques are summarized and compared in Table 2.1.

As we can see from Table 2.1, due to the low computational complexity and higher estimation accuracy, TOA is commonly preferred for broadband wireless communication systems as the high precision of TOA measurement can be facilitated by high time resolution of broadband wireless signals. Although it requires a synchronized network, the BSs in a conventional cellular network are already synchronized through GPS or pre-existing backhaul network and the local clock of the mobile users is not necessarily required to be synchronized with the network time as the clock difference can be eliminated by adding one additional TOA measurement as shown in (2.3).

2.2.5 Technical Challenges of TOA-Based Positioning System

In dense multipath scenarios where the direct signal propagation path is often blocked by various obstacles such as buildings, pedestrians and slowly moving vehicles, the power of FAP is significantly weaker than those of LAPs from scattering, reflection

Table 2.1: Comparison of different location techniques

Location Techniques	Advantages	Disadvantages
RSS	• low hardware implementation cost • simple signal processing algorithm • low computational complexity	• dramatic signal's strength variation in dense multipath environment • low accurate path loss model and low location estimation accuracy
AOA	• simple signal processing algorithm • no requirement of clock synchronization	• high implementation cost due to the size and complexity of antenna array • low location estimation accuracy in large cells
TOA	• simple signal processing algorithm • high time resolution of broadband wireless signal • high location estimation accuracy	• requirement of synchronized network

and refraction. Traditional correlation detector for FAP is based on the cross correlation between the received signal and a local preamble signal [21]. The earliest peak that exceeds a particular threshold is determined as the FAP. However, in practical wireless communication systems, there are some factors making the correlation detector significantly challenging:

1. The average power of the FAP in dense multipath environments is very weak

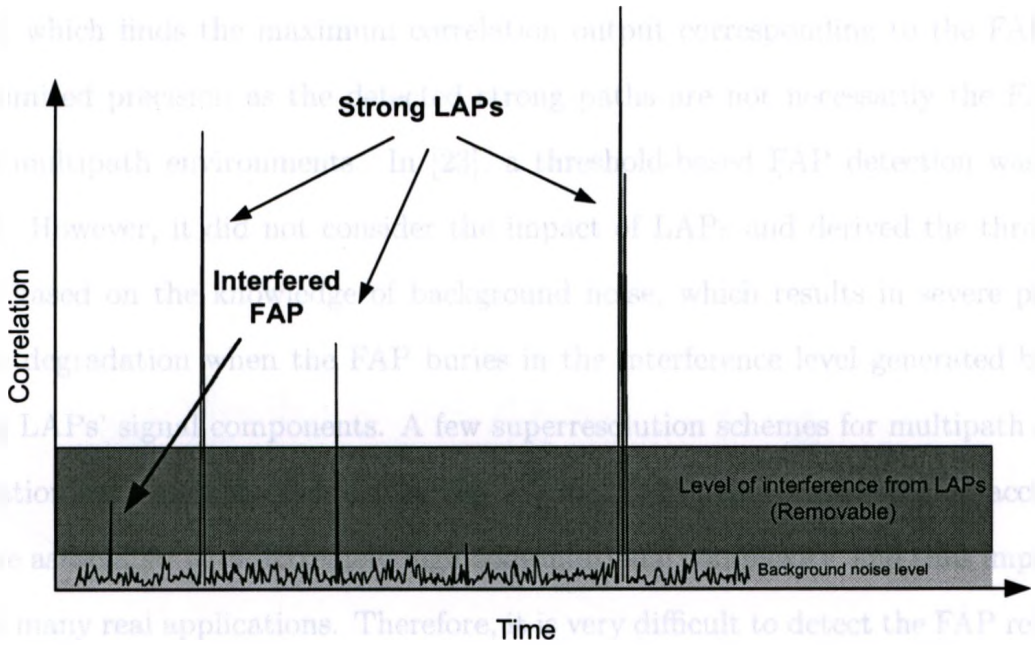

Figure 2.2: Cross-correlation profile for FAP detection in the presence of large LAPs interference.

due to the obstruction of the direct signal propagation path and therefore the FAP can have a very low correlation peak.

2. The length of the preamble signal in conventional communication system is finite due to the transmission efficiency issue and no special design of the preamble is allowed for positioning purpose. Hence, the correlation gain provided by the preamble is limited.

3. The signal strength of the LAPs from the scattering, reflection and refraction paths is much stronger than that of the FAP. The superposition of randomly arrival LAPs' signal components can cause large interference to the FAP.

It can be observed in Fig. 2.2 that the FAP's correlation peak is severely distorted by the large interference from the LAPs. In literature, some FAP detection algorithms have been investigated to achieve accurate location estimation. The scheme

in [22] which finds the maximum correlation output corresponding to the FAP has very limited precision as the detected strong paths are not necessarily the FAP in dense multipath environments. In [23], a threshold-based FAP detection was proposed. However, it did not consider the impact of LAPs and derived the threshold solely based on the knowledge of background noise, which results in severe performance degradation when the FAP buries in the interference level generated by the strong LAPs' signal components. A few superresolution schemes for multipath delay estimation such as that described in [24, 25, 26, 27, 28], can provide higher accuracy but are associated with extremely high computational complexity, and thus impractical for many real applications. Therefore, it is very difficult to detect the FAP reliably from the wireless signals with large LAPs interference and thus, large positioning error is inevitable when the FAP is erroneously identified.

2.3 Muticell Cooperative Networks

2.3.1 Principle of Multicell Cooperation

The conventional cellular networks characterized by *single cell processing* (SCP), have very limited sharing of common system resources due to the resultant large ICI, and therefore preventing the potential enhancement of networks' throughput and coverage [29]. Although SCP scheme generally served well in the past 2G/3G networks, the growing popularity of high-speed wireless applications in recent years poses a looming challenge due to the performance limitation of existing methodology, necessitating a new transmission paradigm referred to as multicell cooperation which exploits the ICI cooperatively by enabling joint signal processing among several interfering BSs.

Multicell cooperation, sometimes also known as *distributed antenna system* or

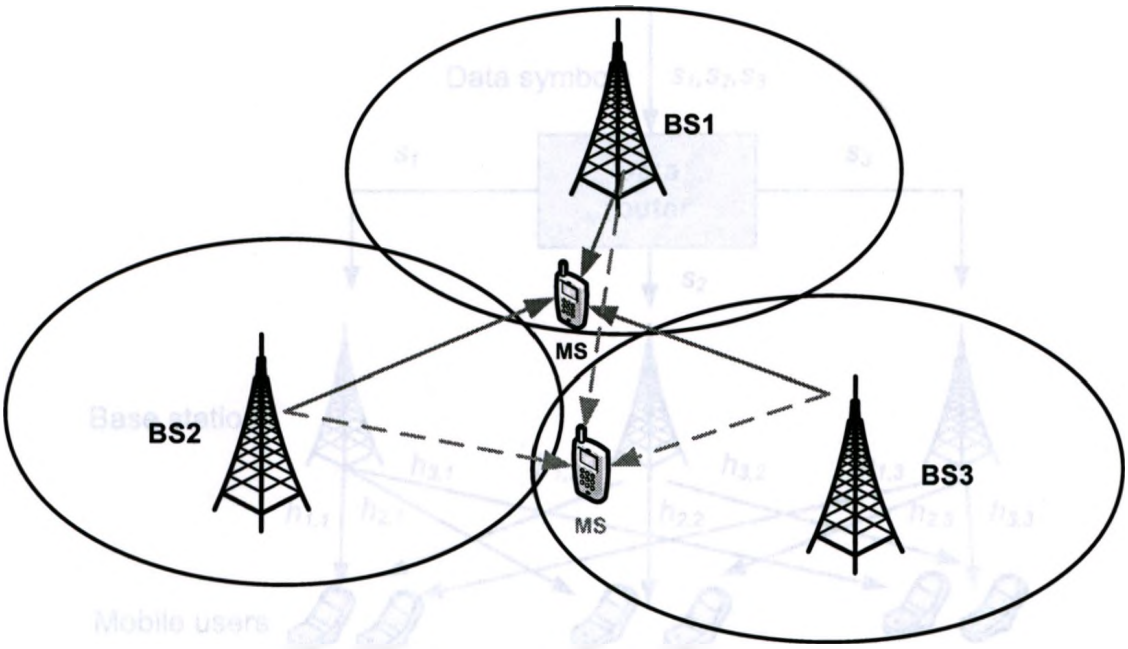

Figure 2.3: Illustration of a cellular network with multicell cooperation.

multicell MIMO, is a revolutionary technique which aims to eliminate the capacity-limiting factor of conventional cellular network and remarkably improve the overall system performance [30, 31, 32, 33]. This intelligent wireless system prescribes coordinated signaling strategies such as power allocation, beamforming directions, user scheduling, and joint encoding/decoding of the transmitted/received signals at the BSs depending on the different levels of multicell cooperation [30]. Recently, it has attracted lots of attention from both industrial and academic communities. For instance, the 3GPP LTE-Advanced [34] standard where the network coordination is known as coordinated multi-point (CoMP) transmission has been calling for standardization of signaling schemes for this technique since September of 2010 for possible consideration in Release 11 of LTE-Advanced. A few pioneering works have been done in literature which evaluate the performance of multicell cooperation through various information-theoretic models with simplified assumptions [35, 36, 37, 38, 39, 40, 41, 42, 43, 44, 45]. In this thesis, we take practi-

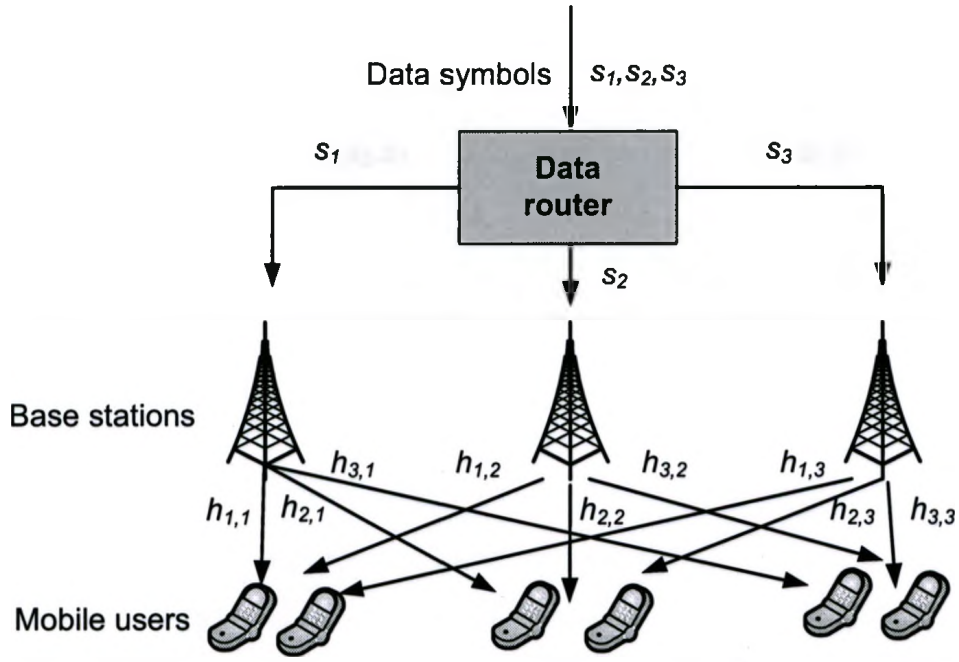

Figure 2.4: Illustration of interference cooperation for the downlink. The BSs acquire and share CSI (but not user data), pertaining to all relevant direct and interfering links, so as to optimize jointly their transmission parameters (time-frequency scheduling, power level, beamforming).

cal implementation-related issues into account and design a new signal transmission scheme which is specially tailored for multicell cooperative networks.

2.3.2 Technical Challenges of Multicell Cooperation

The theoretical performance of cooperative networks have been addressed in literature, however, including some ideal assumptions. With the development of multicell cooperation, the real-world implementation-related issues of cooperative techniques in cellular networks result in significant technical challenges in the design of signal transmission scheme for this new technique:

1) Backhaul issues: Current multicell cooperation techniques are enabled by the presence of a backhaul network with unlimited capacity and free-latency which connects the BSs with each other or with a central processor [46, 47]. Compared to

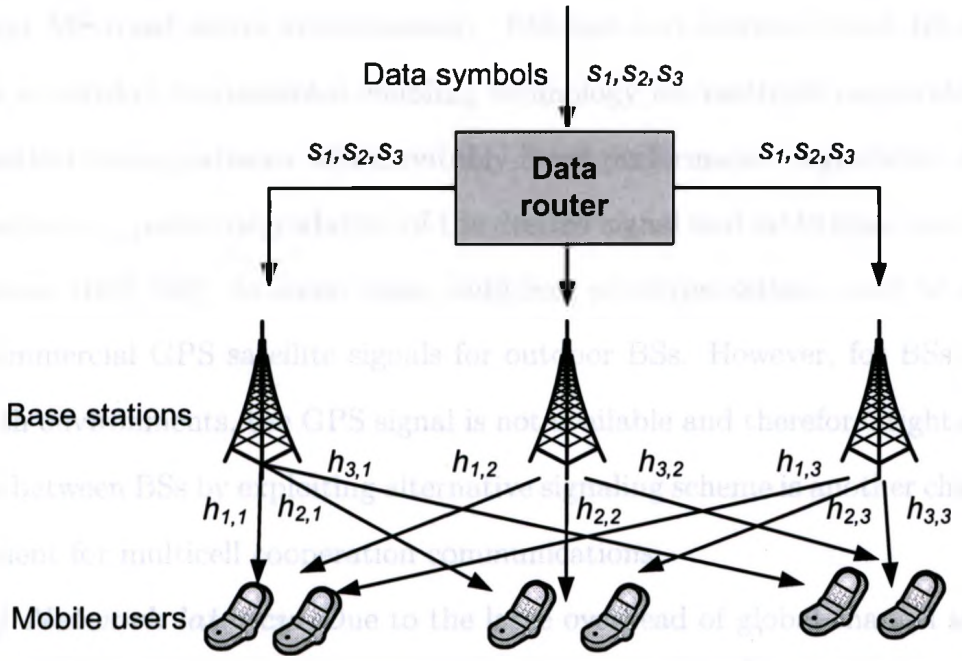

Figure 2.5: Illustration of multicell full cooperation (multicell MIMO) for the downlink. The BSs acquire and share CSI and user data with each other, so as to mimic the behavior of a large MIMO array.

a SCP-based cellular network with no coordination, multicell cooperation techniques require the sharing of certain information among cooperative BSs. For instance, as shown in Fig. 2.4 and Fig. 2.5, interference coordination techniques require the exchange of CSI and full cooperation requires the exchange of both CSI and user data. The data symbols of all users must be known at all cooperative BSs. Since the assumption of unlimited capacity link is quite unrealistic for large scale network, the limited capacity link within the pre-existing infrastructure may be unable to provide sufficient bandwidth for exchanging CSI and user data. As a result, the desired transmission technique should provide a robust signaling for conveying the required information between collaborative BSs to reduce the burden of the low-bandwidth backhaul, or even in the case that the backhaul network does not exist.

2) BS synchronization: To guarantee the mitigation of inter-cell interference, the desired signal components transmitted from different cooperative BSs to

the target MS must arrive synchronously. Efficient and accurate cross BS synchronization is another fundamental enabling technology for multicell cooperation since the imperfect timing advance will inevitably bring performance degradation in different aspects, e.g., power degradation of the desired signal and additional inter symbol interference (ISI) [30]. In some cases, sufficient synchronization could be achieved using commercial GPS satellite signals for outdoor BSs. However, for BSs in dense multipath environments, the GPS signal is not available and therefore, tight synchronization between BSs by exploiting alternative signaling scheme is another challenging requirement for multicell cooperation communications.

3) Network latency: Due to the large overhead of global channel state and user data information and the constrained transmission capability of the backhaul network, the distribution of the necessary information among BSs must be achieved by well-designed cross layer algorithm including Media Access Control (MAC) layer scheduling as well as physical (PHY) layer transmission strategies [48, 49, 50, 51]. The communication between the PHY and higher layers protocols and the traffic routing will naturally bring excessive time delay, especially causing dramatic performance degradation when the delay exceeds the coherence time of the downlink channels.

4) Channel estimation: Coherent combing at the receiver or coherent precombining at the transmitter can provide (signal-to-noise ratio) SNR gain when the CSI is known. Hence, sufficient resources have to be allocated to pilot signals to achieve reliable channel estimation, otherwise, the SNR gain will be significantly reduced due to the imperfect estimation of CSI. In the context of network coordination with spatially distributed BSs, the extent of coordination could depend on the range of reliable channel estimation, and there is a tradeoff between the increasing coordination network size and the increasing pilot overhead.

For estimation of the downlink channels at the transmitter in time-division du-

plex (TDD) networks, the reciprocity of the uplink and downlink channels can be utilized such that the estimated channel on the uplink can also be used for downlink transmission. In this scenario, estimation at the TDD transmitter faces similar challenges as the traditional channel estimation at the receiver. However, TDD system may be associated with additional challenges if the number of users is much larger than to total spatial degree of freedom. Pilot signals and protocols should be well designed to address these issues without leading to excessive training sequence overhead.

Estimation of downlink channels in frequency-division duplex (FDD) networks face much greater challenges. In FDD networks, the channel estimates obtained at the mobile user must be conveyed back to the BS, typically over a limited-bandwidth uplink feedback channel. Quantized channel estimates could be fed back using "codebooks" consisting of fixed precoding vectors.

Therefore, the pilot signals or training sequences should be kept as short as possible in order to reduce the overall overhead of the training while ensuring the acceptable performance of channel estimation. To overcome the contradiction between the large overhead and limited performance caused by the short training, an IDDCE is proposed in this thesis which utilizes the demodulated data to improve the performance of the original estimation provided by the training. Details of IDDCE will be presented in Chapter 5.

2.4 Channel Estimation for OFDM System

2.4.1 Principle of OFDM System

OFDM technique has emerged as one of the most attractive transmission schemes for broadband wireless communications in recent decades [52]. With the ever increasing demand of high data rate transmission in broadband wireless communications, the performance of single carrier modulation schemes is severely affected by large ISI due to the fact that the symbol duration is much shorter than the delay spread of the wireless channel. Therefore, highly complex time domain equalizer is required for good performance in a high data rate system. To solve the challenges, OFDM was first proposed to divide the data stream into multiple substreams to be transmitted over different orthogonal subchannels centered at different subcarrier frequencies. The subchannel bandwidth is less than the coherence bandwidth of the wireless channel, so that the frequency selective fading is now eliminated and the subchannels experience relatively flat fading. This insures that the subchannels will not experience significant ISI.

Furthermore, due to the introduction of a cyclic prefix (CP), not only the impact of ISI in OFDM system is completely removed, but also the received signal can be represented a circular convolution between the transmitted signal and the channel instead of the linear convolution. As a result, a simple one-tap frequency domain equalizer can be adopted to mitigate the effect of the channel which can be modeled as a complex gain on each subchannel/subcarrier. Therefore, OFDM has been widely adopted in various broadband systems such as WLANs, digital video/audio (DVB/DAB), and recently the upcoming fourth generation cellular and mobile radio system such as long term evolution (LTE) [53].

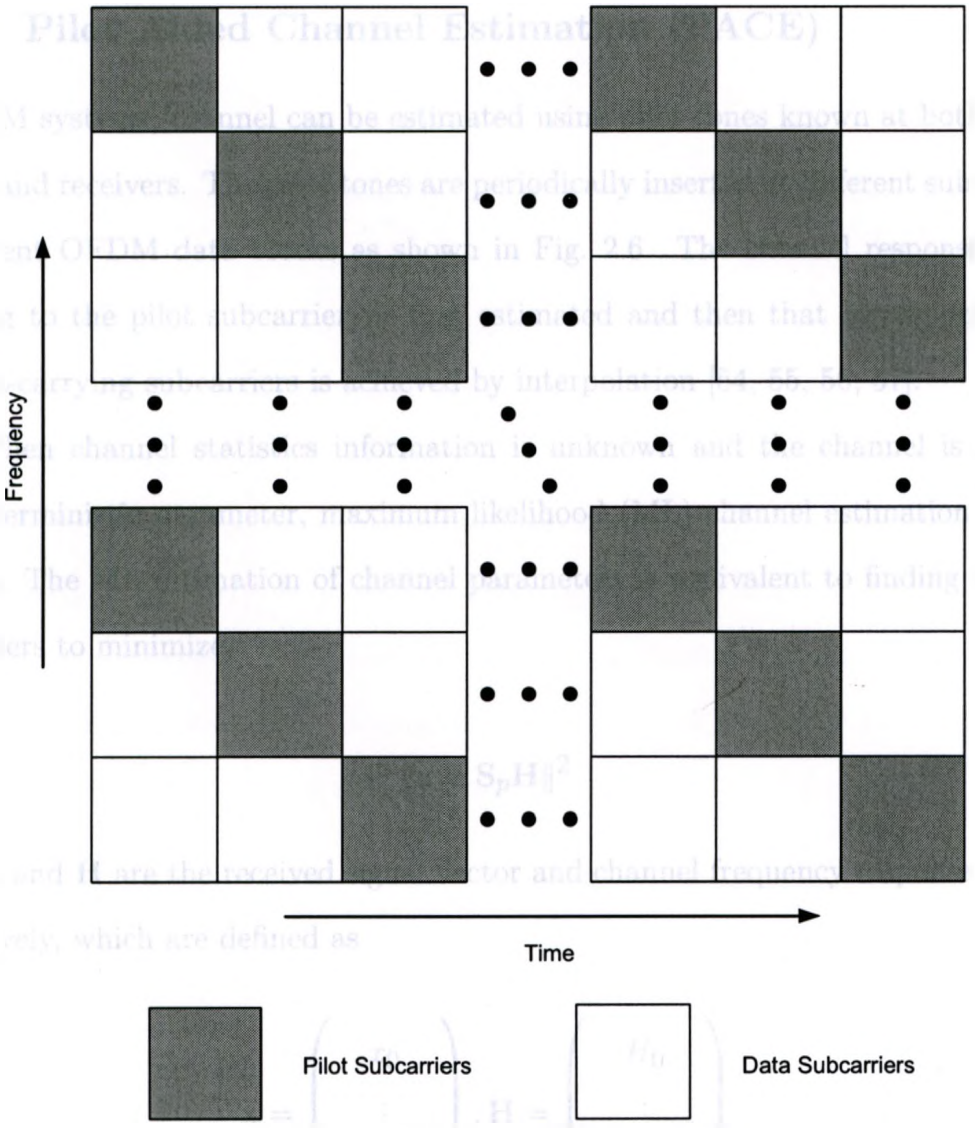

Figure 2.6: Typical pilot arrangement for OFDM systems.

The performance of OFDM systems is generally enhanced through the use of a coherent demodulation process. However, the reliable coherent detection is critically dependent on the accurate channel estimation results. In literature, various channel estimation techniques have been investigated.

2.4.2 Pilot Aided Channel Estimation (PACE)

In OFDM systems, channel can be estimated using pilot tones known at both transmitters and receivers. The pilot tones are periodically inserted at different subcarriers of different OFDM data blocks as shown in Fig. 2.6. The channel response corresponding to the pilot subcarriers is first estimated and then that corresponding to the data-carrying subcarriers is achieved by interpolation [54, 55, 56, 57].

When channel statistics information is unknown and the channel is treated as a deterministic parameter, maximum likelihood (ML) channel estimation will be optimal. The ML estimation of channel parameters is equivalent to finding channel parameters to minimize

$$\|\mathbf{x} - \mathbf{S}_p\mathbf{H}\|^2 \tag{2.4}$$

where $\mathbf{x}$ and $\mathbf{H}$ are the received signal vector and channel frequency response vector, respectively, which are defined as

$$\mathbf{x} = \begin{pmatrix} x_0 \\ \vdots \\ x_{N-1} \end{pmatrix}, \mathbf{H} = \begin{pmatrix} H_0 \\ \vdots \\ H_{N-1} \end{pmatrix} \tag{2.5}$$

and $\mathbf{S}_p$ is the pilot symbol matrix, which can be represented as

$$\mathbf{S}_p = \begin{pmatrix} s_0 & 0 & \cdots & 0 \\ 0 & s_1 & \ddots & 0 \\ \vdots & \ddots & \ddots & \vdots \\ 0 & \cdots & 0 & s_{N-1} \end{pmatrix}. \tag{2.6}$$

It can easily be seen that ML estimation can be solved by the Least Square (LS)

estimation which yields,

$$\hat{\mathbf{H}}_{LS} = \mathbf{S}_p^{-1}\mathbf{x}. \tag{2.7}$$

To reduce the computational complexity of ML or LS channel estimation, $\mathbf{S}_p^{-1}$ can be calculated offline. Estimation in this case neither needs nor exploits the information of channel statistics. Hence, the estimation accuracy is usually not good enough and therefore, it is often applied as initial estimation.

By exploiting channel statistics, channel estimation can significantly be improved. With the information of the correlation matrix of the channel frequency response, $\mathbf{R_H} = \mathrm{E}\left\{\mathbf{H}\mathbf{H}^H\right\}$, linear minimum mean square error (LMMSE) channel estimation can be obtained. For LMMSE estimation, channel frequency responses are regarded as random variables. Estimation of the channel frequency response vector is found to minimize the mean square error (MSE). Therefore we have,

$$\begin{aligned}\hat{\mathbf{H}}_{LMMSE} &= \mathbf{R_H}\left(\mathbf{R_H} + \sigma_n^2\left(\mathbf{S}_p\mathbf{S}_p^H\right)^{-1}\right)^{-1}\mathbf{S}_p^{-1}\mathbf{x} \\ &= \mathbf{R_H}\left(\mathbf{R_H} + \sigma_n^2\left(\mathbf{S}_p\mathbf{S}_p^H\right)^{-1}\right)^{-1}\hat{\mathbf{H}}_{LS}.\end{aligned} \tag{2.8}$$

Compared with LS estimation, LMMSE estimation has much better performance. However, it requires channel statistics information and has much higher computational complexity.

The two major issues which make the PACE methods challenging are pilot design and interpolation:

1): A few optimal design for the pilot pattern, power allocation and pilot number has extensively been studied in [58, 59, 60, 61, 62, 63, 64]. For instance, the impact of pilots on the overall system performance for time-varying channels has first been analyzed in [59]. Then the optimal pilot design for frequency selective channels

has been investigated in [60] and [61], whereas that for doubly selective channels has been investigated in [62]. The pilots have been designed to meet different criteria such as to minimize the MSE of channel estimation [58] or its CRB [63], maximize the channel capacity [60, 61, 62] and optimize the SER [64]. An extensive review on these topics has been addressed in [65].

2): The most challenging problem associated with the PACE is how to design an efficient interpolation method. LMMSE estimation can be applied for joint channel estimation and interpolation. Nevertheless, it requires channel statistics information and very high computational complexity [55, 56] and therefore, low-complexity interpolation algorithms are required for practical communications. Two of the simplest ways are piecewise constant [66] and liner interpolation [54]. However, closely-spaced pilot subcarriers are needed to achieve acceptable performance in frequency selective channels, which results in dramatic bandwidth loss. If channel variation statistics (Power Delay Profile/Doppler spectrum) are known as *a priori*, high-order polynomial can be applied to accurately adapt to wireless channels [54, 67]. Unfortunately, the assumptions on channel information prevents the deployment in practical communication systems.

2.4.3 Training Sequence Based Channel Estimation

In this technique, a training sequence is periodically inserted at the beginning of an or several OFDM data symbols in the time domain depending on the channel variation speed. Therefore, the OFDM frame can be formulated by $\{p[n], c[n], x[n]\}$, where $p[n]$ denotes the training sequence. $c[n]$ and $x[n]$ denote the guard interval (GI)/CP and the OFDM data sequence, respectively.

In the receiver, the channel response can be estimated using the training se-

quence. If we denote the received signal of the training sequence by $\tilde{p}[n]$, it can be expressed as

$$\tilde{p}[n] = p[n] \otimes h[n], \tag{2.9}$$

where $\otimes$ represents the cyclic convolution operation and $h[n]$ denotes the multipath channel. Therefore, in the frequency domain, we have,

$$\tilde{P}[k] = P[k] \cdot H[k]. \tag{2.10}$$

Thus the channel frequency response can be estimated by

$$\tilde{H}[k] = \tilde{P}[k]/P[k]. \tag{2.11}$$

The estimated channel frequency response can then be used to demodulate the subsequent OFDM data symbols.

The main advantage of training sequence-based channel estimation is its low implementation complexity as it does not require the interpolation process, making it as one of the simplest channel estimation schemes. However, several drawbacks exist for the channel estimator:

- The length of the training sequence must be longer than the maximum channel delay spread. Therefore, in the case of estimation of multipath channel with long dispersive time, the overhead of training sequence will result in severe transmission inefficiency.

- For time-varying channels, the training sequence needs to be frequently inserted into the transmitted data stream, e.g., one training sequence for each OFDM

data symbol. In this case, the transmission efficiency will be dramatically reduced.

2.4.4 Superimposed Pilot Based Channel Estimation

A special form of pilot called superimposed pilot, where the pilot is superimposed onto the data symbols before transmission [68, 69], was first proposed for phase synchronization and originally referred to spread spectrum pilot and was later applied for channel estimation [70, 71, 72, 73]. The use of the superimposed pilot enhances both the bandwidth utilization and the transmission efficiency since dedicated pilot subcarriers or training sequences are not required, and therefore representing a more practical approach. However, a certain portion of transmission power must inevitably be allocated to the pilots and therefore, the improvement of the bandwidth utilization is achieved at the expense of a poorer SNR level. Furthermore, the performance of channel estimation using the superimposed pilots also degrades due to the unknown data symbols as large interference.

2.4.5 Decision-Directed Channel Estimation

Motivated by the aforementioned drawbacks of training sequence-based channel estimation, DDCE was proposed to reduce the overhead of the training sequence as well as improve the estimation accuracy [74, 75, 76, 77, 78, 79]. In practical wireless environments, the channel can be assumed to be static over a number of OFDM symbols due to the short symbol duration of broadband communication systems. Therefore, the channel corresponding to the training sequence is first estimated, and then used to demodulate and detect the subsequent OFDM data blocks. The channel can be improved by combing the detected data symbols with the original training sequence

to form an *augmented preamble* such that the length and the resultant total power of this training sequence are virtually extended training sequence are significantly increased.

In literature, there are two main categories of DDCE schemes where the data is detected on either hard decision or soft decision:

(1) Soft Decision: For systems with error-correction coding, redundancy in coding can be exploited to improve the performance of channel estimation, iterative receivers for joint channel estimation and decoding have been proposed in OFDM systems. The scheme performs a combined channel estimation/decoding process according to the maximum *a posteriori* (MAP) criterion, using the expectation-maximization (EM) algorithm. In the iterative receiver, the MAP decoding submodule progressively provides more reliable information on coded bits to the channel estimator submodule. Then it subsequently provides more reliable information on the channel gain to the decoding submodule in an iterative manner. However, the main problem associated with the soft decision feedback is its extremely high implementation complexity due to the iterative decoding procedure [77, 78]. Therefore, it is impractical to implement in real applications.

(2) Hard Decision: The DDCE with hard data decisions can be more suitable for practical OFDM systems with both improved channel estimation accuracy and reduced complexity as compared with the soft data decision. It particularly fits in systems in a slot transmission mode, such as wireless cellular systems. However, this method sometimes can only provide limited performance improvement even degradation in severe frequency selective channels when the data decisions comprise a large portion of hard decision errors [79, 80]. Therefore, in this thesis, we focus on the DDCE with hard decision and propose an iterative DDCE with reliable data feedback selection. Details of the algorithm can be found in Chapter 5.

2.5 Summary

In this chapter, thesis-related technical background, including positioning techniques, multicell cooperation and channel estimation for OFDM systems. Two main types of positioning systems are first introduced. An overview of different location techniques is subsequently presented, based on which, the suitability of these techniques for broadband wireless communication systems is analyzed. In Section 2.3, the principle of multicell cooperative network and its corresponding challenges are presented. Finally, various channel estimation methods including traditional pilot/training-based estimation method and recently proposed DDCE scheme are discussed.

Chapter 3
First Arriving Path Detection in Dense Multipath Environments

3.1 Introduction

Recent development in wireless communication-based location technology brings significant challenge of detecting weak FAP signal for TOA-based techniques in severe dense multipath environments. Due to the common obstruction of the direct signal path, identification of weak FAP in these environments can be very difficult via conventional correlation detector based on the preamble signal in the presence of interference from strong LAPs.

In this chapter, a new FAP detector based on LAPs interference cancellation and preamble extension techniques is proposed for TOA-based positioning system in dense multipath environments. An OFDM-based communication system, which is widely adopted in various broadband wireless applications [52] is considered in this chapter. We first propose an iterative estimator where the channel and the transmitted OFDM data are jointly estimated with progressively improved accuracy. An optimal threshold is subsequently derived to select the significant LAPs that introduce dominant interference to the FAP. The signal components of the LAPs are then reconstructed and removed from the original received signals. FAP detection is performed based on the correlation between the LAPs interference-suppressed signal and

an *augmented preamble* which is the combination of the preamble signal and the demodulated data sequence. As a result, more accurate FAP detection results can be obtained to improve the precision of location estimation. Since the proposed algorithms can be realized by traditional communication transceivers, our system entails neither special preamble signal design nor hardware modification. Furthermore, the performance of the iterative estimator is studied by deriving the semi-analytical expressions of the variance of estimation error, based on which, an automatic stopping criteria is also developed to avoid the unnecessary computational complexity and allow a tradeoff between the performance degradation and computational burden. The overall performance of the algorithm is studied through the mathematical analysis of the FAP's signal-to-noise-and-interference-ratio (SINR). Computer simulations are used to evaluate and verify the performance and effectiveness of different modules as well as the overall algorithm. Simulation results show that the accuracy of location estimation is substantially improved with the proposed algorithm.

The rest of the chapter is organized as follows. The transceiver structure of the OFDM system with the proposed FAP detection is presented in Section 3.2. In Section 3.4, a new FAP detection scheme using the proposed multipath interference cancellation technique is proposed. An automatic stopping criteria is subsequently derived for the sake of power constraint of mobile devices. Performance of the proposed FAP detection is analyzed in Section 3.5 and numerical simulation results are presented in Section 3.6 to validate the performance of the proposed algorithms. Finally, the chapter is summarized in Section 3.7.

3.2 Transceiver of OFDM System with the Proposed Algorithm

We propose to incorporate the proposed FAP detection algorithm into general communication systems. Hence, a traditional OFDM system is considered which is envisioned as a promising technology for broadband wireless communications.

The block diagram of the OFDM system is shown in Fig. 3.1. Basically the TX in Fig. 3.1(a) is exactly the same as that in a traditional OFDM system. For the RX part. it also shares high similarity with conventional OFDM RXs except that the iterative process is used to provide joint LAPs and data estimation with enhanced accuracy. Accordingly, an automatic criterion is also proposed to reduce the associated computational complexity. The other major departure is the LAPs interference canceller and the FAP detector (shaded blocks). However, they can be implemented by simple adder circuits and correlation detector such that no further hardware modification is needed.

Consider the signal frame structure of the OFDM system in Fig. 3.2. We denote the preamble signal as $\mathbf{p} = \left[p_0, p_1, \cdots, p_{N_p-1}\right]$ with length N_p, which is periodically multiplexed with OFDM data blocks for synchronization and channel estimation purposes. Each OFDM data symbol is then generated by N_d-point inverse discrete Fourier transform (IDFT) and given by

$$x_n = \frac{1}{\sqrt{N_d}} \sum_{k=0}^{N_d-1} X_k e^{j\frac{2\pi kn}{N_d}}, n = 0, 1, 2, ..., N_d - 1, \tag{3.1}$$

where X_k denotes the complex data on the kth subcarrier and N_d is the number of total subcarriers. Assume that the guard interval (GI) and the cyclic prefix (CP) are longer than the maximum channel delay spread L and therefore the preamble

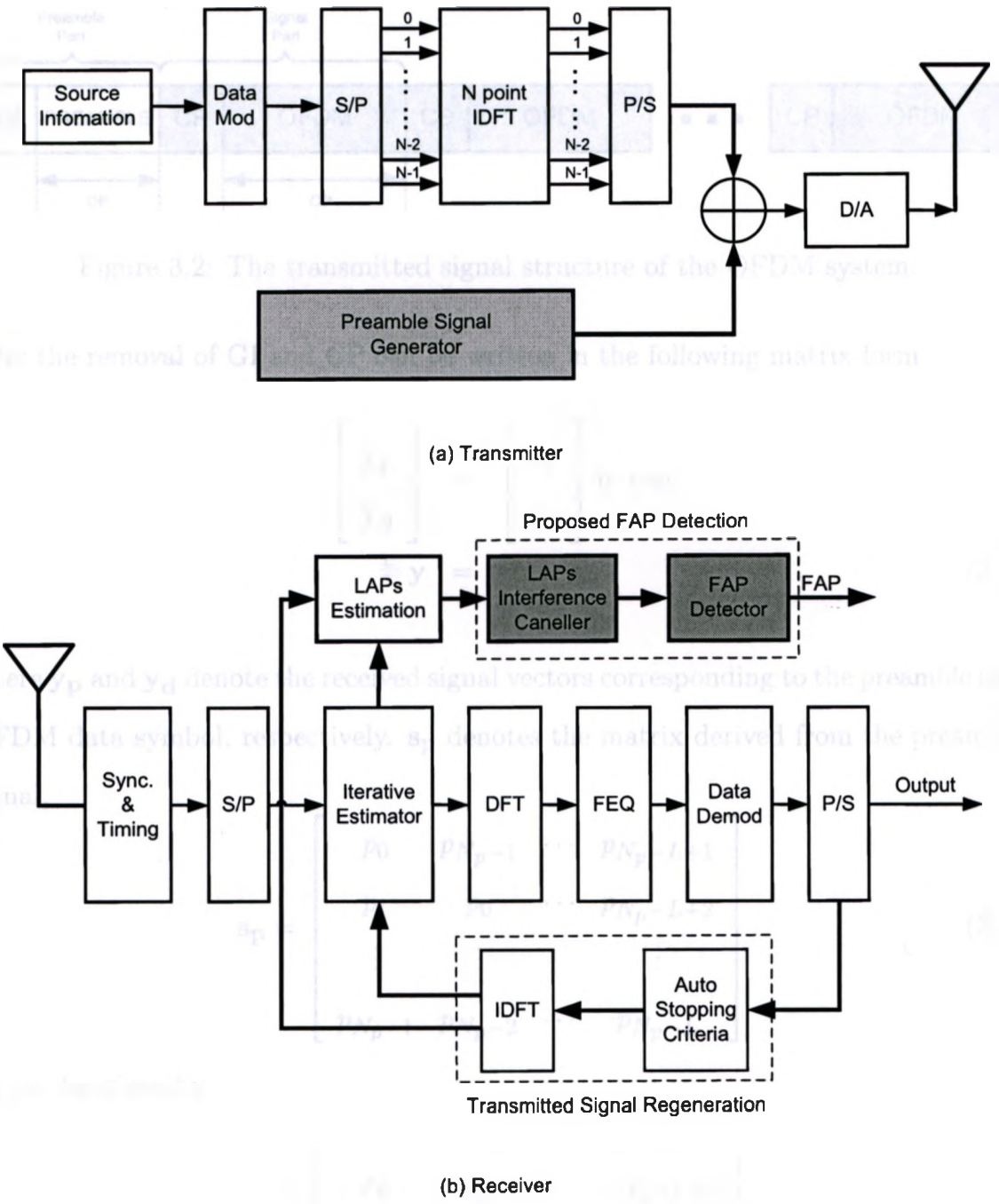

Figure 3.1: Block diagram of the OFDM transceiver with the proposed FAP detection approach: (a) Transmitter (b) Receiver.

signal and OFDM data blocks are free of intersymbol interference (ISI). When the observation periods (OPs) in Fig. 3.2 are adopted at the RX, the received signals

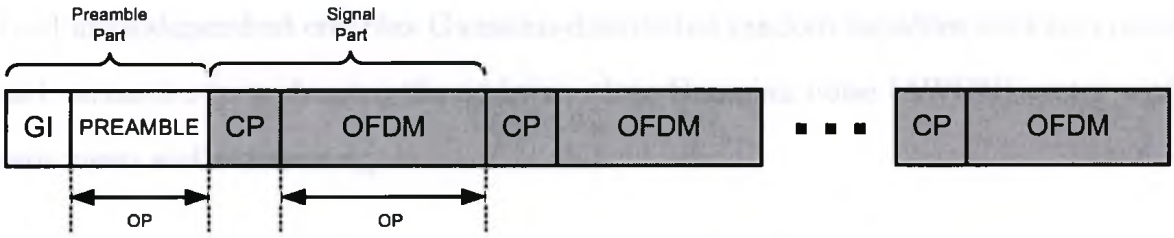

Figure 3.2: The transmitted signal structure of the OFDM system.

after the removal of GI and CP can be written in the following matrix form

$$\begin{bmatrix} \mathbf{y_p} \\ \mathbf{y_d} \end{bmatrix} = \begin{bmatrix} \mathbf{s_p} \\ \mathbf{s_d} \end{bmatrix} \mathbf{h} + \mathbf{w}$$
$$\triangleq \mathbf{y} = \mathbf{sh} + \mathbf{w}, \tag{3.2}$$

where $\mathbf{y_p}$ and $\mathbf{y_d}$ denote the received signal vectors corresponding to the preamble and OFDM data symbol, respectively. $\mathbf{s_p}$ denotes the matrix derived from the preamble signal,

$$\mathbf{s_p} = \begin{bmatrix} p_0 & p_{N_p-1} & \cdots & p_{N_p-L+1} \\ p_1 & p_0 & \cdots & p_{N_p-L+2} \\ \vdots & \vdots & & \vdots \\ p_{N_p-1} & p_{N_p-2} & \cdots & p_{N_p-L} \end{bmatrix}. \tag{3.3}$$

$\mathbf{s_d}$ can be given by

$$\mathbf{s_d} = \begin{bmatrix} x_0 & x_{N_d-1} & \cdots & x_{N_d-L+1} \\ x_1 & x_0 & \cdots & x_{N_d-L+2} \\ \vdots & \vdots & & \vdots \\ x_{N_d-1} & x_{N_d-2} & \cdots & x_{N_d-L} \end{bmatrix}. \tag{3.4}$$

$\mathbf{h} = [h_0, h_1, h_2, \cdots, h_{L-1}]^T$ is the L-tap multipath channel vector where $h_l, 0 \leq l \leq$

$L-1$ are independent complex Gaussian-distributed random variables with zero mean and variance σ_l^2. $\mathbf{w}$ denotes the additive white Gaussian noise (AWGN) vector with zero mean and variance σ_n^2.

3.3 Conventional Correlation Detector for FAP

Traditional scheme to detect the FAP is based on the correlation profile between the received signal and a local preamble. The time index of the first detected peak on the correlation profile is then converted to the corresponding arrival time. However, it is worth mentioning that in traditional communication systems, due to the use of strong error correction coding and the requirement of high transmission efficiency, the length of the preamble signal has to be as short as possible to reduce the corresponding redundancy when the acceptable channel estimation and synchronization performance is achieved. The ideal peak gain of the FAP is therefore limited by the length of the preamble. Furthermore, the peak of the FAP also consists of the LAPs interference components. As we can see in Fig. 2.2, the FAP is severely distorted by the interference from LAPs when the power of the FAP is significantly weaker than those of LAPs.

Mathematically, we can write the correlation between the received signal and the local preamble as follows,

$$R_{yp}(m) = \sum_{n=0}^{N_p-1} y_n p_{n-m}^*, \tag{3.5}$$

The correlation peak corresponding to the FAP can be further arranged as,

$$\begin{aligned} R_{yp}(h_0) &= \sum_{n=0}^{N_p-1}\left[\sum_{l=0}^{L-1} h_l p_{n-l} + w_n\right]\cdot p_n^* \\ &= \sum_{n=0}^{N_p-1}\left[\sum_{l=0}^{L-1} h_l p_{n-l} p_n^* + w_n p_n^*\right] \\ &= \underbrace{N_p h_0}_{\textbf{signal}} + \underbrace{\sum_{l=1}^{L-1} c_l h_l}_{\textbf{LAPs interference}} + \underbrace{\sum_{n=0}^{N_p-1} w_n p_n^*}_{\textbf{noise}}, \end{aligned} \tag{3.6}$$

where $c_l = \sum_{n=0}^{N_p-1} p_{n-l} p_n^*$ denotes the cyclic correlation value of the preamble. In this thesis, an m-sequence will be adopted as the preamble for the following considerations:

1. m-sequence exhibits good correlation properties such that the interference components from LAPs have been minimized by the sequence itself. Even in this case, we will show the significant achievements of our proposed algorithm over the traditional one. Therefore, further enhanced performance gain can be expected when other types of preambles are used.

2. Unlike some complex-valued sequences, the m-sequence is associated with low hardware implementation complexity which is widely employed in various research works and real applications.

Therefore, we have the cyclic correlation value $c_l = -1, \forall l \neq 0$. The SINR on

the FAP's correlation peak $R_{yp}(h_0)$ can be formulated as

$$\begin{aligned}\text{SINR} &= \frac{\mathrm{E}\left[N_p^2|h_0|^2\right]}{\mathrm{E}\left[\sum_{l=1}^{L-1}|h_l|^2\right]+\mathrm{E}\left[\sum_{n=0}^{N_p-1}w_n p_n*\right]} \\ &= \frac{N_p^2\sigma_0^2}{\sum_{l=1}^{L-1}\sigma_l^2+N_p\sigma_n^2},\end{aligned} \tag{3.7}$$

where $\sigma_l^2 = \mathrm{E}\left[|h_l|^2\right]$ denotes the average power of the $l$the channel path. In wireless environments such as indoor or dense commercial areas, the average power of the FAP is often significantly weaker than LAPs due to the blockage of the direct path, e.g., $\sigma_0^2 \ll \sum_{l=1}^{L-1}\sigma_l^2$. Therefore, interference from LAPs shown in (3.6) will have large impact on FAP detection even with a preamble of good correlation properties such as m-sequence. In such circumstances, even a high correlation processing gain N_p cannot guarantee sufficient SINR for accurate FAP detection. The severely interfered correlation sample may result in the wrong peak selection of those LAPs' correlation samples. In order to achieve accurate FAP detection in dense multipath environments, a new FAP detector based on LAPs interference cancellation and preamble extension will be presented in the next section.

3.4 Proposed First Arriving Path Detection Algorithm

The flowchart of the proposed FAP detection approach is shown in Fig. 3.3. In this section, the key modules of the proposed FAP detection algorithm including the iterative estimator for joint channel and data estimation, automatic stopping

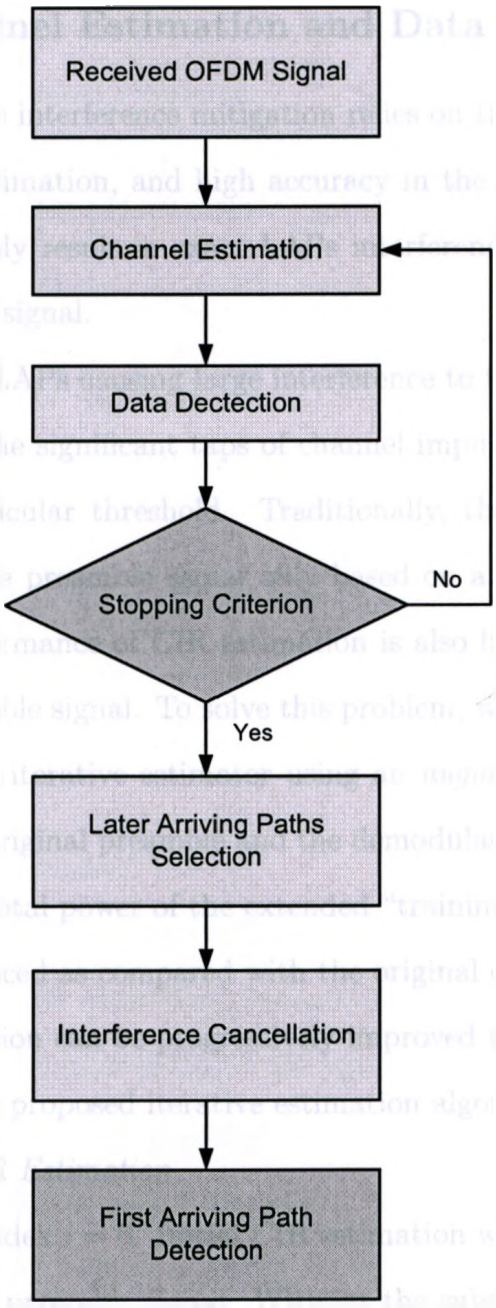

Figure 3.3: The flowchart of the proposed FAP detection approach.

criterion design for the iterative estimator, optimized LAP selection, LAP interference cancellation and FAP detection will be sequentially presented.

3.4.1 Joint Channel Estimation and Data Detection

The accuracy of of LAPs interference mitigation relies on the accuracy of LAPs and the transmitted data estimation, and high accuracy in the acquisition of LAPs and OFDM data will certainly result in exact LAPs interference reconstruction and removal from the received signal.

The predominant LAPs causing large interference to the FAP detection can be estimated by selecting the significant taps of channel impulse response (CIR) which are greater than a particular threshold. Traditionally, the CIR estimation $\hat{\mathbf{h}}$ can be obtained by using the preamble signal only based on a LS or MMSE estimator. Unfortunately, the performance of CIR estimation is also limited by the length and total power of the preamble signal. To solve this problem, we propose to improve the LAPs estimation via an iterative estimator using an *augmented preamble*, which is the combination of the original preamble and the demodulated OFDM symbols. The duration and resultant total power of the extended "training sequence" are expected to be significantly enhanced as compared with the original one. Hence, the accuracy of CIR and data estimation can be progressively improved as the process is iterated.

We summarize the proposed iterative estimation algorithm as follows:

Step 1. Initial CIR Estimation

Set the iteration index $i = 0$. Initial CIR estimation will be derived solely from the original multiplexed preamble signal. Without the subsequent OFDM data, the received signal now is

$$\mathbf{y_p} = \mathbf{s_p}\mathbf{h} + \mathbf{w}. \tag{3.8}$$

The LS estimator can be used to obtain the CIR estimation since no channel statistics information is required,

$$\hat{\mathbf{h}}^{(i)} = (\mathbf{s_p}^H\mathbf{s_p})^{-1}\mathbf{s_p}^H\mathbf{y_p}. \tag{3.9}$$

The variance of the estimation error can be used as a criterion to evaluate the performance of the preamble-based estimator,

$$\begin{aligned}
\sigma^2_{\Delta\mathbf{h}} &= \frac{1}{L}\mathrm{tr}\left(\mathrm{E}\left[\left\{\hat{\mathbf{h}}^{(i)}-\mathbf{h}\right\}^H\left\{\hat{\mathbf{h}}^{(i)}-\mathbf{h}\right\}\right]\right) \\
&= \frac{1}{L}\mathrm{tr}\left(\mathrm{E}\left[\left(\mathbf{s_p}^H\mathbf{s_p}\right)^{-1}\mathbf{s_p}^H\mathbf{w}\mathbf{w}^H\mathbf{s_p}\left(\mathbf{s_p}^H\mathbf{s_p}\right)^{-1}\right]\right) \\
&= \frac{\sigma_n^2}{L}\mathrm{tr}\left(\left(\mathbf{s_p}^H\mathbf{s_p}\right)^{-1}\right) \\
&= \frac{1}{N_p}\sigma_n^2. \qquad (3.10)
\end{aligned}$$

It should be mentioned that the accuracy of the initial estimation is limited by the length of the preamble. Therefore, the performance of LAPs interference cancellation will be dramatically degraded if the LAPs are determined based on the above estimated CIR.

Step 2. Iterative Estimator

The basic idea behind the proposed iterative estimator is that we utilize the *augmented preamble* for CIR estimation instead of using the preamble signal only. The performance of the estimator is then expected to be significantly improved since now the duration and the resultant power of this virtually extended training sequence are enhanced as compared with the original one. However, the *augmented preamble* is not very reliable in the beginning based on the demodulated results from the initial CIR estimation. The OFDM data detection accuracy can be improved when the CIR estimation improves. This indicates an iterative estimator is required to simultaneously enhance the CIR estimation and data detection. The OFDM signal in frequency domain is equalized with the tentative CIR estimation from the previous

step, channel estimates,

$$\tilde{\mathbf{X}}^{(i)} = \frac{\mathrm{DFT}\left\{\mathbf{y_d}\right\}}{\mathrm{DFT}\left\{\hat{\mathbf{h}}^{(i)}\right\}}. \tag{3.11}$$

Make data decisions based on the equalizer output and denote it as $\hat{\mathbf{X}}^{(i)}$. Now the transmitted signal in time domain can be re-modulated using the data after decision,

$$\hat{\mathbf{x}}^{(i)} = \mathrm{IDFT}\left\{\hat{\mathbf{X}}^{(i)}\right\}. \tag{3.12}$$

Similar to (3.4), the matrix of $\hat{\mathbf{x}}^{(i)}$ is constructed by

$$\hat{\mathbf{s_d}}^{(i)} = \begin{bmatrix} \hat{x}_0^{(i)} & \hat{x}_{N_d-1}^{(i)} & \cdots & \hat{x}_{N_d-L+1}^{(i)} \\ \hat{x}_1^{(i)} & \hat{x}_0^{(i)} & \cdots & \hat{x}_{N_d-L+2}^{(i)} \\ \vdots & \vdots & & \vdots \\ \hat{x}_{N_d-1}^{(i)} & \hat{x}_{N_d-2}^{(i)} & \cdots & \hat{x}_{N_d-L}^{(i)} \end{bmatrix}. \tag{3.13}$$

Consequently, the matrix of the *augmented preamble* can then be formulated by

$$\hat{\mathbf{s}}^{(i)} = \begin{bmatrix} \mathbf{s_p} \\ \hat{\mathbf{s_d}}^{(i)} \end{bmatrix}. \tag{3.14}$$

The new channel estimate is updated by the LS estimator, however, the $\mathbf{s_p}$ and $\mathbf{y_p}$ are now replaced by $\hat{\mathbf{s}}^{(i)}$ and $\mathbf{y}$. The CIR estimation is then obtained by using the following

$$\hat{\mathbf{h}}^{(i+1)} = \left((\hat{\mathbf{s}}^{(i)})^H \hat{\mathbf{s}}^{(i)}\right)^{-1} (\hat{\mathbf{s}}^{(i)})^H \mathbf{y}. \tag{3.15}$$

Set iteration index $i = i + 1$.

Repeat Step 2 if necessary until the automatic stopping criterion is fulfilled or a predefined number of iterations is achieved. Details of the automatic stopping

criterion design will be presented in the next subsection.

3.4.2 Automatic Stopping Criterion Design

Due to the limited battery life of the mobile devices, an automatic stopping criterion is proposed to terminate the iterative process as early as possible to avoid unnecessary computations and system latency while the user-specified performance is achieved.

3.4.2.1 Analysis of the estimation error

Before deriving the stopping criterion, it is necessary to study the variance of the estimation error of the iterative process. Given (3.15), the estimation error is straightforward to obtain. (Note that the superscript i has been dropped in for simplicity, unless otherwise stated)

$$\begin{aligned}\mathbf{\Delta h} &= \left(\hat{\mathbf{s}}^H\hat{\mathbf{s}}\right)^{-1}\hat{\mathbf{s}}^H\mathbf{y} - \mathbf{h} \\ &= \left(\hat{\mathbf{s}}^H\hat{\mathbf{s}}\right)^{-1}\hat{\mathbf{s}}^H\mathbf{\Delta s}\mathbf{h} + \left(\hat{\mathbf{s}}^H\hat{\mathbf{s}}\right)^{-1}\hat{\mathbf{s}}^H\mathbf{w} \\ &= \mathbf{\Delta h}_f + \mathbf{\Delta h}_w, \end{aligned} \tag{3.16}$$

where

$$\begin{aligned}\mathbf{\Delta s} &\triangleq \mathbf{s} - \hat{\mathbf{s}} \\ &= \begin{bmatrix}\mathbf{s_p} \\ \mathbf{s_d}\end{bmatrix} - \begin{bmatrix}\mathbf{s_p} \\ \hat{\mathbf{s}}_\mathbf{d}\end{bmatrix} = \begin{bmatrix}\mathbf{0} \\ \mathbf{\Delta s_d}\end{bmatrix}. \end{aligned} \tag{3.17}$$

The terms $\mathbf{\Delta h}_f$ and $\mathbf{\Delta h}_w$ denote the estimation error caused by data decision feedback errors and AWGN, respectively. In (3.16), the approximation holds that

$\left(\hat{\mathbf{s}}^H\hat{\mathbf{s}}\right)^{-1} = \mathbf{I}_L/N$ when $N >> L$ and therefore, the variance of $\mathbf{\Delta h}_w$ can be obtained by

$$\begin{aligned}\sigma^2_{\mathbf{\Delta h}_w} &= \frac{1}{L}\mathrm{tr}\left(\mathrm{E}\left[\mathbf{\Delta h}_w\mathbf{\Delta h}_w^H\right]\right)\\ &= \frac{1}{N}\sigma_n^2,\end{aligned} \tag{3.18}$$

where $N = N_p + N_d$.

For $\mathbf{\Delta h}_f$, it is more difficult to determine the variance which consists of the unknown data decision errors and the multipath channel. We first represent the variance as follows

$$\begin{aligned}\sigma^2_{\mathbf{\Delta h}_f} &= \frac{1}{L}\mathrm{tr}\left(\mathrm{E}\left[\mathbf{\Delta h}_f\mathbf{\Delta h}_f^H\right]\right)\\ &= \frac{1}{N^2L}\mathrm{tr}\left(\mathrm{E}\left[\hat{\mathbf{s}}^H\mathbf{\Delta s}\mathbf{hh}^H\mathbf{\Delta s}^H\hat{\mathbf{s}}\right]\right),\end{aligned} \tag{3.19}$$

note that the term $\hat{\mathbf{s}}^H\mathbf{\Delta s}$ can be written as

$$\begin{aligned}\hat{\mathbf{s}}^H\mathbf{\Delta s} &= \left[\mathbf{s_p}^H, \mathbf{s_d}^H\right]\begin{bmatrix}\mathbf{0}\\ \mathbf{\Delta s_d}\end{bmatrix}\\ &= \mathbf{s_d}^H\mathbf{\Delta s_d}.\end{aligned} \tag{3.20}$$

Thus, (3.19) can be further arranged as

$$\begin{aligned}\sigma^2_{\mathbf{\Delta h}_f} &= \frac{1}{N^2L}\mathrm{tr}\left(\mathrm{E}\left[\hat{\mathbf{s_d}}^H\mathbf{\Delta s_d}\mathbf{hh}^H\mathbf{\Delta s_d}^H\hat{\mathbf{s_d}}\right]\right)\\ &= \frac{1}{N^2L}\mathrm{tr}\left(\mathrm{E}\left[\hat{\mathbf{S_d}}^H\mathbf{F}_N^H\mathbf{F}_N\mathbf{\Delta S_d}\mathbf{hh}^H\mathbf{\Delta S_d}^H\mathbf{F}_N^H\mathbf{F}_N\hat{\mathbf{S_d}}\right]\right)\\ &= \frac{1}{N^2L}\mathrm{tr}\left(\mathrm{E}\left[\hat{\mathbf{S_d}}^H\mathbf{\Delta S_d}\mathbf{hh}^H\mathbf{\Delta S_d}^H\hat{\mathbf{S_d}}\right]\right),\end{aligned} \tag{3.21}$$

where $\mathbf{F}_N$ represents the DFT transform matrix with its element $F(n,k)$ determined by $(e^{j\frac{2\pi kn}{N}}/\sqrt{N})$. $\hat{\mathbf{S}_\mathbf{d}}$ is the frequency domain version of $\hat{\mathbf{s}_\mathbf{d}}$ with its element $\hat{S}_d(n,k) = \hat{X}_{k-n}$ and $\mathbf{\Delta S_d}$ is the frequency domain version of $\mathbf{\Delta s_d}$ with element $\Delta S_d(n,k) = \Delta X_{k-n}$.

As seen from (3.19), due to the trace operation, we only concern the elements on the main diagonal of $\left(\hat{\mathbf{S}}^H \mathbf{\Delta S h h}^H \mathbf{\Delta S}^H \hat{\mathbf{S}}\right)$, which can be represented as

$$\left(\hat{\mathbf{S}_\mathbf{d}}^H \mathbf{\Delta S_d h h}^H \mathbf{\Delta S_d}^H \hat{\mathbf{S}_\mathbf{d}}\right)_{ii} = \sum_{p=1}^{N_d}\sum_{q=1}^{N_d}\sum_{k=0}^{L-1} \hat{X}_{pi}^* \Delta X_{pk} \hat{X}_{qi} \Delta X_{qk}^* |h_k|^2. \tag{3.22}$$

It is straightforward to check that for any $\hat{X}_{im}$, $\hat{X}_{jn}$, ΔX_{im} and ΔX_{jn}, they are independently and identically distributed (i.i.d.) when $(i,m) \neq (j,n)$, then the ex-

pectation of (3.22) can be subsequently obtained by

$$
\begin{aligned}
& \mathrm{E}\left[\left(\hat{\mathbf{S}_\mathbf{d}}^H \mathbf{\Delta S_d h h}^H \mathbf{\Delta S_d}^H \hat{\mathbf{S}_\mathbf{d}}\right)_{ii}\right] \\
= & \sum_{p=1}^{N_d} \sum_{k=0,\ k\neq i}^{L-1} \mathrm{E}\left[\hat{X}_{pi}^* \Delta X_{pk} \hat{X}_{pi} \Delta X_{pk}^*\right] \mathrm{E}\left[|h_k|^2\right] \\
& + \sum_{p=1}^{N_d} \mathrm{E}\left[\hat{X}_{pi}^* \Delta X_{pi} \hat{X}_{pi} \Delta X_{pi}^*\right] \mathrm{E}\left[|h_i|^2\right] \\
& + \sum_{p,q=1,\ p\neq q}^{N_d} \mathrm{E}\left[\hat{X}_{pi}^* \Delta X_{pi} \hat{X}_{qi} \Delta X_{qi}^*\right] \mathrm{E}\left[|h_i|^2\right] \\
= & \sum_{p=1}^{N_d} \sum_{k=0,\ k\neq i}^{L-1} \mathrm{E}\left[\left|\hat{X}_{pi}\right|^2\right] \mathrm{E}\left[\left|\Delta X_{pk}\right|^2\right] \mathrm{E}\left[|h_k|^2\right] \\
& + \sum_{p=1}^{N_d} \mathrm{E}\left[\left|\hat{X}_{pi}\right|^2 \left|\Delta X_{pi}\right|^2\right] \mathrm{E}\left[|h_i|^2\right] \\
& + \sum_{p,q=1,\ p\neq q}^{N_d} \mathrm{E}\left[\hat{X}_{pi}^* \Delta X_{pi}\right] \mathrm{E}\left[\hat{X}_{qi} \Delta X_{qi}^*\right] \mathrm{E}\left[|h_i|^2\right] \\
= & \ \mathcal{V}_1 \sum_{k=0,\ k\neq i}^{L-1} \mathrm{E}\left[|h_k|^2\right] + \mathcal{V}_2 \mathrm{E}\left[|h_i|^2\right] + \mathcal{V}_3 \mathrm{E}\left[|h_i|^2\right]. \qquad (3.23)
\end{aligned}
$$

For analytical simplicity, we drop the subscripts and therefore $\mathcal{V}_i$ can be represented as

$$\mathcal{V}_1 = \mathcal{V}_2 = N_d \mathrm{E}\left[|\hat{X}|^2\right] \cdot \mathrm{E}\left[|\Delta X|^2\right], \qquad (3.24)$$

$$\mathcal{V}_3 = N_d(N_d - 1)\left|\mathrm{E}\left[\hat{X}^* \Delta X\right]\right|^2. \qquad (3.25)$$

Note the values of $\mathcal{V}_i$ may vary depending on the modulation scheme and its corresponding signal constellation. Let P_e denote the symbol error rate of the iterative estimator. We can make further simplifying assumptions that a nearest neighbor

selection is adopted when making symbol detection errors. For a particular point in a given signal constellation, assume that there are m nearest neighboring points with distance $d \triangleq \left|X - \hat{X}\right|$, each equally likely to occur when an decision error has occurred. We also assume zero conditional error probability to nonnearest neighboring points. For instance, if an M-PSK constellation is used, then we have $m = 2$ and $d = 2\sin(\pi/M)$. For QPSK constellation, this yields $d = \sqrt{2}$. Under these assumptions, we have

$$|\Delta X| = \begin{cases} 0, & \text{with probability } 1 - P_e, \\ d, & \text{with probability } P_e, \end{cases} \tag{3.26}$$

which yields

$$\mathrm{E}\left[|\Delta X|^2\right] = d^2 P_e. \tag{3.27}$$

Therefore, $\mathcal{V}_1$ and $\mathcal{V}_2$ can be finalized by

$$\mathcal{V}_1 = \mathcal{V}_2 = N_d d^2 P_e. \tag{3.28}$$

It should be noted that there is no closed form expression for $\mathcal{V}_3$ since it consists of the term $\mathrm{E}\left[\hat{X}^* \Delta X\right]$. Therefore, it can only be obtained through numerical calculations. For instance, for a known M-PSK constellation $\mathcal{A} = \{\alpha_i,\ \imath = 0, 1, \cdots, M-1\}$, considering a particular point $X = \alpha_k$, then the errorous decision falls into its neighboring points $\{\alpha_{k-1}, \alpha_{k+1}\}$ and the corresponding error $\Delta X \in \{\alpha_{k-1} - \alpha_k, \alpha_{k+1} - \alpha_k\}$

with equal probability. Hence, $\mathcal{G}$ can be defined as

$$\begin{aligned}\mathcal{G} &= \mathrm{E}\left[\hat{X}^*\Delta X\right] \\ &= \sum_{k=0}^{M-1}\left\{0.5P_e\alpha_{k-1}^*\cdot(\alpha_{k-1}-\alpha_k)+0.5P_e\alpha_{k+1}^*\cdot(\alpha_{k+1}-\alpha_k)\right\}, \quad (3.29)\end{aligned}$$

consequently, $\mathcal{V}_3$ can be achieved by

$$\mathcal{V}_3 = N_d(N_d-1)|\mathcal{G}|^2. \quad (3.30)$$

By replacing $\mathcal{V}_i$ with the approximated values, $\sigma^2_{\Delta\mathbf{h}_f}$ can be finally obtained by

$$\begin{aligned}\sigma^2_{\Delta\mathbf{h}_f} &= \frac{1}{N^2L}\sum_{i=1}^{L}\left(\mathcal{V}_1\sum_{k=0,k\neq i}^{L-1}\sigma_k^2+\mathcal{V}_2\sigma_i^2+\mathcal{V}_3\sigma_i^2\right) \\ &= \frac{4\sin^2(\pi/M)P_eN_dL+|\mathcal{G}|^2N_d(N_d-1)}{N^2L}, \quad (3.31)\end{aligned}$$

Under the assumption that the overhead of the preamble signal is small, i.e., $N_p \ll N_d$, (3.31) can be further simplified to

$$\sigma^2_{\Delta\mathbf{h}_f} \approx \frac{4\sin^2(\pi/M)P_e}{N}+\frac{|\mathcal{G}|^2}{L}. \quad (3.32)$$

Note that in the above equations, the channel energy $\sigma_H^2 = \sum_{l=0}^{L-1}\sigma_l^2$ is normalized to one. At high SNR range where P_e is sufficiently small, the last term consisting of P_e^2 in (3.31) can be neglected and therefore, (3.31) can be further simplified to

$$\sigma^2_{\Delta\mathbf{h}_f} \approx \frac{4\sin^2(\pi/M)P_e}{N}. \quad (3.33)$$

The final results of $\sigma^2_{\Delta \mathbf{h}_f}$ can be represented as

$$\sigma^2_{\Delta \mathbf{h}_f} = \frac{4\sin^2(\pi/M)P_e}{N} + \frac{|\mathcal{G}|^2}{L}, \tag{3.34}$$

where M is the modulation order and P_e denotes the symbol error probability of the output of the iterative estimator. The definition of $\mathcal{G}$ can be referred to the Appendix. Therefore, the overall variance of the estimation error can be written as

$$\begin{aligned} \sigma^2_{\Delta \mathbf{h}} &= \sigma^2_{\Delta \mathbf{h}_f} + \sigma^2_{\Delta \mathbf{h}_w} \\ &= \frac{4\sin^2(\pi/M)P_e}{N} + \frac{|\mathcal{G}|^2}{L} + \frac{1}{N}\sigma_n^2. \end{aligned} \tag{3.35}$$

3.4.2.2 Automatical Stopping Criterion Design

It can be seen from the previous subsection that $\sigma^2_{\Delta \mathbf{h}} \to \sigma_n^2/N$ as $P_e \to 0$. It should be mentioned that this bias cannot be removed when the length of the preamble and the OFDM data symbol is fixed. In fact, P_e is dependent on SNR and therefore this bias vanishes as SNR$\to \infty$ or $\sigma_n^2 \to 0$. Based on the convergence analysis of the iterative estimator, an automatic stopping criterion can be derived. Consider the relative estimation error between consecutive two iterations at the ith iteration,

$$\begin{aligned} \mathcal{E} &= \frac{\left\|\hat{\mathbf{h}}^{(i)} - \hat{\mathbf{h}}^{(i-1)}\right\|}{\left\|\hat{\mathbf{h}}^{(i-1)}\right\|} \\ &= \frac{\left\|\left(\hat{\mathbf{h}}^{(i)} - \mathbf{h}\right) - \left(\hat{\mathbf{h}}^{(i-1)} - \mathbf{h}\right)\right\|}{\left\|\hat{\mathbf{h}}^{(i-1)}\right\|} \\ &= \frac{\left\|\Delta\mathbf{h}^{(i)} - \Delta\mathbf{h}^{(i-1)}\right\|}{\left\|\hat{\mathbf{h}}^{(i-1)}\right\|}, \end{aligned} \tag{3.36}$$

the iterative process is terminated if the following criterion is fulfilled,

$$\mathcal{E} \leq \varepsilon, \tag{3.37}$$

where ε is a user-defined threshold dependent on the tolerable performance degradation of the receiver. As a small ε which results in less performance degradation is often associated with large number of iterations and vice versa. Therefore, we test the performance of the iterative estimator with different thresholds and it will be discussed in Section 3.6. In real-time application, a tuneable threshold selection device can be equipped such that the user is flexible to adjust the threshold according to its required performance and battery condition.

3.4.3 LAP Selection

After the CIR with improved accuracy is obtained, the significant LAPs which introduce dominant interference to the FAP are to be determined based on the estimated CIR. We proposed a threshold-based scheme to select the significant LAPs. Since the practical multipath channels often show some level of sparsity, where very limited channel paths carry significant energy, the total AWGN perturbation from those nonsignificant paths is usually much higher than the channel energy carried by them. Therefore, choosing a relative high threshold can successfully reject those nonsignificant paths while detecting most of the significant paths.

Remark: It is worth mentioning that the FAP may also be selected in the above process and cancelled in the line-of-sight (LOS) scenario where the direct path between TX and RX is very strong. However, some well-researched non-line-of-sight (NLOS) identification schemes [81, 82, 83] can be adopted before the proposed algorithm to identify the presence of direct path. If the direct path is weak due to the

obstruction, the proposed algorithm is subsequently adopted to remove the impact of LAPs and enhance the FAP detection. Otherwise, conventional FAP detection scheme can be used when the strong FAP is present.

3.4.3.1 Conventional LAP Selection

Motivated by [84], one typical solution is to first determine the strongest estimated path $\hat{h}_{max}$ from the estimated CIR $\hat{\mathbf{h}}$ by $\hat{h}_{max} = \max\{\hat{h}_i, i = 1, \cdots, L-1\}$. The LAPs estimation and the corresponding vector are then given by

$$\tilde{h}_l = \begin{cases} \hat{h}_l, & \text{if } |\hat{h}_l| > \eta|\hat{h}_{max}| \\ 0, & \text{otherwise.} \end{cases}$$
$$\Rightarrow \tilde{\mathbf{h}}_{\mathbf{LAPs}} = \left[0, \tilde{h}_1, \cdots, \tilde{h}_{L-1}\right]^T. \tag{3.38}$$

However, the process of the above LAPs identification has not been optimized which may result in high probabilities of false alarm of noise-only paths (insignificant paths) and missed detection of strong LAPs. In effect, the FAP detection accuracy is not maximized due to the large residual interference after imperfect interference cancellation. In [85, 86, 87], a few other significant-tap-catching schemes have been proposed and can be directly applied to LAPs selection. Unfortunately, adaptation of these schemes in real wireless environments is impractical due to assumptions about the channel statistics or time-consuming pre-simulations for optimization.

3.4.3.2 Optimized LAP Selection

An optimal threshold is derived to maximize the probability of distinguishing between significant LAPs and noise-only taps. The interference of LAPs can then be reformulated optimally and removed to improve the FAP detection. The performance of

LAPs selection is analyzed theoretically by deriving the mean square error (MSE) of LAPs selection.

Note that in our considered propagation scenarios where distinguished power differences exist between the FAP and strong LAPs, the scheme will only choose significant LAPs and therefore the FAP's signal component will be retained in the received signal. The significant LAPs can be determined by

$$\tilde{h}_l = \begin{cases} \hat{h}_l & \text{if } |\hat{h}_l| > \gamma \\ 0 & \text{otherwise} \end{cases}, \quad l = 1, 2, \cdots, L-1, \tag{3.39}$$

where γ denotes the threshold for LAPs selection.

Assuming independent Rayleigh fading for each path of the multipath channel, the optimal threshold can be derived as follows to minimize the error probability of the binary hypothesis testing problem in (3.39). It is straightforward to express the estimated channel $\hat{h}_l$ in two regions R_1 and R_2 which are given by

$$\hat{h}_l = \begin{cases} n', & l \in R_1 \\ h_l + n', & l \in R_2 \end{cases} \tag{3.40}$$

where n' denotes the noise component caused by channel estimation error of the iterative estimator in Section 3.1. In the region R_1 where only noise components exist on the insignificant paths, the probability density function (PDF) of $|\hat{h}_l|$ can be demonstrated by,

$$p_{R_1}(\hat{h}) = \frac{\hat{h}}{\sigma^2_{R_1}} \exp\left(\frac{-\hat{h}^2}{2\sigma^2_{R_1}}\right), \tag{3.41}$$

where $\sigma^2_{R_1} = \sigma^2_{\Delta h}/2$. $\sigma^2_{\Delta h}$ is the variance of the estimation error and derived in (3.35). $\sigma^2_{R_1}$ is identical to the receiver once the modulation scheme and SNR level have been

determined.

In the region R_2, the estimated channel gain consists of the ideal channel path gain and the associated estimation noise. Therefore, the PDF depends on the statistical property of the lth LAP. In Rayleigh channels, the PDF of $|\hat{h}_l|$ can be written as

$$p_{R_2,l}(\hat{h}) = \frac{\hat{h}}{\sigma^2_{R_2,l}} \exp\left(\frac{-\hat{h}^2}{2\sigma^2_{R_2,l}}\right), \tag{3.42}$$

where $\sigma^2_{R_2,l} = \sigma^2_{R_1} + \sigma^2_l/2$ and $\sigma^2_l = \mathrm{E}\left[|h_l|^2\right]$ denotes the average power ratio of the lth LAP to the total channel power. The optimal threshold γ_{opt} can then be derived mathematically to maximize the probability that

$$P_\gamma = \mathrm{Prob}\left\{|\hat{h}_l| < \gamma < |\hat{h}_m|\right\}, l \in R_1, m \in R_2. \tag{3.43}$$

Given the PDFs in (3.41) and (3.42), the above probability can be further represented as

$$\begin{aligned} P_\gamma &= \prod_{l\in R_1}\left(1 - \int_\gamma^\infty p_{R_1}(\hat{h})d\hat{h}\right)\prod_{l\in R_2}\left(1 - \int_0^\gamma p_{R_2,l}(\hat{h})d\hat{h}\right) \\ &= \left(1 - \exp\left(\frac{-\gamma^2}{2\sigma^2_{R_1}}\right)\right)^{L-\mathcal{M}} \prod_{l\in R_2}\exp\left(\frac{-\gamma^2}{2\sigma^2_{R_2,l}}\right), \end{aligned} \tag{3.44}$$

where $\mathcal{M}$ is the number of significant LAPs of the channel. To maximize the probability, we take the first derivative of (3.44) and set it equal to zero. Therefore, the optimal threshold can be shown to be

$$\gamma_{opt} = \sqrt{2\sigma^2_{R_1} \cdot \ln\left(1 + \frac{L-\mathcal{M}}{\sigma^2_{R_1} \cdot \sum_{l\in R_2}\frac{1}{\sigma^2_{R_2,l}}}\right)}. \tag{3.45}$$

Recall the $\sigma^2_{R_1}$ is identical to the receiver. Now the task is to estimate the channel statistics of strong LAPs, e.g., the number and average power. Fortunately, the number of significant LAPs can be obtained through the first step iterative estimator and the average power of these taps can also be achieved through historical observation in a short period of time.

MSE Analysis: The MSE of the proposed optimal LAPs selection is theoretically analyzed as follows. First, we can represent the estimation error $\Delta h_l = |h_l - \tilde{h}_l|$ as follows,

$$\Delta h_l = \begin{cases} 0 & |\hat{h}_l| \leq \gamma, l \in R_1 \\ |n'| & |\hat{h}_l| > \gamma, l \in R_1 \\ |h_l| & |\hat{h}_l| \leq \gamma, l \in R_2 \\ |n'| & |\hat{h}_l| > \gamma, l \in R_2 \end{cases}, \tag{3.46}$$

which indicates that the error is composed of three parts. When an insignificant tap (region R_1) containing only noise components exceeds the threshold, the noise components will contribute to the MSE. While for the significant LAPs (region R_2), if it does not overcome the threshold, the neglected channel energy on that path contributes to the MSE; otherwise, only the noise component contributes to the MSE. Therefore, the distribution of Δh_l can be shown to be,

$$\Delta h_l \sim \begin{cases} 0 & |\hat{h}_l| \leq \gamma, l \in R_1 \\ \exp\left(\frac{\gamma^2}{2\sigma^2_{R_1}}\right)\mathcal{R}\left(\sigma^2_{R_1}\right) & |\hat{h}_l| > \gamma, l \in R_1 \\ \frac{1}{1-\exp\left(-\frac{\gamma^2}{\sigma^2_{R_2,l}}\right)}\mathcal{R}\left(\frac{\sigma^2_{R_2,l}}{2}\right) & |\hat{h}_l| \leq \gamma, l \in R_2 \\ \mathcal{R}\left(\sigma^2_{R_1}\right) & |\hat{h}_l| > \gamma, l \in R_2 \end{cases}, \tag{3.47}$$

where $\mathcal{R}(\cdot)$ denotes the Rayleigh distribution. The total MSE can thus be written as

the sum of the above three different contributions and shown as follows,

$$\begin{aligned}
\mathrm{MSE} &= \sum_{l\in R_1} P\left(|\hat{h}_l| > \gamma\right) \mathrm{E}\left[\Delta h_l^2 \middle| |\hat{h}_l| > \gamma\right] \\
&\quad + \sum_{l\in R_2} \left[P\left(|\hat{h}_l| \le \gamma\right) \mathrm{E}\left[\Delta h_l^2 \middle| |\hat{h}_l| \le \gamma\right] + P\left(|\hat{h}_l| > \gamma\right) \mathrm{E}\left[\Delta h_l^2 \middle| |\hat{h}_l| > \gamma\right] \right] \\
&= \sum_{l\in R_2} \left(1 - \exp\left(-\frac{\gamma^2}{2\sigma^2_{R_2,l}}\right)\right) \left(\sigma_l^2 + \frac{\gamma^2}{1 - \exp\left(\frac{\gamma^2}{\sigma^2_{R_2,l}}\right)}\right) + \sigma^2_{R_1} \exp\left(-\frac{\gamma^2}{2\sigma^2_{R_2,l}}\right) \\
&\quad + (L - \mathcal{M}) \left(\gamma^2 + 2\sigma^2_{R_1}\right) \exp\left(-\frac{\gamma^2}{2\sigma^2_{R_1}}\right). \qquad (3.48)
\end{aligned}$$

3.4.4 LAPs Interference Cancellation and FAP Detection

As we can see from (3.2), the received signal can be decomposed into two parts

$$\mathbf{y} = \mathbf{sh_{FAP}} + \mathbf{sh_{LAPs}} + \mathbf{w}, \qquad (3.49)$$

where $\mathbf{h_{FAP}} = [h_0, 0, \cdots, 0]^T$ and $\mathbf{h_{LAPs}} = [0, h_1, h_2, \cdots, h_{L-1}]^T$ denote the FAP's vector and LAPs' vector, respectively. Basically, $\mathbf{sh_{FAP}}$ is the FAP's signal component that we want to capture. $\mathbf{sh_{LAPs}}$ can be considered as the accumulated interference from all the LAPs' components to the FAP's signal. In order to achieve a high SINR level for accurate FAP detection, the interference has to be mitigated. Fortunately, by utilizing the estimation of LAPs and OFDM signal from the iterative estimator, the LAPs interference can be reconstructed the LAPs interference and then

removed according to

$$\begin{aligned}\hat{\mathbf{y}} &= \mathbf{y} - \hat{\mathbf{s}}\tilde{\mathbf{h}}_{\mathbf{LAPs}} \\ &= \mathbf{sh}_{\mathbf{FAP}} + \mathbf{sh}_{\mathbf{LAPs}} - \hat{\mathbf{s}}\tilde{\mathbf{h}}_{\mathbf{LAPs}} + \mathbf{w} \\ &= \mathbf{sh}_{\mathbf{FAP}} + \hat{\mathbf{w}},\end{aligned} \tag{3.50}$$

where $\hat{\mathbf{s}}\hat{\mathbf{h}}_{\mathbf{LAPs}}$ represents the reconstructed LAPs interference and $\hat{\mathbf{w}}$ is the residual interference and AWGN after cancellation. The successful LAPs interference cancellation can be expected as the regenerated transmitted signal is close to the original transmitted signal, $\hat{\mathbf{s}} \rightarrow \mathbf{s}$ after a few iterations at operating SNRs.

Furthermore, to enhance the FAP's peak gain, an *augmented preamble* is formulated by

$$\hat{\mathbf{p}} = \left[p_0, p_1, \cdots, p_{N_p-1}, \hat{x}_0, \hat{x}_1, \cdots, \hat{x}_{N_d-1}\right], \tag{3.51}$$

which consists of the original preamble signal and the recovered OFDM signal.

The cross-correlation is then performed between the LAPs interference-suppressed signal $\hat{\mathbf{y}}$ and the *augmented preamble* $\hat{\mathbf{p}}$,

$$R_{\hat{y}\hat{p}}(m) = \sum_{n=0}^{N-1} \hat{y}_n \hat{p}^*_{n-m}. \tag{3.52}$$

A threshold needs to be set up to select the FAP. As the correlation peak now becomes so distinctive, the threshold is easy to find. Denote by k_0 the time index of the detected FAP, the corresponding arrival time at the RX can be obtained via $t_0 = k_0 \cdot T_s$ where T_s is the sampling period. However, as mentioned in Section 2.2.3, there is usually a clock drift between the RX the TXs' networks, and therefore at least four TXs are required for RX's location estimation.

3.5 Performance Analysis of the Proposed FAP Detection

The performance of the proposed FAP detection scheme is analyzed in this section by evaluating the FAP's SINR level and this can be achieved by calculating the SINR on the FAP's sample of the cross-correlation profile given by (3.52). We denote the FAP's correlation peak as $R_{\hat{y}\hat{p}}(h_0)$ and it is shown in detail as follows,

$$R_{\hat{y}\hat{p}}(h_0) = \underbrace{h_0 \left(\sum_{n=0}^{N_p-1} p_n p_n^* + \sum_{n=0}^{N_d-1} x_n \hat{x}_n^* \right)}_{\textbf{signal}}$$
$$+ \underbrace{\sum_{l \in \textbf{LAPs}} \left[h_l \sum_{n=0}^{N_d-1} \Delta x_{n-l} \hat{x}_n^* + \Delta h_l \left(\sum_{n=0}^{N_p-1} p_{n-l} p_n^* + \sum_{n=0}^{N_d-1} x_{n-l} \hat{x}_n^* \right) \right]}_{\textbf{interference}} + \underbrace{\sum_{n=0}^{N-1} w_n \hat{p}_n^*}_{\textbf{noise}}, \tag{3.53}$$

where **LAPs** denotes the set of LAPs' indices which can be determined by (3.38), $\textbf{LAPs} = \left\{ l, h_l \in \tilde{\mathbf{h}}_{\textbf{LAPs}} \right\}$. Note that the impact of the non-significant paths has been neglected in (3.53). Denote the signal part in (3.53) as P and the interference and noise parts as I which is contaminated by residual interference from the LAPs interference components and background noise.

The power of P can be first calculated as

$$\begin{aligned}
\sigma_P^2 &= \mathrm{E}\left[|h_0|^2 \cdot \left|N_p + \sum_{n=0}^{N_d-1} x_n \hat{x}_n^*\right|^2\right] \\
&= \sigma_0^2 \left[N_p^2 + N_p \sum_{n=0}^{N_d-1} \mathrm{E}\left[x_n \hat{x}_n^*\right] + N_p \sum_{n=0}^{N_d-1} \mathrm{E}\left[x_n^* \hat{x}_n\right] + \mathrm{E}\left[\left|\sum_{n=0}^{N_d-1} x_n \hat{x}_n^*\right|\right]^2\right] \\
&= \sigma_0^2 \left[N_p^2 + 2N_p N_d \Re\left\{r_{x_n,\hat{x}_n}\right\} + \sum_{n=0}^{N_d-1} \mathrm{E}\left[|x_n|^2 |\hat{x}_n|^2\right] + \binom{2}{N_d} \left|r_{x_n,\hat{x}_n}\right|^2\right] \\
&= \sigma_0^2 \left[N_p^2 + 2N_p N_d \Re\left\{r_{x_n,\hat{x}_n}\right\} + N_d + \binom{2}{N_d} \left|r_{x_n,\hat{x}_n}\right|^2\right] \qquad (3.54)
\end{aligned}$$

where

$$r_{x_n,\hat{x}_n} = \mathrm{E}\left[x_n \hat{x}_n^*\right], \qquad (3.55)$$

The power of I can then be represented as

$$\begin{aligned}
\sigma_I^2 = &\sum_{l \in \mathbf{LAPs}} \mathrm{E}\left[|\Delta h_l|^2\right] \mathrm{E}\left[\left|-1 + \sum_{n=0}^{N_d-1} x_{n-l} \hat{x}_n^*\right|^2\right] \\
&+ \sum_{l \in \mathbf{LAPs}} \mathrm{E}\left[|h_l|^2\right] \mathrm{E}\left[\left|\sum_{n=0}^{N_d-1} \Delta x_{n-l} \hat{x}_n^*\right|\right] + \sum_{n=0}^{N-1} \mathrm{E}\left[|n|^2\right]. \qquad (3.56)
\end{aligned}$$

Note that by assuming the OFDM signals at different sample period are identical, independently distributed (i.i.d.) such that $\mathrm{E}\left[x_k x_l *\right] = 0$, if $k \neq l$, it is straightforward to check that

- $\mathrm{E}\left[x_k \hat{x}_l *\right] = 0$,

- $\mathrm{E}\left[\Delta x_k \hat{x}_l^*\right] = 0$, when $k \neq l$.

Therefore, (3.56) results in

$$\begin{aligned}
\sigma_I^2 &= \mathrm{MSE} \cdot \left[1 + \sum_{n=0}^{N_d-1} \mathrm{E}\left[|x_{n-l}|^2\right] \mathrm{E}\left[|\hat{x}_n|^2\right]\right] \\
&\quad + \sum_{l \in \mathbf{LAPs}} \sigma_l^2 \cdot \mathrm{E}\left[|\Delta x_{n-l}|^2\right] \mathrm{E}\left[|\hat{x}_n|^2\right] + \sum_{n=0}^{N-1} \mathrm{E}\left[|n|^2\right] \\
&= \mathrm{MSE}(1 + N_d) + N_d r_{\Delta x, \Delta x} \sum_{l \in \mathbf{LAPs}} \sigma_l^2 + N\sigma_n^2 \\
&\approx \mathrm{MSE}\,(1 + N_d) + N_d r_{\Delta x, \Delta x} + N\sigma_n^2,
\end{aligned} \tag{3.57}$$

where we assume that these significant LAPs carry most of the channel energy such that $\sum_{l \in \mathbf{LAPs}} \sigma_l^2 \approx 1$, and MSE is defined as $\mathrm{MSE} = \sigma_{\mathbf{\Delta h}}^2 \cdot \mathcal{M}$, where $\mathcal{M}$ is the number of the significant LAPs. $r_{\Delta x, \Delta x}$ is defined as,

$$r_{\Delta x, \Delta x} = \mathrm{E}\left[|\Delta x_n|^2\right]. \tag{3.58}$$

The SINR on the FAP's correlation peak can be determined by

$$\mathrm{SINR} = \frac{\sigma_P^2}{\sigma_I^2}. \tag{3.59}$$

Note for practical communication systems where strong error correction coding is used at operating SNR, the SER is normally sufficiently low such that the probability that $\hat{x}_n = x_n$ is close to unity. With the perfect estimation of the OFDM signal, we have

$$r_{x_n, \hat{x}_n} \to 1, \tag{3.60}$$

$$r_{\Delta x, \Delta x} \to 0, \tag{3.61}$$

almost surely, as $P_e \to 0$.

Therefore, we have the following SINR,

$$\text{SINR} = \frac{(N_p + N_d)^2 \sigma_0^2}{\text{MSE}\,(1 + N_d) + N\sigma_n^2}. \tag{3.62}$$

It can be seen that the SINR is inversely proportional to the variance of the estimation error which shows that more accurate CIR estimation is required from the iterative estimator than the conventional LS estimator.

Recall the SINR of the traditional correlation detector for FAP in (3.7), the SINR gain of the proposed approach can be represented as

$$\begin{aligned}\frac{\text{SINR}_{\text{pro}}}{\text{SINR}_{\text{con}}} &= \left(\frac{N}{N_p}\right)^2 \frac{\sum\limits_{l=1}^{L-1} \sigma_l^2 + N_p\sigma_n^2}{\text{MSE}(1 + N_d) + N\sigma_n^2} \\ &= \left(\frac{N}{N_p}\right)^2 \frac{1 + N_p\sigma_n^2 / \sum_{l=1}^{L-1} \sigma_l^2}{\text{MSE}/\sum\limits_{l=1}^{L-1} \sigma_l^2 (1 + N_d) + N\sigma_n^2 / \sum\limits_{l=1}^{L-1} \sigma_l^2},\end{aligned} \tag{3.63}$$

where $\sigma_n^2 / \sum_{l=1}^{L-1} \sigma_l^2$ can be approximated to the inverse SNR and $\text{MSE}/\sum_{l=1}^{L-1} \sigma_l^2$ is defined as normalized MSE (NMSE). In operating SNR ranges, the NMSE can be assumed to be close to zero. Therefore, (3.63) can be further simplified by

$$\begin{aligned}\frac{\text{SINR}_{\text{pro}}}{\text{SINR}_{\text{con}}} &= \left(\frac{N}{N_p}\right)^2 \frac{1 + N_p/\text{SNR}}{N/\text{SNR}} \\ &= \frac{N}{N_p^2}\text{SNR} + \frac{N}{N_p}.\end{aligned} \tag{3.64}$$

Since the length of the *augmented preamble* N is much longer than that of the original preamble N_p, significant SINR gain can be achieved by the proposed algorithm which will certainly result in more accurate FAP detection. This conclusion will be further

verified through computer simulations in the next section.

3.6 Simulation Results and Discussions

3.6.1 Performance of the Proposed FAP Detection

Numerical simulations have been performed to quantify the performance of each block of the proposed system as well as the overall algorithm. The demonstration system considered is an OFDM system with subcarrier number 512 and CP ratio 1/16 and the preamble signal is an m-sequence with length 15. The modulation scheme chosen is QPSK.

We consider three 8-tap multipath channels with each path independently Rayleigh fading. The average power delay profiles are reported in Table 3.1. Channel I is the modified version of 3GPP LTE Extended Pedestrian A (EPA) channel model [88] where the strongest direct path is replaced by a significantly weaker path. The power of the FAP is set to around 20dB below the strongest LAP, which simulates the scenario with blocked direct signal path in dense multipath environments. Channel II is a variation of Channel I with a stronger FAP. Channel III has a very short delay spread which is close to AWGN case. All the results are obtained over 10000 independent channel realizations.

It should be mentioned that the scenarios simulated in this section are just several specific examples since our purpose is to verify the performance of the proposed algorithm in dense multipath environments and the LAP selection criterion in (3.38) is used and the threshold factor η is set to -8dB in all cases. Note that the performance of the derived optimal LAP selection threshold will be presented in the next subsection.

Table 3.1: Average power delay profiles of multipath channels used in the simulations

	Channel I	Channel II	Channel III
Normalized Path Delay	Average Power(dB)		
0	-21.4	-12.8	-21.4
1	-1.7	-1.9	-0.032
2	-5.1	-5.3	$-\infty$
3	-20.5	-20.7	$-\infty$
7	-24.1	-24.3	$-\infty$

3.6.1.1 Performance of the Iterative Estimator for Joint Channel and Data Estimation

To evaluate the performance of the iterative estimator proposed in Section 3.4.1, the MSE of channel estimation is simulated under Channel II and plotted in Fig. 3.4. The "0 iteration" curve is obtained by the conventional LS estimator and the lower bound is achieved when the transmitted OFDM signal is perfectly regenerated and subsequently used for channel estimation. It can be observed that the accuracy of CIR estimation improves with an increase in iteration number. It is also shown that only one iteration is needed to achieve the lower bound at the SNR level of 20dB. However, more iterations are required for better performance at middle SNR ranges. This is because at the middle SNR, the accuracy of channel estimation is more sensitive to the SER improvement during the iteration process. However, the cases are different for low or high SNR ranges. At extremely low SNR, the SER of iterative estimator is very high such that the *augmented preamble* may consist of large portion of decision errors. Therefore, limited performance improvement can be achieved over the previous iteration when this unreliable preamble is used. On the contrary, the SER of data detection from the 0 iteration is already sufficiently low at high SNR and therefore only one iteration can reach the lower bound. The performance characteristics of the

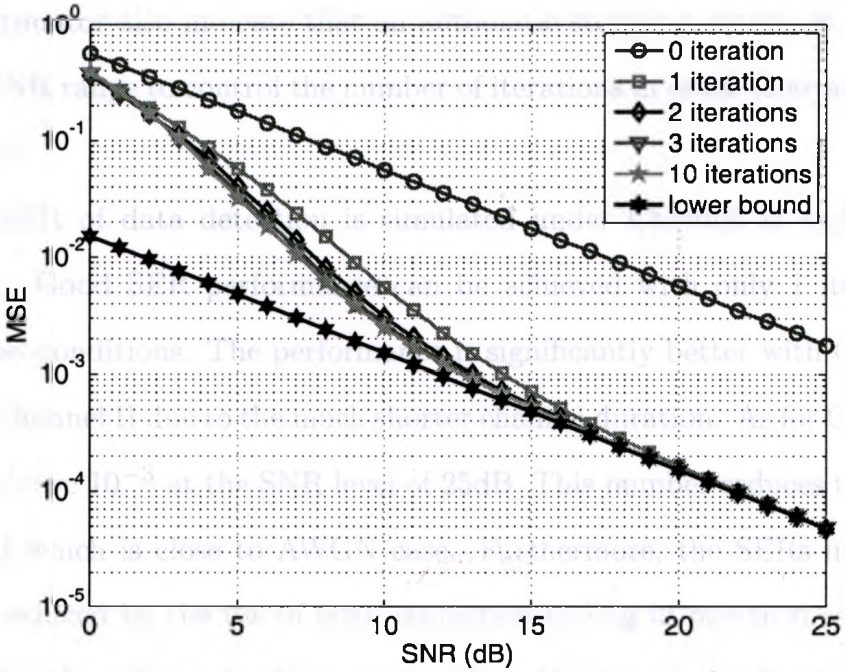

Figure 3.4: Mean square error of the iterative estimator for the OFDM system with 4-QAM modulation.

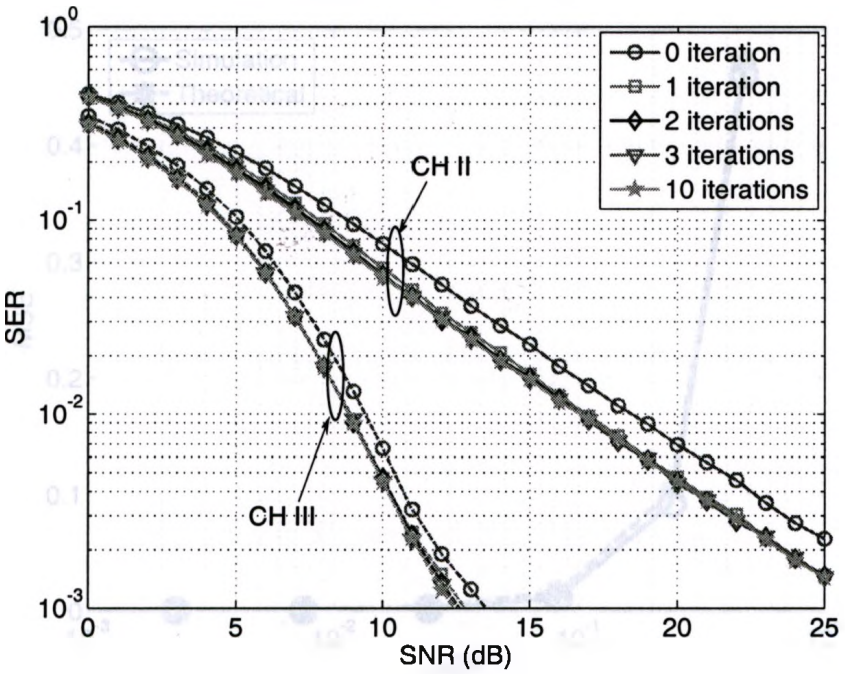

Figure 3.5: Symbol error rate of the iterative estimator for the OFDM system with 4-QAM modulation.

iterative estimator also indicate that an automatic stopping criteria is needed at the moderate SNR range to control the number of iterations in order to avoid unnecessary computation.

The SER of data detection is simulated under Channel II and Channel III in Fig. 3.5. Good SER performance can be achieved with only 1 iteration under both channel conditions. The performance is significantly better with Channel III as compared Channel II due to the much shorter channel duration. As for Channel II, the SER can achieve 10^{-3} at the SNR level of 25dB. This number reduces to 12dB under Channel III which is close to AWGN case. Furthermore, the SERs in Fig. 3.5 can be further reduced by the use of error correction coding in practical communication systems. Therefore, it can be demonstrated that the iterative estimator is capable of providing accurate LAPs and data estimation under various channel conditions.

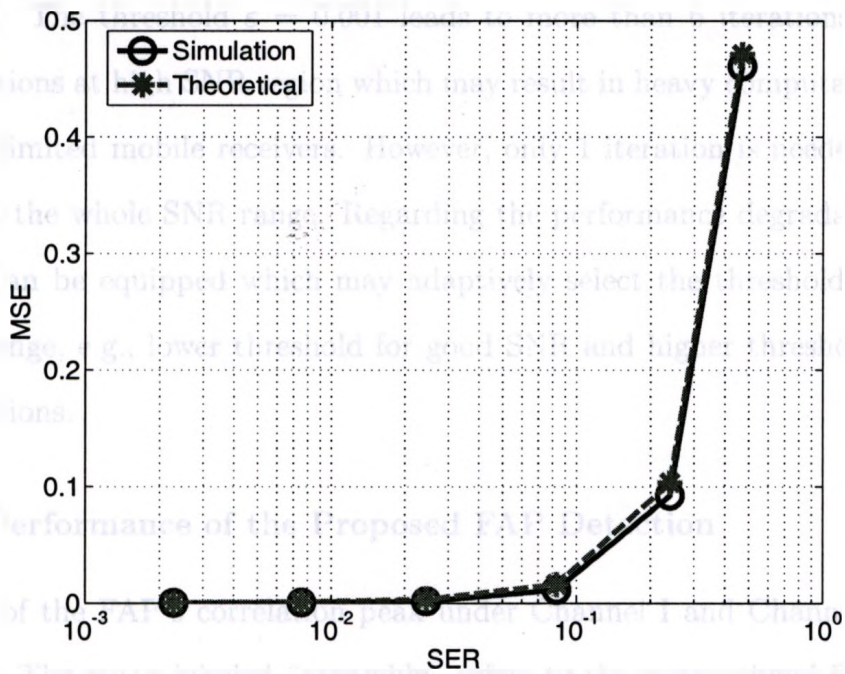

Figure 3.6: Comparison between theoretical values and simulations on MSE versus SER.

To verify the theoretical MSE derived in Section 3.4.2, we replace P_e in (3.34)

with the SER values from 0 iteration under Channel II (the red solid curve in Fig. 3.5), and the corresponding theoretical MSE of 1 iteration is obtained. It is compared with the simulated MSE in Fig. 3.6. The observation implies that the theoretical results match the simulation results well, which also demonstrates the convergence of the iterative estimator with respect to SER.

3.6.1.2 Impact of the Automatic Stopping Criterion

The impact of different threshold ε in (3.36) is evaluated in terms of estimation accuracy and the corresponding required average iterations. The MSE performance degradation of different thresholds as compared with the fixed 10 iterations is shown in Fig. 3.7. It can be found that the lower threshold we set, the better MSE we can achieve. Consequently, the lower threshold also requires more computations as shown in Fig. 3.8. The threshold $\varepsilon = 0.001$ leads to more than 6 iterations at low SNR and 2 iterations at high SNR region which may result in heavy computational burden to battery-limited mobile receivers. However, only 1 iteration is needed for $\varepsilon = 0.1$ throughout the whole SNR range. Regarding the performance degradation, an SNR estimator can be equipped which may adaptively select the threshold according to the SNR range, e.g., lower threshold for good SNR and higher threshold for middle SNR conditions.

3.6.1.3 Performance of the Proposed FAP Detection

The SINR of the FAP's correlation peak under Channel I and Channel II is shown in Fig. 3.9. The curve labeled "preamble" refers to the conventional FAP detection scheme based on preamble correlation. Fig. 3.9 shows due to the weak FAP's power, the SINR is extremely low under both channels with the traditional method. It is

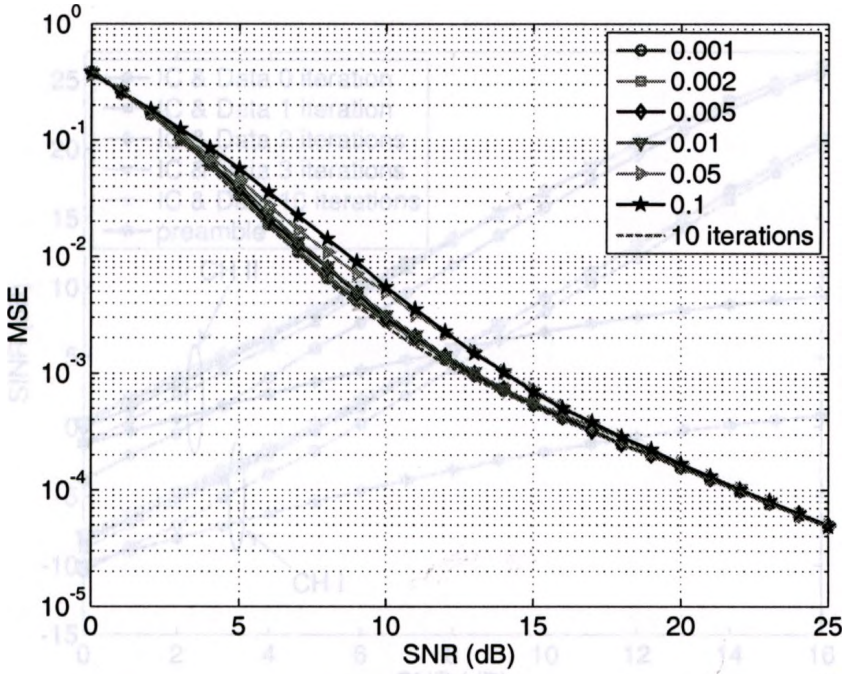

Figure 3.7: Mean square error of the iterative estimator with different stopping criterion threshold.

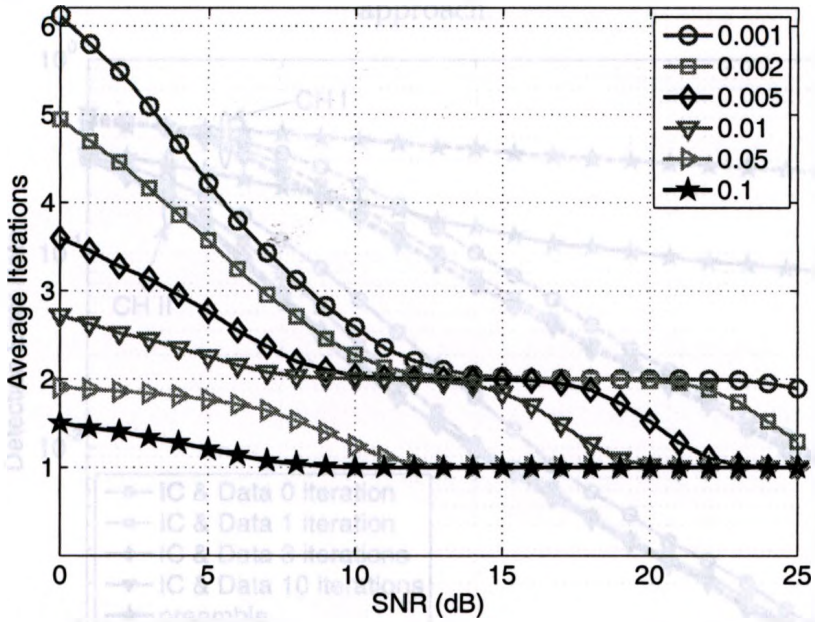

Figure 3.8: The average iterations with different stopping criterion threshold.

obvious that the SINR level provided by this method cannot achieve acceptable accuracy of FAP detection. However, as analyzed in Section IV, the SINR significantly

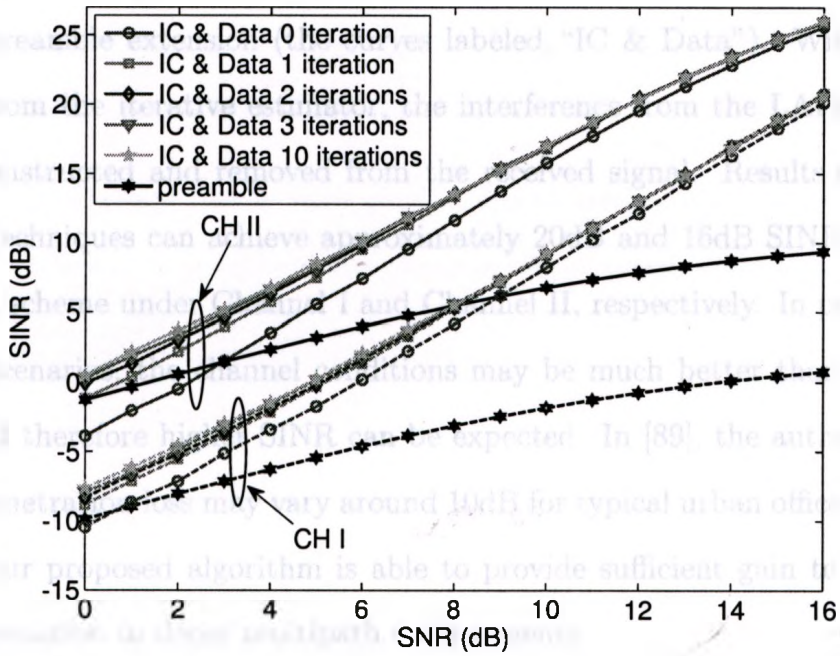

Figure 3.9: SINR of FAP's correlation peak with and without the proposed approach.

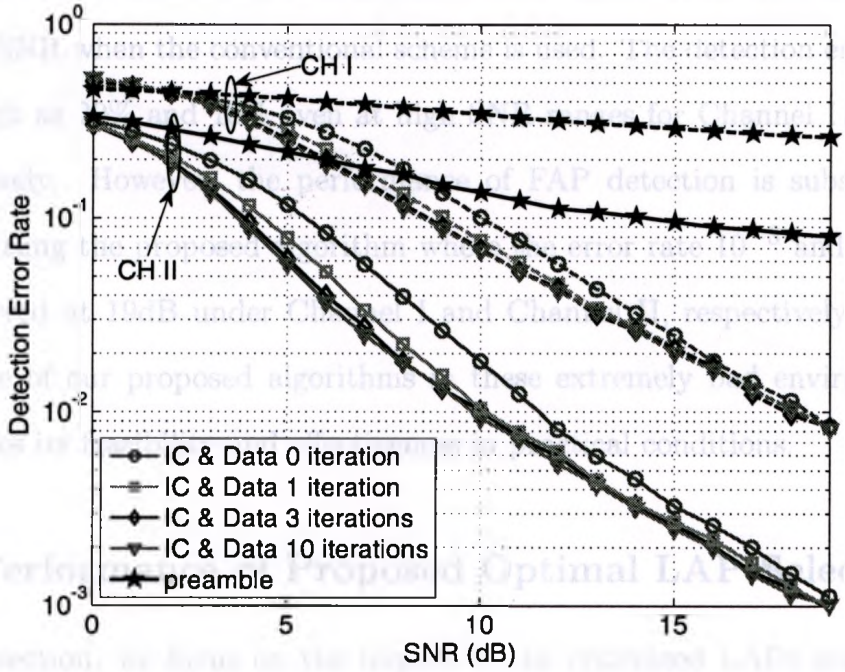

Figure 3.10: FAP detection error rate with and without the proposed approach.

improves with the proposed the proposed algorithm based on interference cancellation and preamble extension (the curves labeled "IC & Data"). With as few as 1 iteration from the iterative estimator, the interference from the LAPs can be accurately reconstructed and removed from the received signal. Results show that our proposed techniques can achieve approximately 20dB and 16dB SINR gain over the traditional scheme under Channel I and Channel II, respectively. In practical indoor or urban scenarios, the channel conditions may be much better than these specific models and therefore higher SINR can be expected. In [89], the author pointed out that the penetration loss may vary around 10dB for typical urban office buildings and therefore our proposed algorithm is able to provide sufficient gain to overcome the severe attenuation in dense multipath environments.

The FAP detection error rate is simulated under Channel I and Channel II in Fig. 3.10. It can be found that the detection error rate reduces very slowly with an increase in SNR when the conventional scheme is used. The detection error probability is as high as 20% and 10% even at high SNR ranges for Channel I and Channel II, respectively. However, the performance of FAP detection is substantially enhanced by using the proposed algorithm where the error rate 10^{-3} and 10^{-2} can be easily achieved at 19dB under Channel I and Channel II, respectively. Again, the performance of our proposed algorithms in these extremely bad environments also demonstrates its feasibility and effectiveness in practical conditions.

3.6.2 Performance of Proposed Optimal LAP Selection

In this subsection, we focus on the impact of the optimized LAPs selection under a more severe multipath channel with an average power delay profile reported in Table 3.2. The channel represents a typical dense multipath scenario with a very

weak FAP where the LAPs dominate the total channel energy and it is assumed to be quasi-stationary during the transmission of one preamble and one OFDM symbol. The results are obtained over 10000 channel realizations.

Table 3.2: Average power delay profile of the multipath channel used in the simulations

Relative Delay	0	15	18	21	29
Average Power (dB)	-21.37	-8.33	-1.58	-9.32	-17.85

3.6.2.1 Demonstration of the Optimal Threshold γ_{opt}

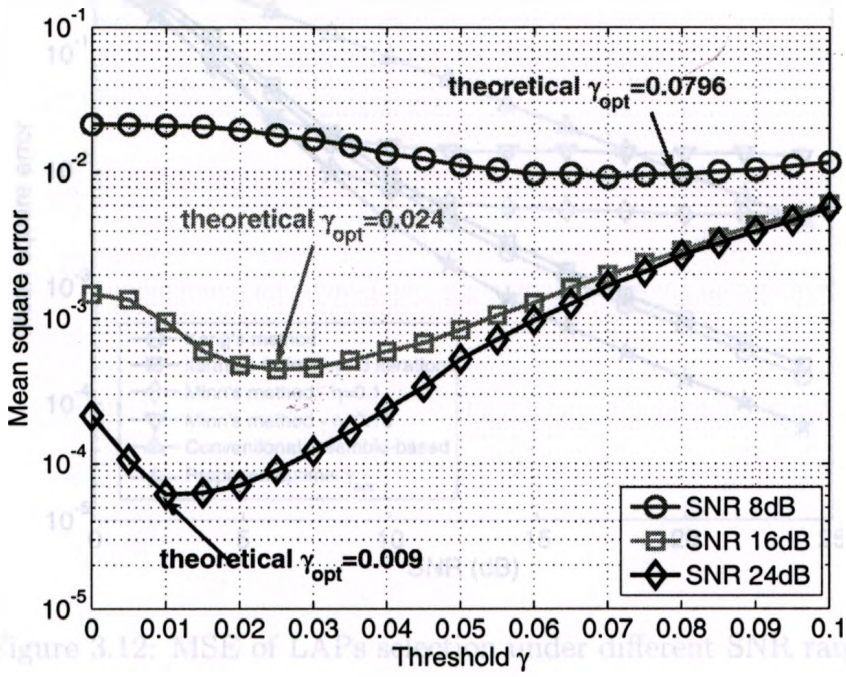

Figure 3.11: MSE of LAPs selection with different threshold values.

We first demonstrate the optimal threshold γ_{opt} derived in (3.45) by simulating the LAPs selection using different values of γ over a wide range of SNR values. The MSE here is defined as MSE $= \sum_{l=1}^{L-1} |\tilde{h}_l - h_l|^2$. It is observed in Fig. 3.11 that the derived optimal thresholds (indicated by text arrows) are in close agreement with the

simulation results (points with minimum MSE) under different SNRs. Furthermore, the ratio of the minimum MSE value with the optimal threshold to the MSE without the LAPs selection process ($\gamma = 0$ case) becomes smaller with a decrease in SNR. This is because at low SNR, the estimation error from the iterative estimator (Section 3.4.1) is sufficiently large and comparable to those true LAPs. In other words, the noise-only taps are more likely to be determined as significant LAPs.

3.6.2.2 MSE Performance Comparison of Different Schemes

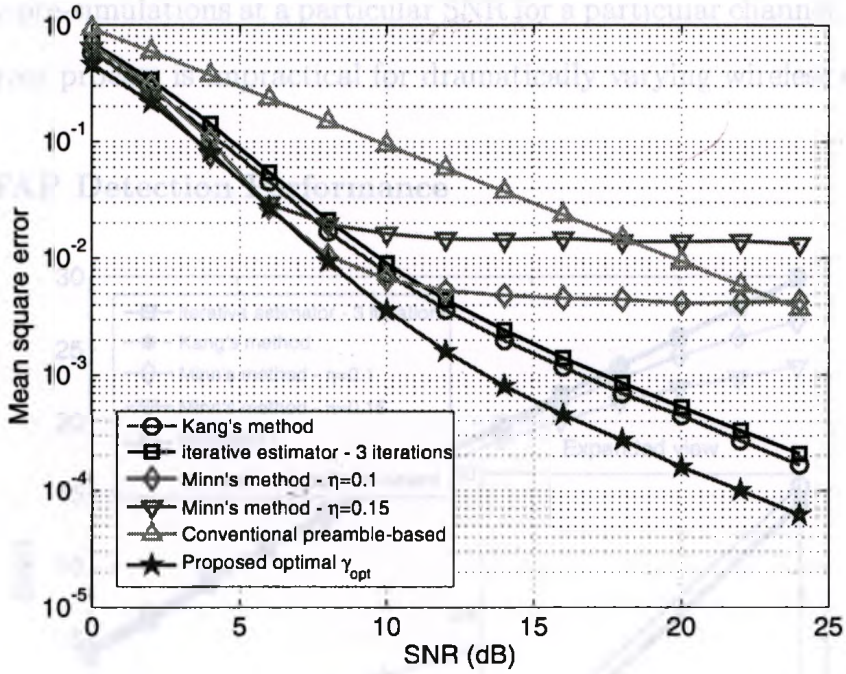

Figure 3.12: MSE of LAPs selection under different SNR ranges.

The MSE of LAPs selection is evaluated with different schemes including the LS estimator in (3.9), the proposed iterative estimator without threshold, Minn's scheme [86], Kang's scheme [87], and the proposed optimal threshold. It can be observed in Fig. 3.12 that the proposed optimal threshold always gives the best performance under different SNR ranges since it successfully selects the dominant LAPs and suppresses

those noise-only taps. Kang's scheme only provides slight improvement over the iterative estimator without LAPs selection. The proposed optimal LAPs selection can achieve approximately 4 – 5dB gain over both Kang's scheme and the iterative estimator. Furthermore, it can be found that the error floors occur for Minn's method with different threshold factors. This is because the actual criteria utilized in [86] is $\eta|\hat{h}_{max}|$, where η is the threshold factor and $|\hat{h}_{max}|$ is the largest estimated channel tap gain. Since $|\hat{h}_{max}|$ is itself a random variable, a fixed η cannot be optimal for various SNRs. It is worth mentioning that [86] pointed out that the optimal η can be achieved by pre-simulations at a particular SNR for a particular channel. However, the trial and error process is impractical for dramatically varying wireless environments.

3.6.2.3 FAP Detection Performance

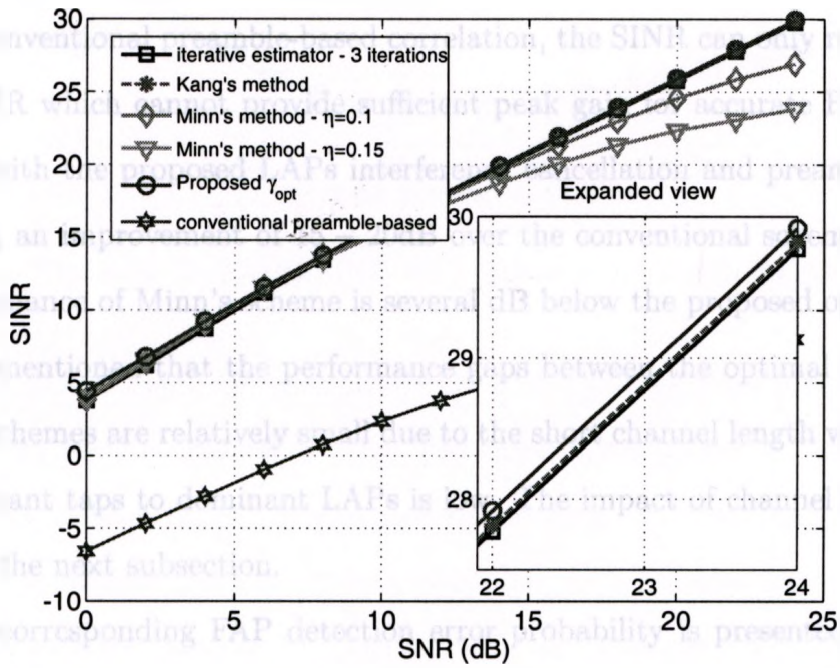

Figure 3.13: FAP's SINR under different SNR ranges.

The SINR on FAP's correlation sample is evaluated in Fig. 3.13. It is found that

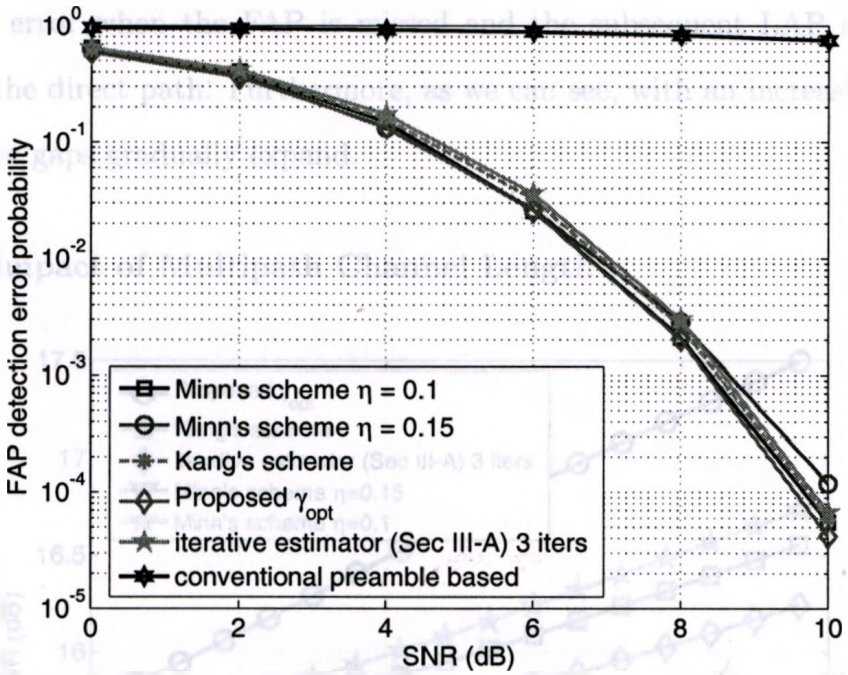

Figure 3.14: FAP's detection error probability under different SNR ranges.

with the conventional preamble-based correlation, the SINR can only reach 8dB even at high SNR which cannot provide sufficient peak gain for accurate FAP detection. However, with the proposed LAPs interference cancellation and preamble extension techniques, an improvement of 15 – 20dB over the conventional scheme is observed. The performance of Minn's scheme is several dB below the proposed optimal one. It should be mentioned that the performance gaps between the optimal threshold and the other schemes are relatively small due to the short channel length where the ratio of insignificant taps to dominant LAPs is low. The impact of channel length will be studied in the next subsection.

The corresponding FAP detection error probability is presented in Fig. 3.14. It indicates that an approximate 50% performance gain over other schemes can be obtained at 10dB when the optimal threshold is adopted. Although at this SNR the performance difference is not significantly large, it could cause large location

estimation error when the FAP is missed and the subsequent LAP is erroneously judged as the direct path. Furthermore, as we can see, with an increase in SNR, the performance gaps gradually expand.

3.6.2.4 Impact of Multipath Channel Length

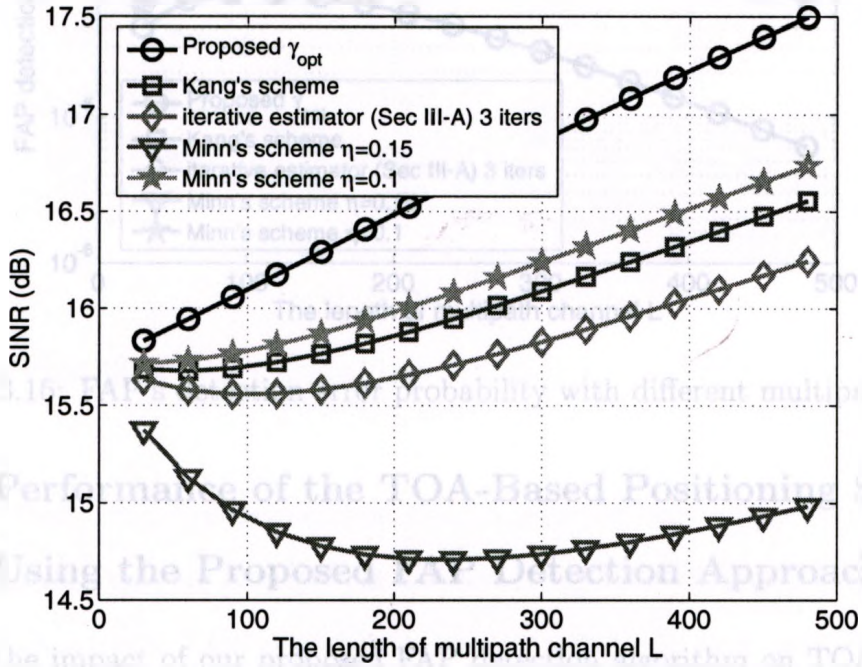

Figure 3.15: FAP's SINR with different multipath length.

Fig. 3.15 and Fig. 3.16 demonstrate the SINR and the error probability of FAP detection with various channel lengths. The same power profile in Table 3.2 is used; however, the channel length is increased by padding zeros between two dominant paths and the relative position of each dominant path remains unchanged. Distinguished performance gain can be observed with the proposed FAP detection scheme over others for both SINR and detection error probability.

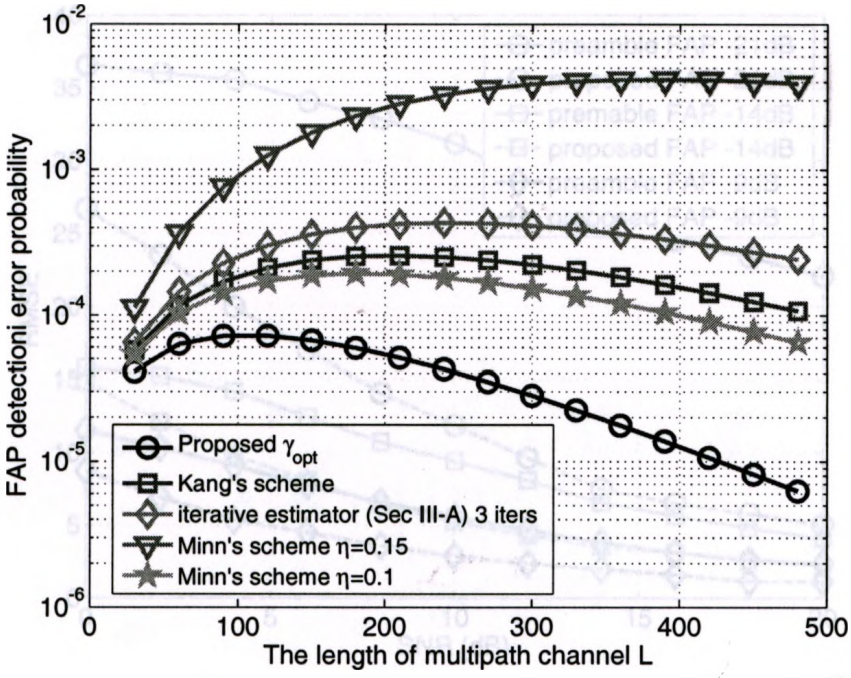

Figure 3.16: FAP's detection error probability with different multipath length.

3.6.3 Performance of the TOA-Based Positioning System Using the Proposed FAP Detection Approach

To study the impact of our proposed FAP detection algorithm on TOA positioning system, a more realistic signal propagation scenario is considered in this subsection where the length of multipath channel is set to 60 with 4 LAPs randomly placed in the tap range [20, 59]. Different FAP's average power is considered in this simulation. The average power of LAPs is also randomly chosen and the sum is normalized to $1-\sigma_0^2$. The length of preamble signal is correspondingly increased to 63 samples. We evaluate the root mean square error (RMSE) of the normalized arrival time of FAP under wide range of SNR. It can be observed in Fig. 3.17 that the proposed FAP detection algorithm can achieve significant gain over the conventional preamble-based detection with different FAP's power. At high SNR range, very accurate arrival time estimates (less than 1 tap) can be achieved with the proposed FAP detection algo-

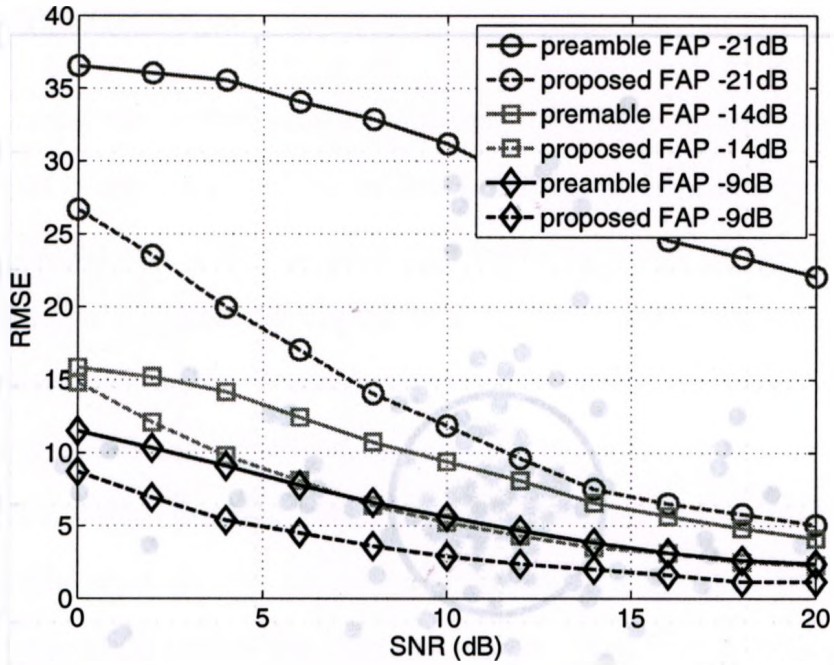

Figure 3.17: RMSE of FAP's arrival time estimation with and without the proposed FAP detection approach.

rithm. Furthermore, as expected, the RMSE gaps between the proposed algorithm and the conventional one reduce with an increase in FAP's power.

Numerical results for positioning system using our proposed algorithms are shown in Fig. 3.18. Four synchronized TXs with known locations are used in our system. The coordinates of the four TXs are $(0,0),(0,500),(500,0)$ and $(500,500)$ respectively and the RX location is chosen randomly inside the square formed by these TXs. Each circle or star represents one round of location process (Stars are the results with the proposed algorithms). The propagation model used in Fig. 3.18 is considered here. The time resolution ΔT is assumed to be 5ns such that the maximum channel delay spread is around 300ns [89]. The FAP's power is -21dB and SNR 15dB. The accuracy of the positioning process is evaluated by the distance between the estimation and the true location of the RX (origin of the coordinates). The simulation results show that with LAPs interference cancellation and the utilization

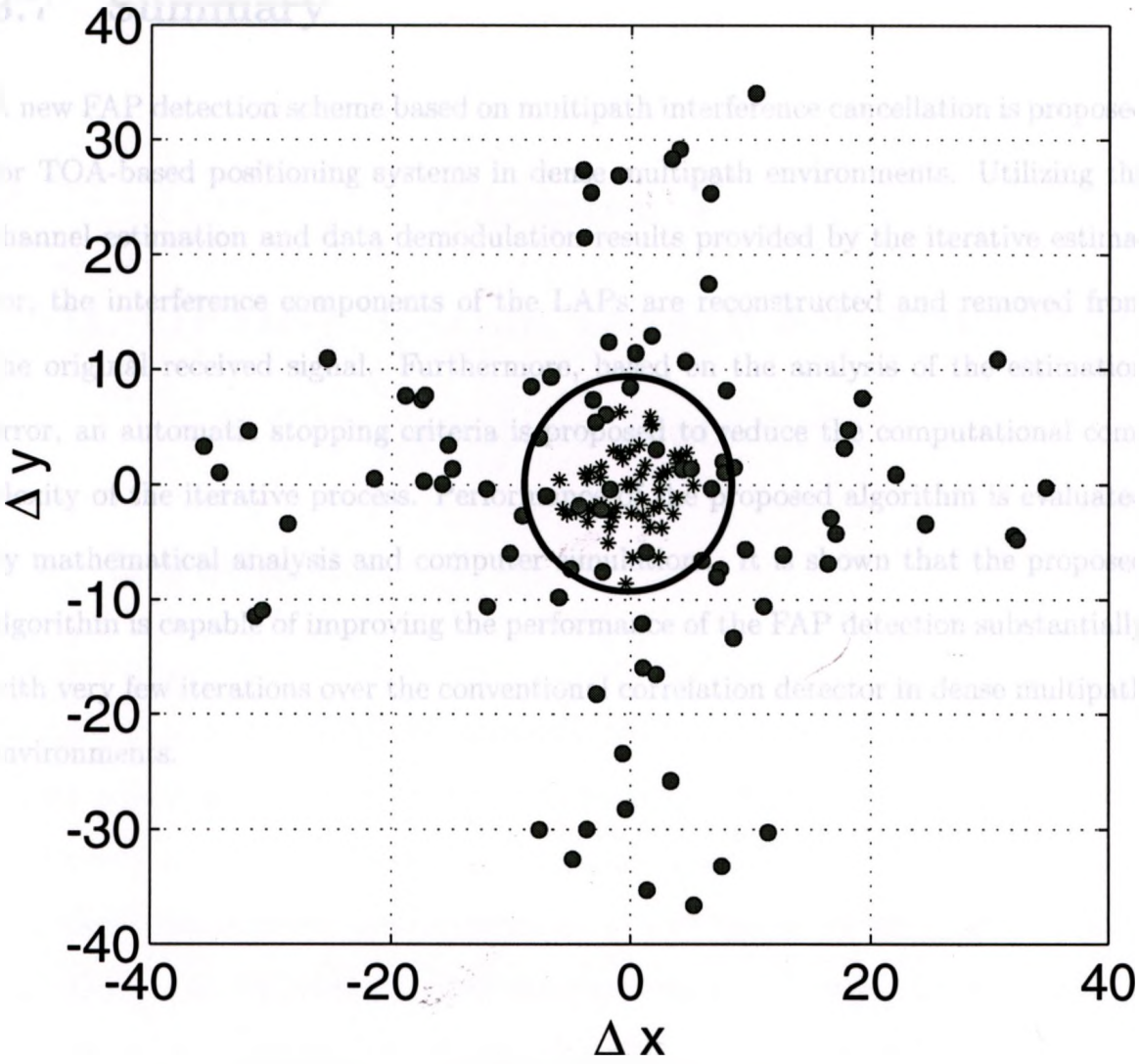

Figure 3.18: Numerical results for the proposed positioning system with and without the proposed FAP detection approach.

of *augmented preamble*, the accuracy of the positioning system using the proposed algorithms is within several meters while for conventional preamble-based location estimation this value is as large as thirty meters.

3.7 Summary

A new FAP detection scheme based on multipath interference cancellation is proposed for TOA-based positioning systems in dense multipath environments. Utilizing the channel estimation and data demodulation results provided by the iterative estimator, the interference components of the LAPs are reconstructed and removed from the original received signal. Furthermore, based on the analysis of the estimation error, an automatic stopping criteria is proposed to reduce the computational complexity of the iterative process. Performance of the proposed algorithm is evaluated by mathematical analysis and computer simulations. It is shown that the proposed algorithm is capable of improving the performance of the FAP detection substantially with very few iterations over the conventional correlation detector in dense multipath environments.

Chapter 4

ML-OFDM System Design for Multicell Cooperative Networks

4.1 Introduction

The performance of conventional cellular networks characterized by SCP can be substantially improved by multicell cooperation technique which enables joint signal processing among several interfering BSs to fulfill the demands of broadband mobile multimedia applications. However, as mentioned earlier in Section 2.3.2, technical challenges arise in practical implementation of multicell cooperation including *backhaul issues*, *network latency* and *BS synchronization*. Therefore, the motivation of this chapter is to address the aforementioned challenges with the proposed *Multi-Layered OFDM* (ML-OFDM) system. As OFDM is envisioned as a key technology for broadband wireless communications and most of the broadband systems (DVB-T, DVB-H, WiMAX and LTE) are already OFDM-based, we propose a ML-OFDM system which provides a robust, efficient and flexible platform specially tailored for the newly conceptual multicell cooperation enabled cellular networks.

The proposed ML-OFDM is illustrated in Fig. 4.1. The *Base Layer* (BL) provides conventional OFDMA-based two-way *unicast* services ("private" information)

for cellular users and the *Enhanced Layers* (ELs) offer several other important functionalities for the cellular network. First, the *broadcast* services ("common" information) [90, 91, 92, 93] including location information of mobile users, ***emergency alerting signal*** or public messages can be delivered by utilizing one EL link to the silent mobile receivers over the entire cell for the design of potential location-assisted applications. The "common" and "private" information is overlaid across both the entire frequency and time domains, and therefore, the tedious procedure to establish sperate infrastructures or design orthogonal multiplexing could be avoided, which significantly reduces the implementation cost and radio resource overhead. Secondly, alternative parallel EL can provide a dedicated over-the-air link among different BSs of exchanging the available information, e.g., CSI pertaining to all relevant direct and interfering links, data symbols sent to the target MS, and transmission parameters including power level, beamforming coefficients, time slot, subcarrier usage etc. These information can be sent concurrently with data-carrying OFDM signal (BL signal) for dynamic BS coordination. Such coordination protocol can be realized by solely exploiting the proposed EL link or using this link to enhance the pre-existing finite capacity backhaul network when a high-bandwidth link is required for information sharing. In addition, the timing synchronization between cooperative BSs can also be easily achieved through additional parallel EL link in PHY layer, eliminating the involvement of MAC layer scheduling, which reduces the potential network latency. Compared with the traditional control channels, which occupy additional spectrum resources for the aforementioned purposes, multiple functionalities are simultaneously supported by the proposed ELs using both the same spectrum band and the timing slot as those of the OFDM data-carrying signal.

The rest of the chapter is structured as follows. The principle and architecture of the proposed ML-OFDM system are presented in Sections 4.2 and Section 4.3. Based

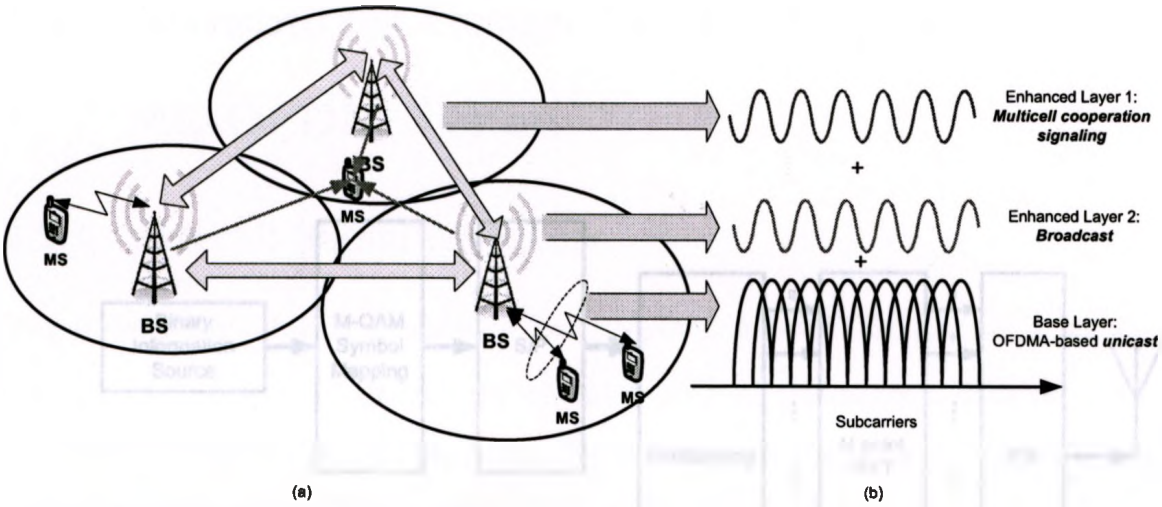

Figure 4.1: Snapshot of a cellular network with *multicell cooperation* using the proposed ML-OFDM. (a) Snapshot of the cellular network (b) The signal frame of the proposed ML-OFDM

on our interference analysis for the proposed ML-OFDM, an efficient EL induced interference cancellation algorithm is proposed. In Section 4.4, we analyze the system performance including the error probability of the proposed EL links and the impact of EL link on the capacity of the BL. Based on these analysis, a power distribution scheme is proposed which optimizes the system performance with a few practical constraints in Section 4.5. Simulation results are provided and discussed to access and validate the performance and feasibility of the proposed system in Section 4.6. The chapter is finally summarized in Section 4.7.

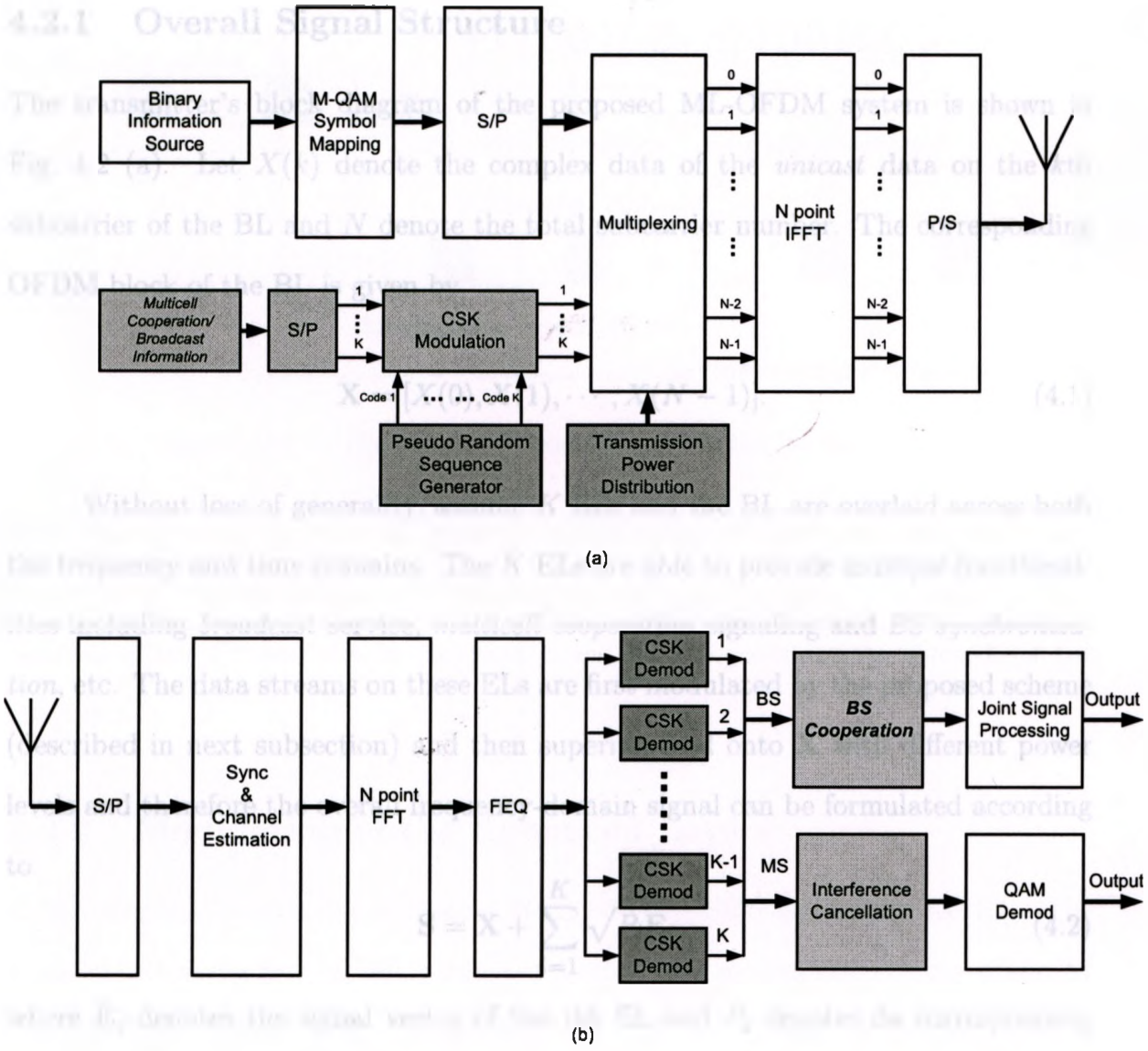

Figure 4.2: Block diagram of the proposed multi-layered OFDM system: (a) Transmitter (b) Receiver.

4.2 Transmitter Design for the Proposed ML-OFDM System

4.2.1 Overall Signal Structure

The transmitter's block diagram of the proposed ML-OFDM system is shown in Fig. 4.2 (a). Let $X(k)$ denote the complex data of the *unicast* data on the kth subcarrier of the BL and N denote the total subcarrier number. The corresponding OFDM block of the BL is given by

$$\mathbf{X} = [X(0), X(1), \cdots, X(N-1)]. \tag{4.1}$$

Without loss of generality, assume K ELs and the BL are overlaid across both the frequency and time domains. The K ELs are able to provide multiple functionalities including *broadcast* service, *multicell cooperation* signaling and *BS synchronization*, etc. The data streams on these ELs are first modulated by the proposed scheme (described in next subsection) and then superimposed onto $\mathbf{X}$ with different power levels and therefore the overall frequency-domain signal can be formulated according to

$$\mathbf{S} = \mathbf{X} + \sum_{i=1}^{K} \sqrt{P_i}\mathbf{E}_i, \tag{4.2}$$

where $\mathbf{E}_i$ denotes the signal vector of the ith EL and P_i denotes its corresponding transmission power. Therefore, each time-domain data block is then generated by N point IDFT,

$$s(n) = \frac{1}{\sqrt{N}} \sum_{k=0}^{N-1} S(k) e^{j\frac{2\pi kn}{N}}, \; n = 0, 1, 2, \cdots, N-1. \tag{4.3}$$

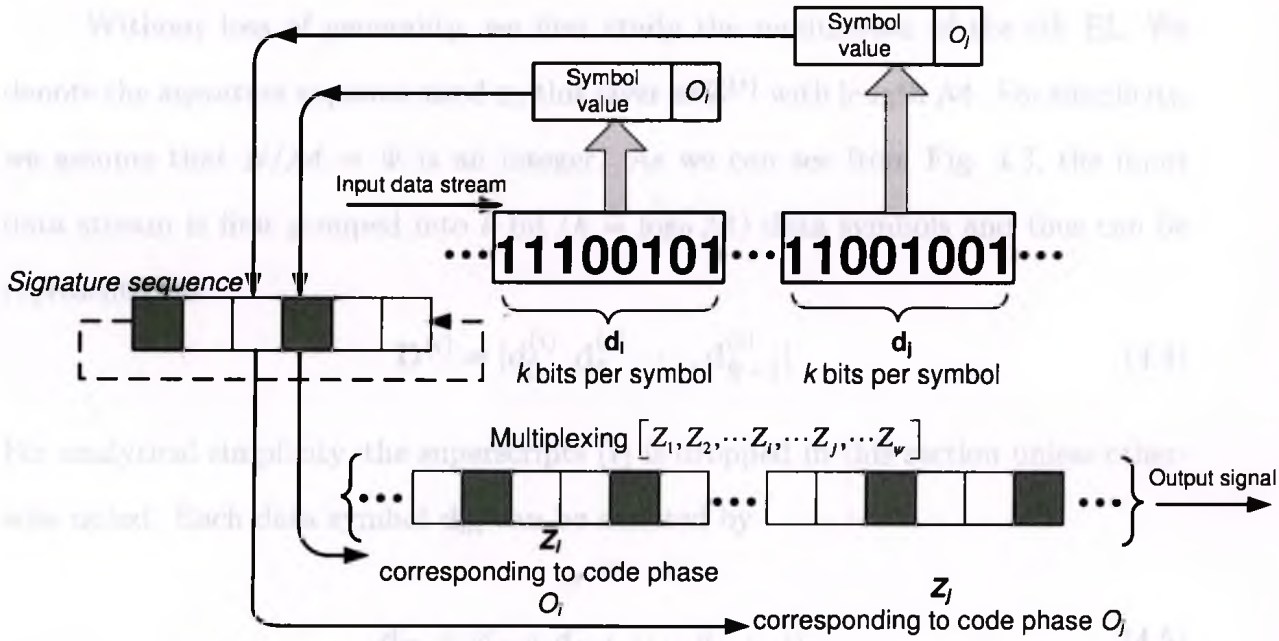

Figure 4.3: Illustration of the proposed modulation scheme for the Enhanced Layers.

Note that by assuming that the CP in our system is longer than the maximum channel delay spread, the transmitted symbols are free of ISI and therefore, the insertion and removal of the CP will not be included in the following discussions throughout the chapter.

4.2.2 Modulation of the Enhanced Layers

In the proposed system, we propose a Modified Code Shift Keying for the ELs. The Code Shift Keying [94, 95, 96] is adopted as the basic modulation scheme where $\mathcal{M}$ different cyclic phase shifts of a *signature sequence* is employed as $\mathcal{M}$-ary signaling to transmit data sequences. As the desired *multicell cooperation signaling* and the *broadcast services* should be very robust in handling strong interference and providing reliable information transmission, Code Shift Keying can offer very high noise and interference immunity such that low rate but error-free data transmission can be achieved.

Without loss of generality, we first study the modulation of the ith EL. We denote the *signature sequence* used on this layer as $\mathbf{Z}^{(i)}$ with length $\mathcal{M}$. For simplicity, we assume that $N/\mathcal{M} = \Psi$ is an integer. As we can see from Fig. 4.3, the input data stream is first grouped into k-bit ($k = \log_2 \mathcal{M}$) data symbols and thus can be represented as

$$\mathbf{D}^{(i)} = [\mathbf{d}_0^{(i)}, \mathbf{d}_1^{(i)}, \cdots, \mathbf{d}_{\Psi-1}^{(i)}]. \tag{4.4}$$

For analytical simplicity, the superscripts (i) is dropped in this section unless otherwise noted. Each data symbol $\mathbf{d}_m$ can be denoted by

$$\mathbf{d}_m = [d_{m,0}, d_{m,1}, \cdots, d_{m,k-1}]. \tag{4.5}$$

According to the symbol value of $\mathbf{d}_m$, the *signature sequence* $\mathbf{Z}$ is cyclicly shifted by a unique phase O_m determined by the symbol value and denoted by $\mathbf{Z}_{O_m}$. Note in our case, the phase O_m takes value of $\{0, 1, \cdots, \mathcal{M}-1\}$. The system parameters of the modulation scheme is shown in Table. 4.1.

Table 4.1: System parameters of the proposed modulation scheme

Sequence Length	Bit Number of Each Data Symbol	Sequence Number of Each OFDM Block	Total Bit Number
$\mathcal{M}$	$k = \log_2 \mathcal{M}$	$\Psi = N/\mathcal{M}$	$\Psi \cdot k$

After code phase shift operation of each data symbol, the output signal on the ith EL can be represented by

$$\mathbf{E}_i = \left[\mathbf{Z}_{O_0}^{(i)}, \mathbf{Z}_{O_1}^{(i)}, \cdots, \mathbf{Z}_{O_{\Psi-1}}^{(i)}\right]. \tag{4.6}$$

The same modulation steps can be applied for the jth EL except that the

signature sequence $\mathbf{Z}^{(i)}$ is now replaced by $\mathbf{Z}^{(j)}$.

We now consider the design of the *signature sequences*. Denote the set of *signature sequences* used by the K ELs by,

$$\mathcal{Z} = \left\{\mathbf{Z}^{(0)}, \mathbf{Z}^{(1)}, \mathbf{Z}^{(2)}, \ldots, \mathbf{Z}^{(K-1)}\right\}. \tag{4.7}$$

The ideal design of the *signature sequences* should meet the following criteria,

$$\sum_{k=0}^{\mathcal{M}-1} Z_{O_m}^{(i)} \cdot Z_{O_n}^{(j)*} = \begin{cases} \mathcal{M}, \text{ if } i = j \bigcap O_m = O_n \\ 0, \text{ if } i \neq j \bigcup O_m \neq O_n \end{cases} \tag{4.8}$$

(4.8) indicates that ideally the *signature sequence* should be orthogonal to its cyclically shifted versions and other sequences regardless of any shift in the set such that the mutual interference between different ELs will be completely eliminated. However, the sequences with the perfect correlation properties do not exist in mathematics. Recently, *Zadoff-Chu* sequence has received considerable attention due to its excellent correlation properties and therefore is adopted by 3GPP LTE air interface as Primary Synchronization Signal (PSS) and Random Access Preamble (PRACH). One important property of *Zadoff-Chu* sequence is that it has perfect cyclic auto-correlation and small cyclic cross-correlation values. Therefore, it is preferred for Code Shift Keying modulation and used as the *signature sequence* in our proposed system.

For clarity of exposition, an example is given where $N = 1024$ and $\mathcal{M} = 64$, then it is possible transmit 6 bits for each sequence and a maximum number of $6 \times 16 = 96$ bits can be transmitted for one EL within one OFDM data block. In the case of 3GPP-LTE Evolved Universal Terrestrial Radio Access (EUTRA) air interface where the symbol duration is $66.7\mu s$, data rate for this EL in the proposed system can be as high as $R_b = 96\text{bits}/66.7\mu s \approx 1.4\text{Mbps}$. The rate is sufficiently high for *broadcast*

services, i.e., video conferencing quality stream (128 – 384kbps) and VCD quality stream (1.15Mbps max), as well as THE *multicell cooperation signaling* between the cooperative base stations.

4.2.3 Flexibility of the Proposed Modulation

The proposed modulation scheme is capable of improving the system flexibility. The total transmitted number of bits is not necessarily fixed to $\Psi \cdot k$ which is shown in Table. 4.1. For instance, when a low-rate data stream such as location information is broadcasted using the proposed EL link, the data symbols can be repeated several times in the data block, e.g., (4.4) can be reformulated as

$$\mathbf{D}^{(i)} = [\underbrace{\mathbf{d}_0^{(i)}, \cdots, \mathbf{d}_0^{(i)}}_{\mathcal{R}}, \cdots, \cdots, \underbrace{\mathbf{d}_{\Psi/\mathcal{R}-1}^{(i)}, \cdots, \mathbf{d}_{\Psi/\mathcal{R}-1}^{(i)}}_{\mathcal{R}}]. \tag{4.9}$$

The benefit of this strategy is that in the receiver side, the averaging can be performed to reduce the associated interference and noise and therefore improve the robustness of the EL link. Furthermore, to achieve the same performance, lots of power budget can be saved at the transmitter side. The same mechanism can also be applied to the *muticell cooperation signaling*, when different quantization techniques are used to reduce the overhead of the shared CSI/user data information [97, 98]. Consequently, our proposed modulation scheme can adapt to future cellular networks in most flexible, efficient and reliable manners.

4.3 Receiver Design for the Proposed System

In order to implement the proposed ML-OFDM system, some modifications are necessary to traditional OFDM receiver. As the overlay ELs' signals appear to be large

interference to the BL's signal, to guarantee the service quality of the *unicast* service on the BL, the first step is to demodulate the data on the ELs. The receiver is then capable of removing the interference induced by the previous demodulated ELs by using the estimated channel and the regenerated signals on the ELs and thus minimizing the impact on the demodulation of the BL.

4.3.1 Data Detection on the Enhanced Layers

Consider a block fading multipath channel $\mathbf{h} = [h_0, h_1, h_2, \cdots, h_{L-1}]$ and its frequency response can be denoted by $\mathbf{H}$ whose element is given by,

$$H(k) = \sum_{l=0}^{L-1} h_l e^{\frac{j2\pi lk}{N}}, \; k = 0, 1, \cdots, N-1. \tag{4.10}$$

We assume that the channel impulse response h_l, $0 \leq l \leq L-1$ are independent complex Gaussian-distributed random variables with zero mean and a variance of σ_l^2, and therefore the kth subcarrier channel frequency response $H(k)$ is also a complex Gaussian random variable with zero mean and variance of $\sigma_H^2 = \sum_{l=0}^{L-1} \sigma_l^2$. Then the received signal in frequency domain after passing through the multipath channel can be represented as

$$Y(k) = X(k)H(k) + \sum_{i=1}^{K} \sqrt{P_i} E_i(k) H(k) + W(k), \; k = 0, 1, \cdots, N-1, \tag{4.11}$$

where $W(k)$ denotes the kth subcarrier AWGN sample with zero mean and variance σ_n^2. For analytical simplicity, we first assume that the channel is estimated and compensated with high accuracy and therefore the signal after frequency-domain

equalization can be written as

$$S'(k) = X(k) + \sum_{i=1}^{K} \sqrt{P_i} E_i(k) + W'(k),\ k = 0, 1, \cdots, N-1, \tag{4.12}$$

where $W'(k) = W(k)/H(k)$ represents the kth subcarrier AWGN scaled by the channel frequency response. As previously analyzed in (4.6), each EL may consist of several modulated *signature sequences* and therefore without loss of generality, we now discuss the demodulation of the mth data symbol of the jth EL. First the cyclic phase embedded in the sequence is detected by computing the frequency domain cross-correlations between the corresponding signal segment and the local generated *signature sequence* with all possible cyclic phase shifts:

$$R(\varphi) = \sum_{k=0}^{\mathcal{M}-1} S'(k + (m-1)\mathcal{M}) Z_{O_\varphi}^{(i)\,*}(k),\quad O_\varphi = 0, 1, \cdots, \mathcal{Z}-1, \tag{4.13}$$

where $Z_{O_\varphi}^{(j)}$ is the locally generated jth EL's *signature sequence* with all the possible cyclic shifts.

Mathematically, (4.13) can be further expanded as

$$
\begin{aligned}
R(\varphi) &= \sum_{k=0}^{\mathcal{M}-1}\left[X(k+(m-1)\mathcal{M}) + \sum_{i=1}^{K}\sqrt{P_i}Z_{O_m}^{(i)}(k) + W'(k)\right] Z_{O_\varphi}^{(i)\,*}(k) \\
&= \sum_{k=0}^{\mathcal{M}-1}\sqrt{P_j}Z_{O_m}^{(j)}(k)Z_{O_\varphi}^{(j)\,*}(k) + \underbrace{\sum_{i=1,i\neq j}^{K}\sum_{k=0}^{\mathcal{M}-1}\sqrt{P_i}Z_{O_m}^{(i)}(k)Z_{O_\varphi}^{(j)\,*}(k)}_{\textbf{mutual Enhanced Layer interference}} \\
&\quad + \underbrace{\sum_{k=0}^{\mathcal{M}-1}\left[X(k+(m-1)\mathcal{M}) + W'(k)\right] Z_{O_\varphi}^{(j)\,*}(k)}_{\textbf{Base Layer interference and noise}} \\
&= \begin{cases} \sqrt{P_j}\sum_{k=0}^{\mathcal{M}-1}\left|Z_{O_m}^{(i)}(k)\right|^2 + \sum_{k=0}^{\mathcal{M}-1}\left[X(k+(m-1)\mathcal{M}) + W'(k)\right] Z_{O_\varphi}^{(j)\,*}(k) & \text{if } O_m = O_\varphi \\ \sum_{k=0}^{\mathcal{M}-1}\left[X(k+(m-1)\mathcal{M}) + W'(k)\right] Z_{O_\varphi}^{(j)\,*}(k) & \text{if } O_m \neq O_\varphi \end{cases}
\end{aligned}
\tag{4.14}
$$

The mutual layer interference can be assumed to be negligible when comparing with the strong interference from the BL and the AWGN,

$$
\sum_{i=1,i\neq j}^{K}\sum_{k=0}^{\mathcal{M}-1}\sqrt{P_i}Z_{O_m}^{(i)}(k)Z_{O_\varphi}^{(j)\,*}(k) \approx 0, \tag{4.15}
$$

Therefore, the local *signature sequence* with cyclic phase shift O_φ that leads to the maximum correlation output is the phase encoded from the transmitted data bits. With the one to one mapping between the decimal value of the input data sequence and the cyclic phase shift O_φ, the original data $\mathbf{d}_m^{(j)}$ in (4.4) can be retrieved.

4.3.2 Interference Cancellation of Enhanced Layers

The superimposition of ELs' signals may cause large interference to the demodulation of OFDM data on the BL. However, due to the significantly large gap between the

regenerated ELs' signals $\mathbf{E}'_i = \mathbf{E}_i$ is close to unity. Hence, $\mathbf{E}'_i$ can be subtracted from the received signal according to,

$$\mathbf{S}' - \sum_{i=1}^{K} \sqrt{P_i}\mathbf{E}'_i. \tag{4.17}$$

In practical wireless communications, the interference cancellation can be imperfect due to the channel estimation errors and data detection errors, resulting in residual interference after the subtraction. If we denote the estimated channel frequency response as $\mathbf{H}'$ and the residual interference can be written as

$$\begin{aligned}\mathbf{I} &= \sum_{i=1}^{K} \mathbf{E}_i\mathbf{H} - \mathbf{E}'_i\mathbf{H}' \\ &= \sum_{i=1}^{K} \mathbf{E}_i\mathbf{\Delta H} + \mathbf{\Delta E}_i\mathbf{H} + \mathbf{\Delta E}_i\mathbf{\Delta H},\end{aligned} \tag{4.18}$$

where $\mathbf{\Delta H} = \mathbf{H} - \mathbf{H}'$ and $\mathbf{\Delta E}_i = \mathbf{E}_i - \mathbf{E}'_i$ denote the error of channel estimation and regenerated signal, respectively. Note that the last term in (4.17) is small in magnitude and can be neglected. Then the variance of $\mathbf{I}$ can be calculated,

$$\sigma_I^2 = \sum_{i=1}^{K} P_i\sigma_{\Delta H}^2 + 2P_{e,i}P_i\sigma_H^2, \tag{4.19}$$

where $P_{e,i}$ denotes the SER of the ith EL and $\sigma_{\Delta H}^2$ denotes the variance of channel estimation error. The residual interference is influenced by both channel estimation and data detection results. Nevertheless, as $P_{e,i}$ is already sufficiently small ($\approx 10^{-6}$), the second term on the right hand side of (4.18) can be significantly weaker than the first term. (4.18) also implies that the accumulated residual interference from all the ELs may dramatically reduce the BL's performance. As a result, further power

distribution scheme is definitely required to optimize the overall system performance as we will discuss later in the following sections.

After interference cancellation, hard data decisions can be made upon the interference-suppressed signal and the OFDM data on the BL can be retrieved.

4.4 Performance Evaluation of the Proposed System

4.4.1 Error Performance Analysis of Enhanced Layers

As the proposed modulation scheme is similar to conventional $\mathcal{M}$-ary signaling, the BER expression given by [99] can be used to evaluate the performance of the proposed modulation. However, it is difficult to obtain a closed-form expression and thus the computational complexity for the potential power distribution will be extremely high if the exact BER expression is used as a constraint. For efficiency improvement of further power distribution scheme, a simple BER upper bound is derived in this subsection.

In order to evaluate the robustness of the proposed modulation scheme, the Peak-to-Noise Ratio (PNR) of the correlation output is first analyzed. For analytical simplicity, the correlation output in (4.14) can be rewritten as

$$R(\varphi) = \begin{cases} \mathcal{A} + n \text{ if } O_m = O_\varphi \\ n \quad \text{ if } O_m \neq O_\varphi \end{cases} \tag{4.20}$$

where $\mathcal{A} = \sqrt{P_j}\sum_{k=0}^{\mathcal{M}-1}\left|Z_{O_m}^{(i)}(k)\right|^2 = \sqrt{P_j}\mathcal{M}$ denotes the ideal peak value and $n = \sum_{k=0}^{\mathcal{M}-1}\left[X(k+(m-1)\mathcal{M}) + W'(k)\right] Z_{O_\varphi}^{(j)^*}(k)$ denotes the associated interfer-

ence and noise term on the peak. It is obvious that n is Gaussian distributed and satisfies,

$$n \sim \mathcal{N}\left(0, \sigma_w^2\right), \tag{4.21}$$

where the variance $\sigma_w^2 = \mathcal{M}\sigma_d^2 + \mathcal{M}\sigma_n'^2$. $\sigma_n'^2$ represents the variance of the $W'(k)$ and can be calculated according to

$$\sigma_n'^2 = \int_0^\infty \frac{\sigma_n^2}{|H(k)|^2} p(|H(k)|) d|H(k)|, \tag{4.22}$$

where $p(|H(k)|)$ denotes the probability density of the magnitude of the channel frequency response,

$$p(|H(k)|) = \frac{|H(k)|}{\sigma_H^2/2} \exp\left(-\frac{|H(k)|^2}{\sigma_H^2}\right). \tag{4.23}$$

Therefore the PNR of the correlation output can be represented by

$$\begin{aligned}
\text{PNR} &= \frac{\mathcal{A}^2}{\sigma_w^2} \\
&= \frac{P_j \mathcal{M}^2}{\mathrm{E}\left[\left|\sum_{k=0}^{\mathcal{M}-1} \left[X(k+(m-1)\mathcal{M}) + W'(k)\right] Z_{O_\varphi}^{(j)*}(k)\right|^2\right]} \\
&= \frac{P_j \mathcal{M}^2}{\mathcal{M}\sigma_d^2 + \mathcal{M}\sigma_n'^2}
\end{aligned} \tag{4.24}$$

It can be observed in (4.23) that the PNR is dominated by the sequence length $\mathcal{M}$ and the power level P_j. Longer *signature sequence* and higher transmission power can be allocated to achieve more robust transmission for the *multicell cooperation* and *broadcast* signaling. However, as shown in Table. 4.1, the corresponding transmission data rate is reduced and the resultant interference to the BL (*unicast services*) will

also be increased.

It is worth mentioning that in the case of (4.9), where each modulated sequence on the EL is repeated by $\mathcal{R}$ times for robustness enhancement, then the corresponding segments can be averaged prior to correlation. Therefore, the correlation output can be rewritten as

$$\sqrt{P_j}\sum_{k=0}^{\mathcal{M}-1}\left|Z_{O_m}^{(i)}(k)\right|^2+\sum_{k=0}^{\mathcal{M}-1}\left[\overline{X(k)}+\overline{W'(k)}\right]Z_{O_\varphi}^{(j)\,*}(k)\ \text{ if }\ O_m=O_\varphi \tag{4.25}$$

where $\overline{X(k)}$ is the averaged OFDM symbol with variance $\sigma_d^2/\mathcal{R}$ and $\overline{W'(k)}$ is the averaged noise with variance $\sigma'^2_n/\mathcal{R}$. The corresponding PNR can then be reformulated by,

$$\text{PNR}=\frac{P_j\mathcal{M}^2\cdot\mathcal{R}}{\mathcal{M}\sigma_d^2+\mathcal{M}\sigma_n'^2}. \tag{4.26}$$

As we can see from (4.19), the correct detection of the cyclic shift (phase) for the $\mathcal{M}-1$ comparisons should meet the criteria $\mathcal{A}>n+n$. Now let us consider a new variable $y=2n$ and its probability density can be derived as follows

$$\begin{aligned}
p_Y(y)&=\int_{-\infty}^{\infty}p_N(n)p_N(y-n)dn\\
&=\int_{-\infty}^{\infty}\frac{1}{\sqrt{2\pi\sigma_w^2}}e^{-\frac{n^2}{2\sigma_w^2}}\frac{1}{\sqrt{2\pi\sigma_w^2}}e^{-\frac{(y-n)^2}{2\sigma_w^2}}dn\\
&=\frac{1}{\sqrt{2\pi\sigma_w^2}}e^{-\frac{y^2}{2\sigma_w^2}}\int_{-\infty}^{\infty}\frac{1}{\sqrt{2\pi\sigma_w^2}}e^{-\frac{2(n-y/2)^2-y^2/2}{2\sigma_w^2}}\\
&=\frac{1}{2\sqrt{\pi}\sigma_w}e^{-\frac{y^2}{4\sigma_w^2}}.
\end{aligned} \tag{4.27}$$

The correct detection should meet the criteria that $y<\mathcal{A}$ for all $\mathcal{M}-1$ correlation

comparisons and therefore the false detection probability for one comparison is given by

$$
\begin{aligned}
P_c &= \int_{\mathcal{A}}^{\infty} p_Y(y)dy \\
&= \int_{\mathcal{A}}^{\infty} \frac{1}{2\sqrt{\pi}\sigma_w} e^{-\frac{y^2}{4\sigma_w^2}} dy \\
&= \mathcal{Q}\left(\frac{\mathcal{A}}{\sqrt{2}\sigma_w^2}\right) \\
&= \mathcal{Q}\left(\sqrt{\frac{\mathrm{PNR}}{2}}\right).
\end{aligned} \tag{4.28}
$$

The false peak detection is then upper bounded by its union bound,

$$
P_f = (\mathcal{M}-1)P_c. \tag{4.29}
$$

Assume that all the bits in one data symbol $\mathbf{d}_i$ are equally likely. Since one symbol is composed of k bits, the BER of the $j$the EL is therefore upper bounded by

$$
\begin{aligned}
P_{b,j} &= \frac{2^{k-1}}{2^k-1} P_f = 2^{k-1}\mathcal{Q}\left(\sqrt{\frac{P_j \cdot \mathrm{NPNR}_j}{2}}\right) \\
&\leq \frac{\mathcal{M}-1}{2} \exp\left(-\frac{P_j \cdot \mathrm{NPNR}_j}{4}\right),
\end{aligned} \tag{4.30}
$$

where we define the normalized PNR of the jth EL as $\mathrm{NPNR}_j = \mathrm{PNR}_j/P_j$.

4.4.2 Capacity Loss Analysis of Base Layer

The average channel capacity of the BL is derived in this subsection to study the impact of EL's transmission on the overall system performance. After interference

cancellation, the effective received signal of the BL can be represented as

$$\mathbf{Y}' = \mathbf{XH} + \mathbf{I} + \mathbf{W}. \tag{4.31}$$

Assume that the LS or MMSE estimators using training sequences are used for channel estimation in the proposed system and if the length of the training sequence is N_t, when L/N_t is sufficiently small, the residual interference term $\mathbf{I}$ in is essentially uncorrelated with $\mathbf{W}$. Therefore, $\mathbf{I}+\mathbf{W}$ in (4.30) can be considered as a Gaussian vector with zero mean and covariance matrix of $\left(\sum_{i=1}^{K} P_i\sigma_{\Delta H}^2 + 2P_{e,i}P_i\sigma_H^2 + \sigma_n^2\right)\mathbf{I}_N$, where $\mathbf{I}_N$ is an identity matrix of order N. Based on the analysis of the average channel capacity for flat fading channels given in [100], we derive the average channel capacity of BL C_{BL} by summing over all the subcarriers,

$$C_{BL} = \frac{1}{N}\sum_{k=0}^{N-1} \mathrm{E}\left[\log\left(1 + \frac{P_B \cdot |H_k'|^2}{P_B\sigma_{\Delta H}^2 + \sum_{i=1}^{K} P_i\sigma_{\Delta H}^2 + 2P_{e,i}P_i\sigma_H^2 + \sigma_n^2}\right)\right] \tag{4.32}$$

where P_B denotes the power of BL and it has been normalized to one. For analytical simplicity, the following Gaussian random variable with zero mean and unit variance is introduced, $g \triangleq H_k'/\sqrt{\mathrm{Var}\left(H_k'\right)}$. Therefore, (4.31) can be reformulated as

$$C_{BL} = \frac{1}{N}\sum_{k=0}^{N-1} \mathrm{E}\left[\log\left(1 + \frac{P_B \cdot \mathrm{Var}\left(H_k'\right)|g|^2}{P_{total}\sigma_{\Delta H}^2 + \sum\limits_{i=1}^{K} 2P_{e,i}P_i\sigma_H^2 + \sigma_n^2}\right)\right], \tag{4.33}$$

where $P_{total} = P_B + \sum_{i=1}^{K} P_i$. Furthermore, the assumption that the normalized channel estimation error $\sigma_{\Delta H}^2/\sigma_H^2$ is sufficiently small holds when accurate channel estimation techniques are adopted and therefore $\mathrm{Var}\left(H_k'\right)$ can be approximated to

σ_H^2. Then the capacity can be further approximated as

$$C_{BL} = \frac{1}{N}\sum_{k=0}^{N-1} \mathrm{E}\left[\log\left(1 + \frac{P_B \cdot \sigma_H^2 |g|^2}{P_{total}\sigma_{\Delta H}^2 + \sum_{i=1}^{K} 2P_{e,i}P_i\sigma_H^2 + \sigma_n^2}\right)\right]$$
$$= \log\left(1 + \frac{P_B \cdot \sigma_H^2 |g|^2}{P_{total}\sigma_{\Delta H}^2 + \sum_{i=1}^{K} 2P_{e,i}P_i\sigma_H^2 + \sigma_n^2}\right). \tag{4.34}$$

In the absence of ELs' transmission, the upper bound of BL's capacity can be written as

$$\overline{C}_{BL} = \frac{1}{N}\sum_{k=0}^{N-1} \log\left(1 + \frac{P_B \cdot \sigma_H^2 |g|^2}{P_B\sigma_{\Delta H}^2 + \sigma_n^2}\right). \tag{4.35}$$

By introducing the maximum allowed capacity loss ΔC, the ELs' transmission is enabled in the ML-OFDM system only when the following constraint is satisfied

$$\overline{C}_{BL} - C_{BL} \leq \Delta C. \tag{4.36}$$

The above constraint is referred to as the BL's capacity loss constraint and can be reformulated as

$$C_{BL} \geq C, \tag{4.37}$$

where $C \triangleq \overline{C}_{BL} - \Delta C$. The above constraint is essential for the multi-layered system design as it reflects the impact of ELs' transmission on the BL. If the capacity loss is sufficiently large that the BL cannot tolerate, no ELs' transmission is allowed. Therefore, the constraint will further be used in the power distribution scheme as we will discuss in the next section.

4.5 Power Distribution for Enhanced Layers' transmission

Power distribution scheme for different ELs is discussed in this section. The objective is to optimize the overall system performance by balancing the tradeoff between the ELs and the BL. Therefore, we propose to optimize the overall error performance of the ELs given the constraint on the BL's capacity loss. Furthermore, by considering the different service quality of different ELs, we introduce the proportional BER constraints into our system. The benefit of the proportional constraints is that we can flexibly control the reliability of different signaling and therefore provide different target quality for different purposes.

The power allocation can be expressed mathematically as,

$$\min_{P_i} \overline{\text{BER}} = \frac{\sum_{i=1}^{K} k_i P_{b,i}}{\sum_{i=1}^{K} k_i}, \tag{4.38}$$

subject to,

$$\sum_{i=1}^{K} P_i \leq P_{E,total} \tag{4.39}$$

$$C_{BL} \geq C \tag{4.40}$$

$$P_{b,1} : P_{b,2} : \cdots : P_{b,K} = \gamma_1 : \gamma_2 : \cdots : \gamma_K, \tag{4.41}$$

where $P_{b,i}$ denotes the BER upper bound of the ith EL as derived in (4.29). k_i denotes the effective transmitted bit number on the ith EL. $P_{E,total}$ is the total transmission power budget for the ELs. $\{\gamma_i\}_{i=1}^{K}$ is the set of the predefined values which are used to ensure the proportion of BER on different EL. The purpose of introducing the proportional BER constraints is to support various reliability/coverage requirements

of different signaling, i.e., *BS coordination* signaling needs more robust transmission of CSI information than the *broadcast*; the constraints can be flexibly adjusted according to system design targets. Note that the nonlinear inequality constraint $-C_{BL} \leq C$ makes the optimization problem in (4.37) nonconvex. Iterative methods, such as Newton-Raphson or quasi-Newton methods can be used to obtain the solutions, however, with a large amount of computational complexity. However, under ceratin conditions, the optimal or near-optimal solutions of problem can be found with low complexity. Since the operating SNR range for the ELs is much lower than that of the BL. Therefore, we analyze the case where certain approximations can be made.

Under traditional OFDM's operating SNR range, the SER of the ELs $P_{e,i}, i = 1, 2, \cdots, K$ are already very low and the variance of channel estimation error $\sigma^2_{\Delta h}$ can be considered to be much larger as compared with $P_{e,i}$. Therefore, the term $\sum_{i=1}^{K} 2P_{e,i}P_i\sigma^2_H$ in (4.33) is significantly smaller than the other interference and background noise $P_{total}\sigma^2_{\Delta H} + \sigma^2_n$; the capacity of BL given by (4.33) can be further simplified to

$$C_{BL} = \log\left(1 + \frac{P_B \cdot \sigma^2_H |g|^2}{P_B\sigma^2_{\Delta H} + \sum_{i=1}^{K} P_i\sigma^2_{\Delta H} + \sigma^2_n}\right). \tag{4.42}$$

It is obvious that now the approximated capacity is concave function with respect to P_i, therefore, the problem becomes convex. Its global optimal solution can be

obtained by Karush-Kuhn-Tucker (KKT) conditions [101] as follows,

$$\frac{\partial \overline{\mathrm{BER}}}{\partial P_i} + \lambda + \mu \frac{\partial C_{BL}}{\partial P_i} + \sum_{i=1}^{K-1} \varpi_i \frac{\partial \left(P_{b,1} - \frac{\gamma_1}{\gamma_i} P_{b,i} \right)}{\partial P_i} = 0 \tag{4.43}$$

$$\lambda \left(\sum_{i=1}^{K} P_i - P_{total} \right) = 0 \tag{4.44}$$

$$\mu \left(\log \left(1 + \frac{P_B \cdot \sigma_H^2}{P_B \sigma_{\Delta H}^2 + \sum_{i=1}^{K} P_i \sigma_{\Delta H}^2} \right) + C \right) = 0 \tag{4.45}$$

$$\varpi_i \left(\exp \left(-\frac{P_1 \cdot \mathrm{NPNR}_1}{4} \right) - \frac{\gamma_1}{\gamma_i} \exp \left(-\frac{P_i \cdot \mathrm{NPNR}_i}{4} \right) \right) = 0 \tag{4.46}$$

where λ, μ, and ϖ_i are the Lagrange multipliers. $\forall i \in \{1, \cdots, K\}$ $\lambda \geq 0$, $\mu \geq 0$, and $\varpi_i \geq 0$.

Note that the capacity given by (4.33) is a monotonously increasing function of P_i. Therefore the constraint (4.39) can be reformulated by

$$\sum_{i=1}^{K} P_i \leq \frac{10^C - 1}{P_B \sigma_H^2 \sigma_{\Delta H}^2} - P_B \triangleq \chi, \tag{4.47}$$

where the right hand side of the above inequality is denoted by χ.

From (4.43) and (4.44), we note that λ and μ are not allowed to be synchronously nonzero which means

$$\lambda \neq 0 \Rightarrow \sum_{i=1}^{K} P_i = \chi \tag{4.48}$$

$$\mu \neq 0 \Rightarrow \sum_{i=1}^{K} P_i = P_{E,total}, \tag{4.49}$$

when $\chi \neq P_{total}$. Therefore, the problem can be discussed in the following two circumstances:

A. When $\chi < P_{total}$

With this condition, we can obtain $\sum_{i=1}^{K} P_i < P_{E,total}$ since $\sum_{i=1}^{K} P_i \leq \chi$. Therefore, according to (4.47), $\lambda = 0$ is obtained. Therefore, (4.42) can be furthered expanded and solved by

$$\frac{k_i}{\sum\limits_{i=1}^{K} k_i} \cdot \left(-\frac{\mathrm{NPNR}_i}{4}\right) P_{b,i} + \mu + \varpi_i \left(-\frac{\gamma_1}{\gamma_i}\right) \cdot \left(-\frac{\mathrm{PNR}_i}{4}\right) P_{b,i} = 0$$

$$\Rightarrow P_i = -4 \log \left\{ \frac{8\mu}{(\mathcal{M}-1)\,\mathrm{NPNR}_i} / \eta_i \right\} / \mathrm{NPNR}_i, \tag{4.50}$$

where $\eta_i = \frac{k_i}{\sum\limits_{k=1}^{K} k_i} - \frac{\gamma_1}{\gamma_i}\varpi_i$. Note that when $\mu = \lambda = 0$, then it is easy to obtain $P_i \to \infty$, which is impossible for real implementation. Therefore, this circumstance is not allowed to occur. μ and λ must not be synchronously zero.

B. When $\chi \geq P_{total}$

Similarly, we can obtain that $\sum_{i=1}^{K} P_i < \chi$ since $\sum_{i=1}^{K} P_i \leq P_{E,total}$. Thus, $\mu = 0$ in this circumstance. The solution is thus given by with μ replaced by λ

$$P_i = -4 \log \left\{ \frac{8\lambda}{(\mathcal{M}-1)\,\mathrm{NPNR}_i} / \eta_i \right\} / \mathrm{NPNR}_i. \tag{4.51}$$

Also μ and λ are not allowed to be synchronously zero.

From the optimal power distribution solution for the ELs, it implies that the power level for different ELs depends on the parameters λ, μ, and ϖ_i. λ is the dual variable associated with the total transmission power budget. It is straightforward that a lager transmission power budget will result in a smaller λ and thus a higher power level, and vice versa. μ is the dual variable associated with the tolerable capacity loss of the base layer. If the base layer can accommodate a larger residual interference introduced by the transmission of ELs, μ would be smaller, and therefore

a higher allowed transmission power level, and vice versa. For instance, in an extreme case where the base layer cannot accommodate any interference or in other words, the capacity loss constraint for the BL is zero, then μ would be infinity and the resultant zero power level indicates that no ELs' signals superimposed onto the BL is allowed in this condition. Similarly, the analysis can be also applied to ϖ_i which is associated with the proportional BER constraints of the ELs.

4.6 Simulation Results and Discussions

Numerical simulation results are presented to evaluate the performance of the proposed ML-OFDM. The OFDM system with 1024 subcarriers and CP of length 1/8 of the symbol duration is considered in the simulation. The modulation scheme for the BL is chosen as 4-QAM. In additional. two ELs are considered in the demonstration system which are designated to the *BS cooperation signaling* and the *broadcast service*, respectively. Two nearly orthogonal *Zadoff-Chu* sequences with length $\mathcal{M} = 64$ are used as the *signature sequences* for the two ELs. To improve the robustness of the ELs, the signals are formulated according to

$$\begin{aligned} \mathbf{D}^{(1)} &= \left[\underbrace{\mathbf{d}_0^{(1)}, \cdots, \mathbf{d}_0^{(1)}}_{8}, \underbrace{\mathbf{d}_1^{(1)}, \cdots, \mathbf{d}_1^{(1)}}_{8}\right], \\ \mathbf{D}^{(2)} &= \left[\mathbf{d}_0^{(2)}, \mathbf{d}_1^{(2)}, \cdots, \cdots, \mathbf{d}_{14}^{(2)}, \mathbf{d}_{15}^{(2)}\right]. \end{aligned} \tag{4.52}$$

Each data symbols are repeated by 8 times on EL1 and therefore the total transmitted bit number becomes $k_1 = 12$ bits for EL1 and $k_2 = 96$ bits for EL2. Note that the repetition time can be flexibly adjusted according to the system requirements, i.e., the BSs share the CSI information by using the global vector quantization (GVQ)

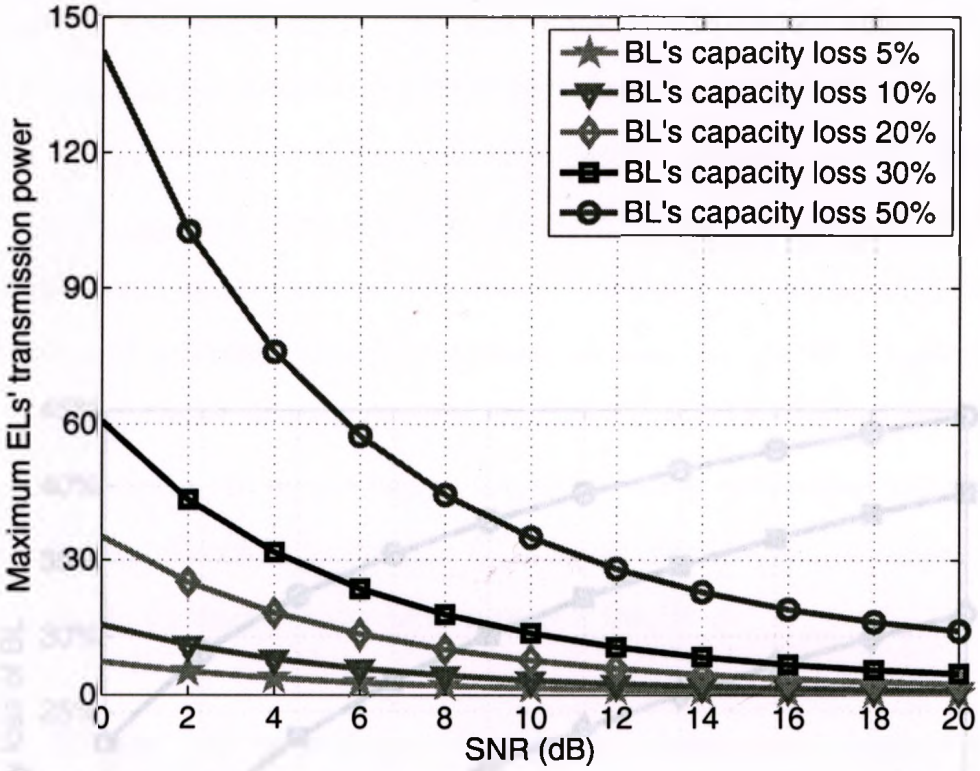

Figure 4.4: Effect of varying capacity loss constraints on the maximum ELs' transmission power (with fixed channel estimation error $\sigma^2_{\Delta H} = 0.10$).

approach [98] to reduce the overhead. In this example, EL1 is used for *BS cooperation signaling* and EL2 is utilized to broadcast public information.

4.6.1 The Impact of Base Layer's Capacity Loss Constraint

In this subsection, we first examine the impact of the BL's capacity loss constraint in (4.35) on the performance of the ELs. Fig. 4.4 shows the maximum allowed total transmission power for the ELs with different BL's capacity loss constraints. It can be observed in Fig. 4.4 that as the capacity loss constraint becomes looser, higher transmission power is allowed for the ELs, which will significantly improve the reliability/coverage of the *multicell cooperation signaling* and the *broadcast service*; however, the performance of *unicast services* is dramatically degraded. It is also apparent that

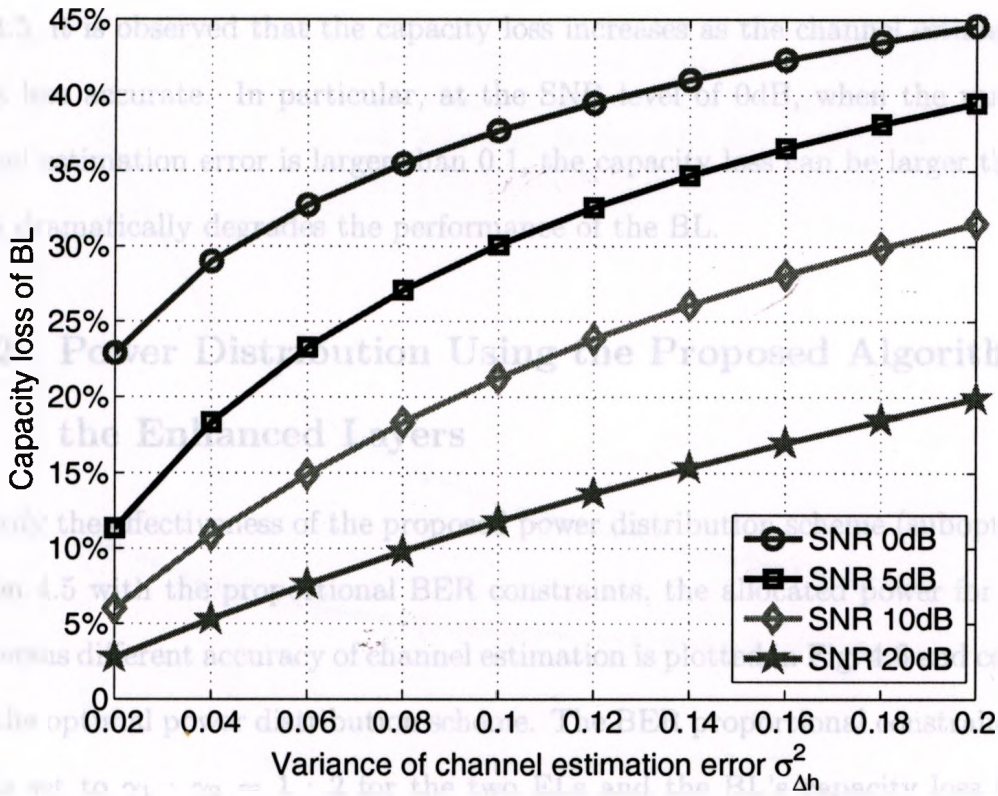

Figure 4.5: Effect of channel estimation accuracy on the capacity loss of the BL (with fixed ELs total transmission power $P_{E,total} = 1$).

an increase in SNR will result in a decrease in the attained total transmission power. This is because as the variance of AWGN reduces, the capacity loss is dominated by the term $\sum_{i=1}^{K} P_i \cdot \sigma_{\Delta H}^2$. If there exists large channel estimation error, then a small increase in $P_{E,total}$ will cause dramatic reduction in BL's capacity and therefore no ELs' transmission is beneficial in this case. Therefore, we subsequently assess the consequences of different channel estimation accuracy on the BL's capacity. From Fig. 4.5, it is observed that the capacity loss increases as the channel estimation becomes less accurate. In particular, at the SNR level of 0dB, when the variance of channel estimation error is larger than 0.1, the capacity loss can be larger than 35% which dramatically degrades the performance of the BL.

4.6.2 Power Distribution Using the Proposed Algorithm for the Enhanced Layers

To verify the effectiveness of the proposed power distribution scheme (suboptimal) in Section 4.5 with the proportional BER constraints, the allocated power for the two ELs versus different accuracy of channel estimation is plotted in Fig. 4.6 and compared with the optimal power distribution scheme. The BER proportional constraint in this case is set to $\gamma_1 : \gamma_2 = 1 : 2$ for the two ELs and the BL's capacity loss is set to 10%. The optimal power distribution scheme uses the exact BER expressions given by [99] instead of the derived BER upper bound. The exact BER expressions can represented as

$$P_e = \frac{1}{\sqrt{2\pi}} \int_{-\infty}^{\infty} \left[1 - (1 - Q(x))^{\mathcal{M}-1}\right] e^{-\frac{(x-\sqrt{\text{PNR}})^2}{2}} dx \tag{4.53}$$

$$P_b = \frac{2^{k-1}}{2^k - 1} P_e. \tag{4.54}$$

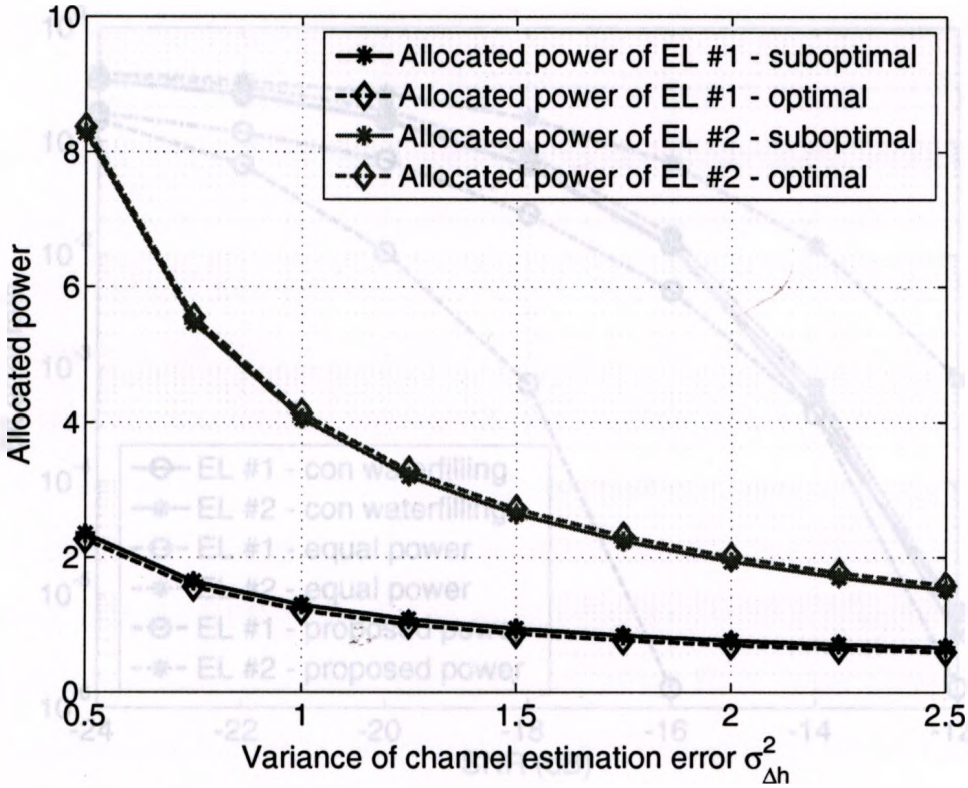

Figure 4.6: The allocated power to different ELs with the proposed power distribution scheme and the optimal power distribution scheme.

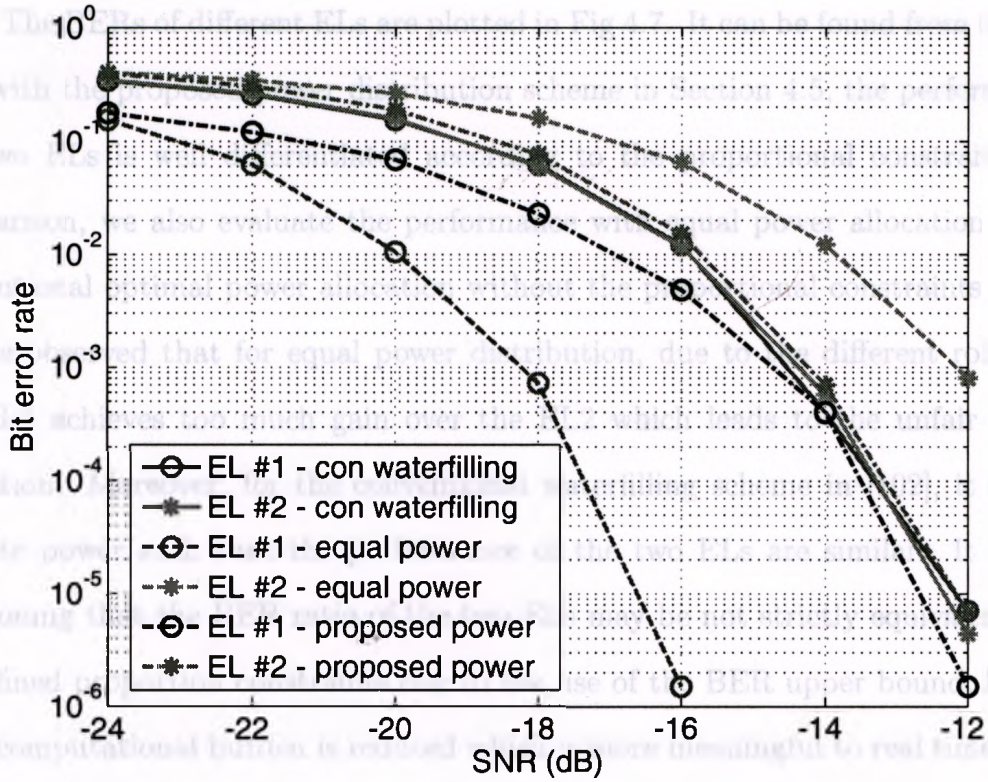

Figure 4.7: BER of different ELs using the proposed power distribution scheme and other schemes.

The above expressions can only be calculated numerically and therefore, an exhaustive searching is carried out to find the optimal P_1 and P_2 for the two ELs to satisfy the proportional BER constraints and therefore the required computational burden can be extremely high. Fig. 4.6 shows that the gap between the optimal and the proposed algorithm is almost invisible and therefore it confirms the feasibility of the proposed power distribution scheme.

The BERs of different ELs are plotted in Fig 4.7. It can be found from the figure that with the proposed power distribution scheme in Section 4.5, the performance of the two ELs is well differentiated according to the proportional constraints. For comparison, we also evaluate the performance with equal power allocation and the conventional optimal power allocation without the proportional constraints [102]. It can be observed that for equal power distribution, due to the different robustness, the EL1 achieves too much gain over the EL2 which leads to the unfair resource allocation. Moreover, for the conventional waterfilling scheme in [102], it tends to allocate power such that the performance of the two ELs are similar. It is worth mentioning that the BER ratio of the two ELs may be not strictly equivalent to the predefined proportion constraints due to the use of the BER upper bound, however, large computational burden is reduced which is more meaningful to real time cellular network scenario.

To evaluate more intuitively how good the proposed power distribution scheme satisfies the BER proportional constraints, a new metric is defined. Let $P_{k,i}$ be the BER of the kth EL for the ith Monte Carlo run and therefore $\tilde{P}_{k,i} = P_{k,i}/\sum_{k=1}^{K} P_{k,i}$ be the normalized BER for the kth EL. Also, the normalized BER proportional constraints is defined as $\tilde{\gamma}_k = \gamma_k/\sum_{k=1}^{K}\gamma_k$. The normalized variance of the BER

proportional constraints for the ith Monte Carlo run is defined as

$$\mathcal{V}_i = \sum_{k=1}^{K} |\tilde{P}_{k,i} - \tilde{\gamma}_k|^2. \tag{4.55}$$

Table 4.2: Average variance of the BER proportional constraints under different SNRs

SNR(dB)	-24	-22	-20	-18	-16	-14	-12
$\gamma_1 : \gamma_2$	0.5	0.5	0.5	0.5	0.5	0.5	0.5
$\overline{\mathcal{V}}$, proposed	0.0012	0.0052	0.0092	0.0217	0.0170	0.0021	0.0476
$\overline{\mathcal{V}}$, equal	0.0065	0.0651	0.1743	0.2162	0.2222	-	-
$\overline{\mathcal{V}}$, [102]	0.0535	0.0527	0.0515	0.0603	0.0628	0.0127	0.1591

The average variance over total I Monte Carlo runs, denoted by $\overline{\mathcal{V}} = \sum_{i=1}^{I} \mathcal{V}_i / I$, is reported in Table 4.2. Note that the ideal $\overline{\mathcal{V}}$ is supposed to be close to zero if the allocated power strictly satisfies the constraints. It can be observed that the variance of the proposed power distribution scheme is orders of magnitude smaller than those obtained by equal power distribution and conventional waterfilling algorithm in [102].

4.6.3 The Effects of Enhanced Layers' Transmission on Base Layer

After the power distribution of the ELs, the SER of the BL is examined in the presence of ELs' transmission with different channel estimation accuracy in Fig. 4.8. The curve labeled "ideal coherent detection" refers to the SER obtained with perfect channel estimation. Large gaps can be found in Fig. 4.8 between the curves with relatively large estimation error and ideal coherent detection. However, when highly accurate channel estimation scheme is used, the SER degradation is almost indistinguishable.

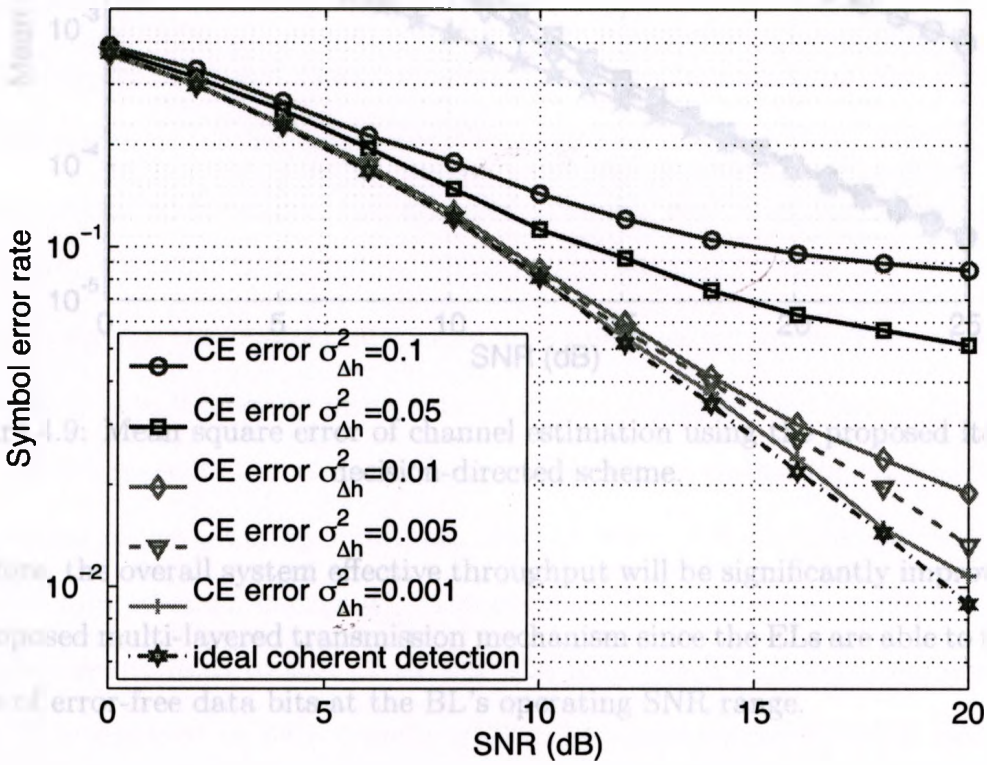

Figure 4.8: Effect of ELs' transmission on BL's performance with difference variance of channel estimation error.

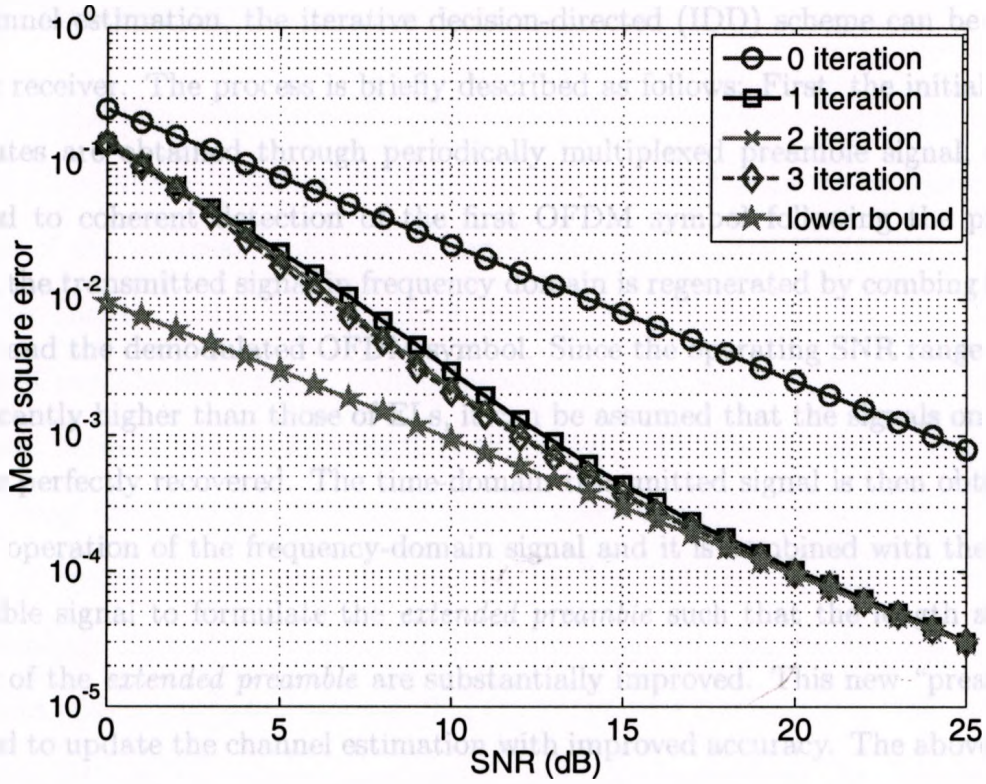

Figure 4.9: Mean square error of channel estimation using the proposed iterative decision-directed scheme.

Therefore, the overall system effective throughput will be significantly improved with the proposed multi-layered transmission mechanism since the ELs are able to transmit dozens of error-free data bits at the BL's operating SNR range.

4.6.4 Accuracy Improvement of Channel Estimation

As we can see from the previous results, the accuracy of channel estimation has large impact on the performance of the overall system. With higher accurate channel estimation, the maximum allowed ELs' transmission power will be increased which results in the corresponding enhanced performance of the ELs. On the other hand, the capacity loss of the BL due to the interference of ELs will also be reduced in the presence of more accurate of channel estimates. Therefore, to improve the quality

of channel estimation, the iterative decision-directed (IDD) scheme can be adopted at the receiver. The process is briefly described as follows: First, the initial channel estimates are obtained through periodically multiplexed preamble signal, which is applied to coherent detection of the first OFDM symbol following the preamble. Then, the transmitted signal in frequency domain is regenerated by combing the EL's signal and the demodulated OFDM symbol. Since the operating SNR range of BL is significantly higher than those of ELs, it can be assumed that the signals on the ELs can be perfectly recovered. The time-domain transmitted signal is then obtained by IDFT operation of the frequency-domain signal and it is combined with the original preamble signal to formulate the *extended preamble* such that the length and total power of the *extended preamble* are substantially improved. This new "preamble" is utilized to update the channel estimation with improved accuracy. The above process is iterated to simultaneously provide more accurate channel and data estimation.

Fig. 4.9 presents the mean square error of channel estimation with and without IDD process under a 10-tap multipath channel with uniform average power profile while the total channel energy σ_H^2 is normalized to 1. One EL is assumed and its allocated power equals to that of BL and the total power is normalized to one. The preamble is assumed to be a pseudo random sequence consisting of 40 samples. 4-QAM modulation is also assumed for the BL. In the figure, the label "0 iteration" represents the conventional channel estimation scheme by only utilizing preamble signal. The lower bound represents the case where the transmitted signal can be perfectly regenerated and subsequently used as part of the *extended preamble.* It can be observed that the IDD process substantially outperforms the conventional preamble based channel estimation scheme. With the increase of iterations, the corresponding MSE of channel estimation also reduces. The results also show that with 3 iterations, the lower bound can be achieved at the SNR level of 20dB.

4.7 Summary

A new ML-OFDM supporting multicell cooperative network is presented in this chapter. The flexibility of the new OFDM platform is derived from the concurrent transmission of the necessary information among the cooperative BSs together with the OFDMA-based *unicast service*. By encoding the CSI/data information using the proposed modulation scheme, tedious procedure to establish additional signaling or backhaul network can be substantially simplified. The BSs are tightly synchronized by utilizing the proposed *Enhanced Layer*, which significantly improve the performance of *multicell cooperation*. In addition, the parallel *Enhanced Layer* provides the *cell broadcast* capability, eliminating the requirement of separate wireless infrastructures and additional radio resource. The corresponding transceiver is designed for the proposed ML-OFDM system based on the proposed modem for the *Enhanced Layer* and the interference cancellation algorithm. Practical power distribution scheme is also proposed to optimize the overall system performance by considering a set of BER proportional constraints. The performance of the ML-OFDM is analyzed theoretically and verified through numerical simulations. With the ML-OFDM platform, *BS coordination* as well as various wireless demands will become more efficient and flexible and can easily be achieved.

Chapter 5

Optimal Iterative Channel Estimation for OFDM Systems

5.1 Introduction

Due to the extremely short symbol duration of broadband wireless communication systems, the wireless environments can commonly be modeled as quasi-static where the multipath channel is static over a few OFDM symbols. In this case, *Decision-Directed Channel Estimation* can be used to improve the estimation accuracy with the aid of the detected OFDM data. In traditional DDCE with hard decision feedback, the improvement of channel estimation is sometimes limited due to the data decision errors when all the demodulated data is fed back for the next round estimation. Motivated by the drawback, a reliable region decision DDCE scheme was proposed in [79]. The high BER region and low BER region are separated based on the magnitude of channel frequency response (CFR). Unfortunately, the performance of the scheme dramatically degrades under severe frequency selective channels. Recently, a DDCE method using partial hard decision was proposed in [80]. However, the scheme, which minimizes the variance of data decision error, may not necessarily reduce the variance of channel estimation error.

In this chapter, a new *Iterative Decision-Directed Channel Estimation* with reliable data feedback selection is proposed for OFDM system. The unreliable data

decisions are eliminated on the subcarriers suffering from noise enhancement where the magnitude of CFR is lower than a threshold. By investigating the variance of the channel estimation error, the optimal value of the threshold is derived to minimize the variance. Computer simulations are used to validate the performance of the proposed scheme.

The reminder of the chapter is organized as follows. Section 5.2 introduces the OFDM system model with proposed IDDCE. In Section 5.3, the proposed IDDCE is presented and the performance in terms of its variance of estimation error is also studied. In Section 5.4, the optimal threshold to select the reliable data decision feedback is derived. Simulation results and discussions are presented in Section 5.5. Finally, the chapter is summarized in Section 5.6.

5.2 System Model

We consider the same OFDM frame structure as shown in Fig. 3.2, where the preamble signal is denoted by $\mathbf{p} = [p(0), p(1), \cdots, p(N_p - 1)]$ and the OFDM data symbol by $\mathbf{x} = [x(0), x(1), \cdots, x(N_d - 1)]$. N_p and N_d are the length of the preamble signal and number of total subcarriers of the OFDM data symbol, respectively. Each element of $\mathbf{x}$ is generated by N_d- point IDFT,

$$x(n) = \frac{1}{\sqrt{N_d}} \sum_{k=0}^{N_d-1} X(k) \exp\left(\frac{j2\pi kn}{N_d}\right), \tag{5.1}$$

where $X(k)$ denotes the complex data on the kth subcarrier.

According to Section 3.2, the received signal after the removal of the GI and

the CP can be represented in the following matrix form,

$$\begin{bmatrix} \mathbf{y_p} \\ \mathbf{y_d} \end{bmatrix} = \begin{bmatrix} \mathbf{s_p} \\ \mathbf{s_d} \end{bmatrix} \mathbf{h} + \mathbf{w} \triangleq \mathbf{y} = \mathbf{sh} + \mathbf{w}, \tag{5.2}$$

where $\mathbf{y_p}$ and $\mathbf{y_d}$ denote the received vectors of $\mathbf{p}$ and $\mathbf{x}$, respectively. $\mathbf{s_p}$ and $\mathbf{s_d}$ are the matrices derived from $\mathbf{p}$ and $\mathbf{x}$ with size $N_p \times L$ and $N_d \times L$ whose first columns are given by $\mathbf{p}^T$ and $\mathbf{x}^T$, respectively. The remaining columns are each cyclic shift of $\mathbf{p}^T$ and $\mathbf{x}^T$ with an offset equal to the column indices, respectively. $\mathbf{h}$ is a column vector of multipath channel with L taps and $\mathbf{w}$ is the AWGN vector with zero mean and variance σ_w^2.

5.3 Iterative Decision-Directed Channel Estimation

5.3.1 Proposed IDDCE Algorithm

The basic idea of the IDDCE is to utilize an *augmented preamble* which is the combination of the original preamble and the demodulated data such that the duration and total power of this extended training sequence is significantly enhanced as compared with the original one. The initial channel estimate is obtained by the original preamble and then used to provide the tentative estimate of $\mathbf{x}$. Then the iterative estimator can progressively update the channel and data estimation with the *augmented preamble*. Therefore, the channel and data estimates are simultaneously improved as the process is iterated. However, as the data estimates include decision errors, a few data feedback may introduce large interference to the iterative estimator, resulting in limited performance improvement even degradation.

In the data decision process, due to the impact of frequency selective channel, the noise effect may be enlarged on the subcarriers with low CFR and thus the wrong decisions are more likely to occur after equalization on these subcarriers. Therefore, it is necessary to select reliable data decision feedback by comparing the magnitude of CFR with a certain threshold.

The proposed IDDCE algorithm is summarized as follows.

1. Perform the initial channel estimation. Since the preamble signal is known to the receiver, the LS or MMSE estimator can be used to obtain the initial channel estimate. As the MMSE requires the channel characteristics such as the variance of each channel tap, here for practical consideration, we consider the LS estimator in this chapter. The channel estimate is obtained by using the circulant matrix of preamble signal $\mathbf{s_p}$ and its corresponding received samples $\mathbf{y_p}$ according to

$$\hat{\mathbf{h}} = \left(\mathbf{s_p}^H \mathbf{s_p}\right)^{-1} \mathbf{s_p}^H \mathbf{y_p}. \tag{5.3}$$

Therefore the corresponding estimation error of LS estimator can be formulated by

$$\mathbf{\Delta h} = \left(\mathbf{s_p}^H \mathbf{s_p}\right)^{-1} \mathbf{s_p}^H \mathbf{w}, \tag{5.4}$$

where $\left(\mathbf{s_p}^H \mathbf{s_p}\right)^{-1} = \mathbf{I}_L / N_p$. The variance of estimation error can be calculated as

$$\begin{aligned} \sigma^2_{\Delta h} &= \frac{1}{L} \mathrm{tr}\left\{\mathrm{E}\left[\mathbf{\Delta h \Delta h}^H\right]\right\} \\ &= \frac{1}{N_p^2 L} \mathrm{tr}\left\{\sigma_w^2 \mathbf{I}_{N_p}\right\} \\ &= \frac{1}{N_p} \sigma_w^2, \end{aligned} \tag{5.5}$$

where tr $\{\cdot\}$ denotes the trace operation of a matrix.

2. Equalize the OFDM signal in frequency domain with the current channel estimates,

$$\tilde{\mathbf{X}} = \frac{\mathrm{DFT}\{\mathbf{y_d}\}}{\mathrm{DFT}\left\{\hat{\mathbf{h}}\right\}}. \tag{5.6}$$

3. Make data decisions based on the equalizer output and denote it as $\hat{\mathbf{X}}$. As previously analyzed, the error probability of the noise-enhanced subcarriers is relatively high as compared with others and the resultant data decision feedback is less reliable on these subcarriers. Therefore, after obataining the estimate of CFR by $\hat{\mathbf{H}} = \mathrm{DFT}\left\{\hat{\mathbf{h}}\right\}$, the following selection criteria is proposed based on the current CFR estimate:

$$\hat{X}(k) = \begin{cases} \hat{X}(k) & |\hat{H}(k)| \geq \eta \\ 0 & |\hat{H}(k)| < \eta, \end{cases} \quad k = 0, 1, \cdots, N_d - 1. \tag{5.7}$$

Note that the corresponding received sample $Y(k)$ is also forced to be zero when the magnitude of CFR is lower than the threshold η.

4. Re-modulate the transmitted signal in time domain using the selected data from the previous step,

$$\hat{\mathbf{x}} = \mathrm{IDFT}\left\{\hat{\mathbf{X}}\right\}. \tag{5.8}$$

Consequently the circulant matrix of $\hat{\mathbf{x}}$ is also obtained and denoted as $\hat{\mathbf{s}}_{\mathbf{d}}$.

5. The channel estimate is updated by the LS estimator. However, the $\mathbf{s_p}$ and $\mathbf{y_p}$ are replaced by $\hat{\mathbf{s}}$ and $\mathbf{y}$ as defined in (4.2),

$$\hat{\mathbf{h}} = \left(\hat{\mathbf{s}}^H \hat{\mathbf{s}}\right)^{-1} \hat{\mathbf{s}}^H \mathbf{y}, \tag{5.9}$$

where

$$\hat{\mathbf{s}} = \begin{bmatrix} \mathbf{s_p} \\ \hat{\mathbf{s_d}} \end{bmatrix}. \tag{5.10}$$

6. Repeat steps 2) to 5) if necessary until the channel estimates converge or a predefined number of iterations is achieved.

5.3.2 Performance Analysis of the Proposed IDDCE

In this subsection, we analyze the performance of the proposed IDDCE in terms of the variance of the channel estimation error. First, the estimation error of the iterative estimator can be represented as

$$\begin{aligned} \mathbf{\Delta h} &= \left(\hat{\mathbf{s}}^H \hat{\mathbf{s}}\right)^{-1} \hat{\mathbf{s}}^H \mathbf{y} - \mathbf{h} \\ &= \left(\hat{\mathbf{s}}^H \hat{\mathbf{s}}\right)^{-1} \hat{\mathbf{s}}^H \mathbf{\Delta s h} + \left(\hat{\mathbf{s}}^H \hat{\mathbf{s}}\right)^{-1} \hat{\mathbf{s}}^H \mathbf{w} \\ &= \mathbf{\Delta h_f} + \mathbf{\Delta h_w}, \end{aligned} \tag{5.11}$$

where

$$\mathbf{\Delta s} = \mathbf{s} - \hat{\mathbf{s}} = \begin{bmatrix} \mathbf{0} \\ \mathbf{\Delta s_d} \end{bmatrix}. \tag{5.12}$$

$\mathbf{\Delta h_f}$ and $\mathbf{\Delta h_w}$ denote the estimation error from the data decision errors and the AWGN, respectively. $\mathbf{\Delta h_w}$ is straightforward to obtain

$$\sigma^2_{\Delta h_w} = \frac{1}{L}\mathrm{tr}\left\{\mathrm{E}\left[\mathbf{\Delta h_w} \mathbf{\Delta h_w}^H\right]\right\} = \frac{1}{N}\sigma^2_w, \tag{5.13}$$

For $\mathbf{\Delta h_f}$, it can be shown that

$$\begin{aligned}\sigma^2_{\Delta h_f} &= \frac{1}{N^2 L}\mathrm{tr}\left(\mathrm{E}\left[\hat{\mathbf{s}}^H \mathbf{\Delta s h h}^H \mathbf{\Delta s}^H \hat{\mathbf{s}}\right]\right) \\ &= \frac{1}{N^2 L}\mathrm{tr}\left(\mathrm{E}\left[\hat{\mathbf{S}}^H \mathbf{F}_N^H \mathbf{F}_N \mathbf{\Delta S h h}^H \mathbf{\Delta S}^H \mathbf{F}_N^H \mathbf{F}_N \hat{\mathbf{S}}\right]\right) \\ &= \frac{1}{N^2 L}\mathrm{tr}\left(\mathrm{E}\left[\hat{\mathbf{S}}^H \mathbf{\Delta S h h}^H \mathbf{\Delta S}^H \hat{\mathbf{S}}\right]\right), \end{aligned} \tag{5.14}$$

where $\mathbf{F}_N$ denotes the DFT transform matrix with the element $F(n,k) = e^{j\frac{2\pi kn}{N}}/\sqrt{N}$. $\hat{\mathbf{S}}$ and $\mathbf{\Delta S}$ denote the frequency domain version of $\hat{\mathbf{s}}$ and $\mathbf{\Delta s}$, respectively. Note that $\mathbf{\Delta S}$ only contains errors from the OFDM symbol. $N = N_p + N'_d$ is the total length of the *augmented preamble* where N'_d is the number of the non-zero components of $\hat{\mathbf{X}}$ selected by the criteria in (5.7). The trace operation in (5.14) only concerns the diagonal elements in $\left(\hat{\mathbf{S}}^H \mathbf{\Delta S h h}^H \mathbf{\Delta S}^H \hat{\mathbf{S}}\right)$ and it can be given by

$$\begin{aligned}&\left(\hat{\mathbf{S}}^H \mathbf{\Delta S h h}^H \mathbf{\Delta S}^H \hat{\mathbf{S}}\right)_{ii} \\ &= \sum_{p=1}^{N'_d}\sum_{q=1}^{N'_d}\sum_{k=0}^{L-1} \hat{X}^*_{pi}\Delta X_{pk}\hat{X}_{qi}\Delta X^*_{qk}|h_k|^2. \end{aligned} \tag{5.15}$$

The expectation of (5.15) can be subsequently given by

$$\begin{aligned}
&\mathrm{E}\left[\left(\hat{\mathbf{S}}^H \Delta \mathbf{S} \mathbf{h} \mathbf{h}^H \Delta \mathbf{S}^H \hat{\mathbf{S}}\right)_{ii}\right] \\
&= \sum_{p=1}^{N'_d} \sum_{k=0\ k\neq i}^{L-1} \mathrm{E}\left[\hat{X}^*_{pi} \Delta X_{pk} \hat{X}_{pi} \Delta X^*_{pk}\right] \mathrm{E}\left[|h_k|^2\right] \\
&+ \sum_{p=1}^{N'_d} \mathrm{E}\left[\hat{X}^*_{pi} \Delta X_{pi} \hat{X}_{pi} \Delta X^*_{pi}\right] \mathrm{E}\left[|h_i|^2\right] \\
&+ \sum_{p,q=1,\ p\neq q}^{N'_d} \mathrm{E}\left[\hat{X}^*_{pi} \Delta X_{pi} \hat{X}_{qi} \Delta X^*_{qi}\right] \mathrm{E}\left[|h_i|^2\right] \\
&= \mathcal{V}_1 \sum_{k=0\ k\neq i}^{L-1} \mathrm{E}\left[|h_k|^2\right] + \mathcal{V}_2 \mathrm{E}\left[|h_i|^2\right] + \mathcal{V}_3 \mathrm{E}\left[|h_i|^2\right]. \qquad (5.16)
\end{aligned}$$

Since the data symbols are mutually independent, the values of $\mathcal{V}_i$ can be calculated according to,

$$\mathcal{V}_1 = \mathcal{V}_2 = N'_d \mathrm{E}\left[|\hat{X}|^2\right] \cdot \mathrm{E}\left[|\Delta X|^2\right] \qquad (5.17)$$

$$\mathcal{V}_3 = N'_d (N'_d - 1) \left|\mathrm{E}\left[\hat{X}^* \Delta X\right]\right|^2 \qquad (5.18)$$

Finally, $\sigma^2_{\Delta h_f}$ is given by

$$\begin{aligned}
\sigma^2_{\Delta h_f} &= \frac{1}{N^2 L} \sum_{i=1}^{L} \left(\mathcal{V}_1 \sum_{k=0, k\neq i}^{L-1} \sigma^2_{h_k} + \mathcal{V}_2 \sigma^2_{h_i} + \mathcal{V}_3 \sigma^2_{h_i} \right) \\
&= \frac{\mathcal{V}_1 L + \mathcal{V}_3}{N^2 L}, \qquad (5.19)
\end{aligned}$$

where the total channel energy is normalized such that $\sigma^2_H = \sum_{l=0}^{L-1} \sigma^2_l = 1$. It is worth mentioning that the values of $\mathcal{V}_1$ and $\mathcal{V}_3$ vary depending on different mod-

ulation types. However, $\mathcal{V}_1$ and $\mathcal{V}_3$ are straightforward to obtain when the signal constellations are known. Therefore, the overall variance of the estimation error can be formulated as

$$\sigma^2_{\Delta h} = \sigma^2_{\Delta h_w} + \sigma^2_{\Delta h_f}. \tag{5.20}$$

5.4 Derivation of the Optimal Threshold

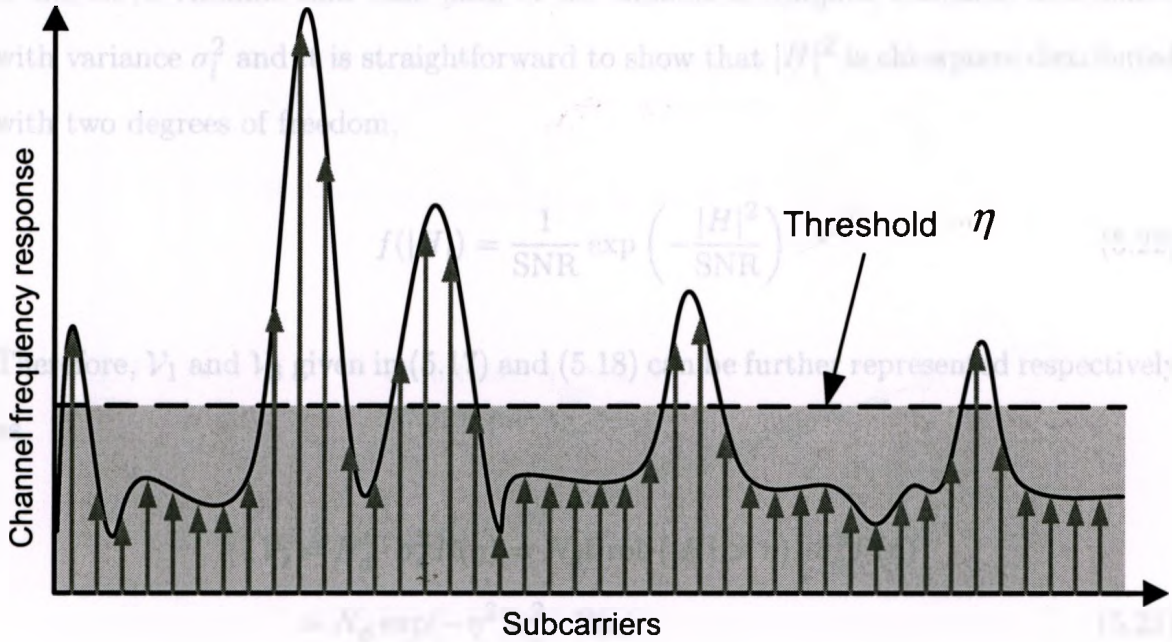

Figure 5.1: Illustration of the proposed reliable data decision feedback selection.

The principle of the proposed IDDCE with reliable data feedback selection is shown in Fig. 5.1. The shaded area below the dashed line represents the subcarriers associated with unreliable data decisions. In this section, the optimal threshold is derived which minimizes the variance of the channel estimation derived in the previous section. Here 4-QAM constellation is considered as basic modulation scheme and the proposed scheme can be easily extended to higher order modulation.

First, the average SER over the selected subcarriers with the proposed threshold can be represented as

$$P(\eta) = \int_{\eta}^{\infty} Q\left(\sqrt{\mathrm{SNR}} \cdot |H|\right) f\left(|H|\right) d\,|H|\,, \tag{5.21}$$

where $Q(x) = 1/\sqrt{2\pi}\int_x^{\infty} e^{-\frac{t^2}{2}}\,dt$ and $f(\cdot)$ represents the probability density function of the CFR. Assume that each path of the channel is complex Gaussian distributed with variance σ_l^2 and it is straightforward to show that $|H|^2$ is chi-square distributed with two degrees of freedom,

$$f(|H|) = \frac{1}{\mathrm{SNR}} \exp\left(-\frac{|H|^2}{\mathrm{SNR}}\right). \tag{5.22}$$

Therefore, $\mathcal{V}_1$ and $\mathcal{V}_3$ given in (5.17) and (5.18) can be further represented respectively as

$$\begin{aligned}\mathcal{V}_1 &= N_d' \cdot \sigma_e^2 P(\eta) = N_d \mathrm{Prob}\left(|H| > \eta\right) \cdot \sigma_e^2 P(\eta) \\ &= N_d \exp(-\eta^2)\sigma_e^2 \cdot P(\eta), \end{aligned} \tag{5.23}$$

$$\mathcal{V}_3 = N_d^2 \exp^2(-\eta^2) \cdot \sigma_e'^2 P^2(\eta), \tag{5.24}$$

where σ_e^2 and $\sigma_e'^2$ can be approximated to 8/3 and 16/9 under the assumption that the probabilities of each possible decision error ΔX in $\left\{-\sqrt{2}, -\sqrt{2}j, -\sqrt{2}-\sqrt{2}j\right\}$ are equally likely. Therefore, with the assumption that $N_d \gg N_p$, the variance of the channel estimation error can be reformulated as

$$\sigma_{\Delta h}^2(\eta) \approx \frac{\sigma_w^2}{N_p + N_d \exp(\eta^2)} + \frac{\frac{8}{3}P(\eta)}{N_d \exp(\eta^2)} + \frac{\frac{16}{9}P^2(\eta)}{L}. \tag{5.25}$$

To minimize the above variance, we set the first derivative of the above equation with respect to η equal to zero,

$$\frac{d\sigma^2_{\Delta h}(\eta)}{d\eta} = 0. \tag{5.26}$$

The above equation can be solved offline to achieve the optimal threshold and thus it does not contribute to the computational complexity in real applications.

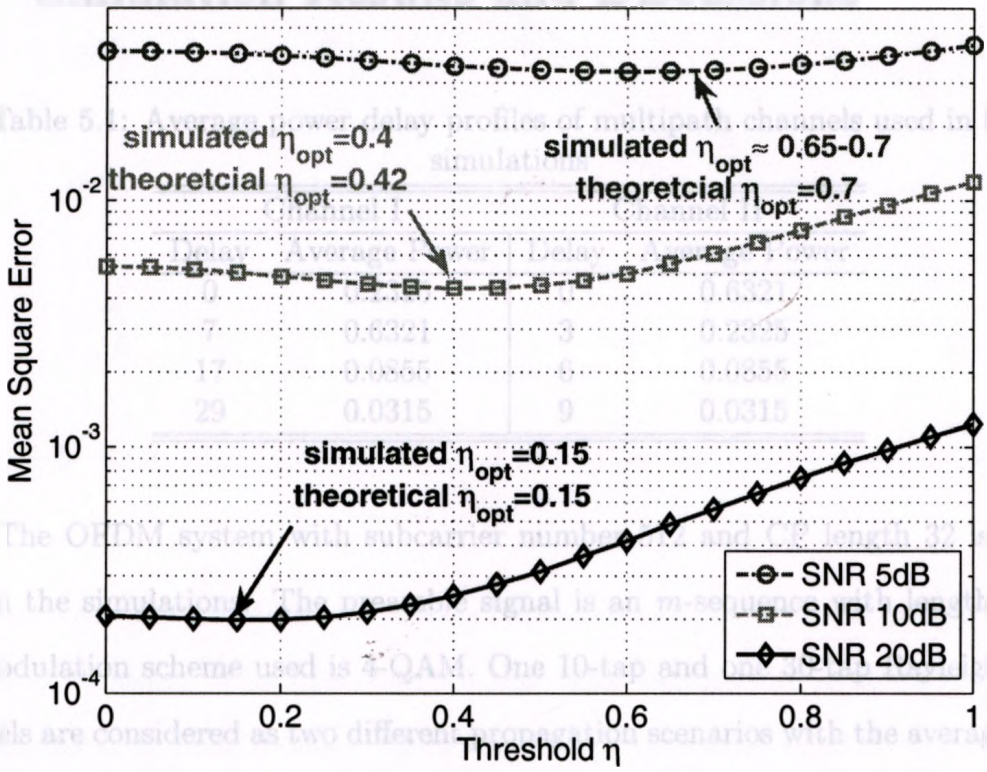

Figure 5.2: Mean square error of channel estimation versus different thresholds. The initial channel estimation is obtained via a preamble signal of length 31. The results are obtained via one iteration with the proposed data feedback selection threshold.

To verify the derived optimal selection threshold, Fig. 5.2 presents the simulated MSE of channel estimation with IDDCE and the proposed selection criteria. The simulated optimal thresholds (minimum MSE points) and the theoretical optimal thresholds (calculated by (5.25) and (5.26)) are pointed out by the text arrows. It can be found that the theoretical values well match the simulated ones. Moreover, with

the increase of SNR, the value of the optimal threshold decreases correspondingly. With the observed trend, it can be concluded that when the SNR is sufficiently large, the conventional method which uses all the data decision feedback may become the optimal one.

5.5 Simulation Results and Discussions

Table 5.1: Average power delay profiles of multipath channels used in the simulations

Channel I		Channel II	
Delay	Average Power	Delay	Average Power
0	0.2325	0	0.6321
7	0.6321	3	0.2325
17	0.0855	6	0.0855
29	0.0315	9	0.0315

The OFDM system with subcarrier number 512 and CP length 32 is considered in the simulations. The preamble signal is an m-sequence with length 31 and the modulation scheme used is 4-QAM. One 10-tap and one 30-tap Rayleigh fading channels are considered as two different propagation scenarios with the average power delay profiles reported in Table 5.1. The channels are assumed to be static during the transmission of one preamble and one OFDM symbol. Basically, Channel I represents a more hostile scenario than Channel II due to its long dispersive time and low power of first arriving path. Numerical results are obtained by averaging over 10000 independent Monte Carlo runs.

We first exploit the performance characteristics of the proposed IDDCE under different channel conditions and therefore the threshold of data feedback selection in (5.7) is set to zero. The MSE of the proposed IDDCE is presented in Fig. 5.3

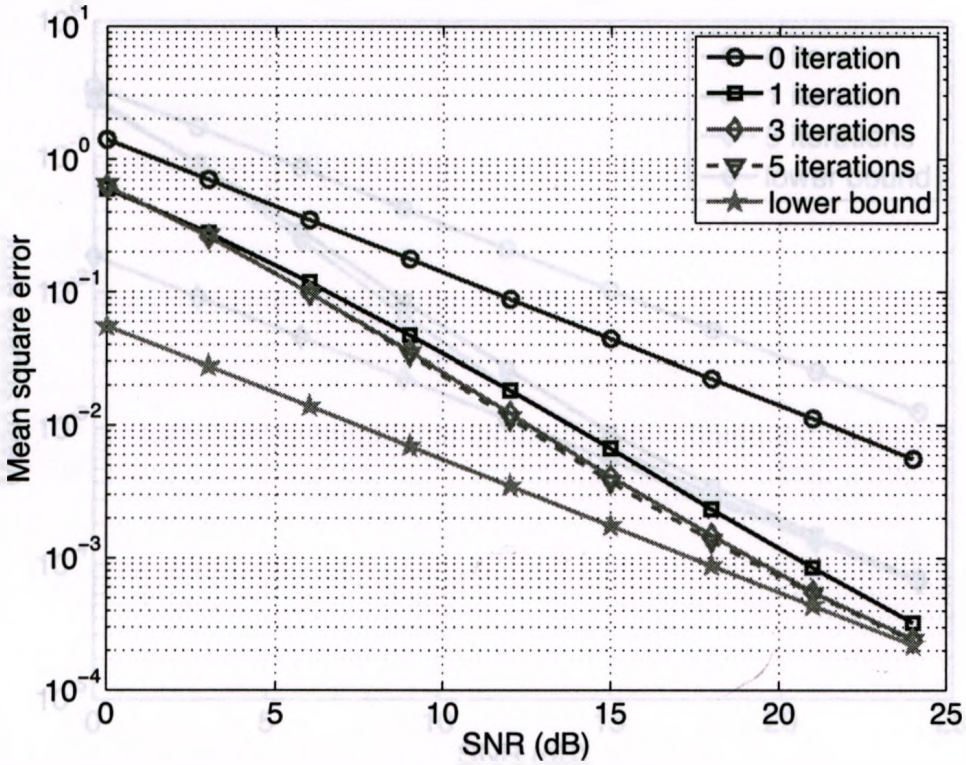

Figure 5.3: Mean square error of channel estimation with different iterations under Channel I.

and Fig. 5.4. The "0 iteration" curves represent the conventional preamble-based channel estimation. It can be observed that with the increase of iteration number, the corresponding MSE reduces. The lower bound is obtained when the data feedback consists of no decision errors. The results show that for Channel I, three iterations are needed to approach the lower bound at high SNR while this number reduces to one for Channel II to approach the lower bound at 20dB. This again demonstrates that Channel I is more hostile than Channel II. However, for both channels at moderate SNR, better performance is obtained with more iterations. This is because the MSE is sensitive to BER improvement at middle SNR. However, the case may not be applied to low and high SNR ranges. Since for the extremely low SNR, the BER is very high and most of the data decision feedback may be unreliable for next iteration. Therefore

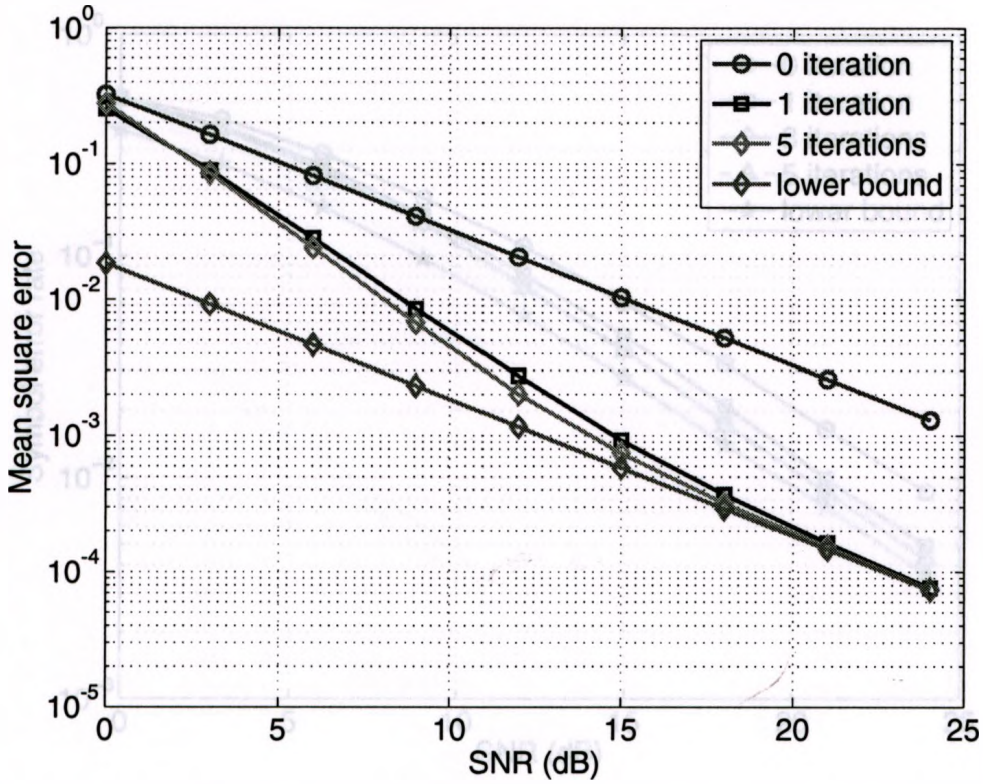

Figure 5.4: Mean square error of channel estimation with different iterations under Channel II.

the iterative process may not necessarily improve the performance. However, for high SNR, the BER is already sufficiently low such that only one iteration can achieve the lower bound.

The SER of the OFDM system with the proposed IDDCE is presented in Fig. 5.5 and Fig. 5.6. The "0 iteration" curves have the worst performance since the corresponding MSE of channel estimation is much larger than others with iteration process. The lower bound is obtained with the ideal coherent detection (perfectly known multipath channel). Significantly better SER performance can be obtained with more iterations as compared with the conventional one. The scheme also indicates that under multipath conditions where the channel is static over several OFDM symbols, the performance can be further enhanced when the subsequent demodulated symbols

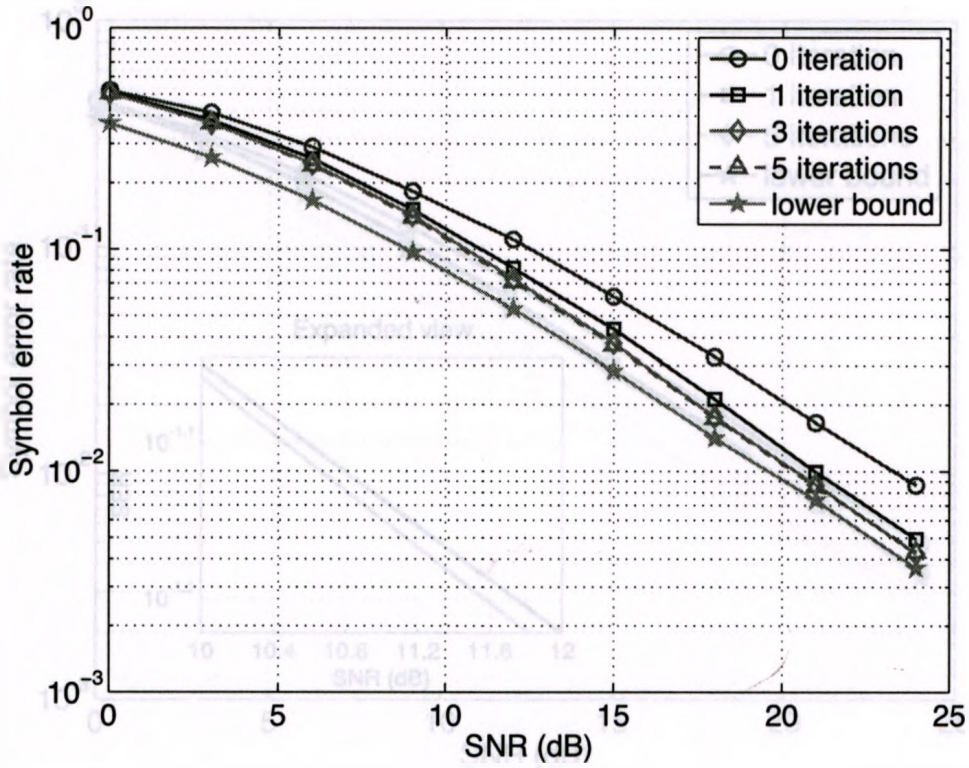

Figure 5.5: Symbol error rate at the receiver using the proposed IDDCE with different iterations under Channel I.

are also used to extend the "training". It is also found that the performance gaps between different iterations under Channel I are larger than those under Channel II since Channel II has a much shorter duration such that the SER is less sensitive to the MSE improvement.

To evaluate the performance of the proposed optimal threshold, the MSE of channel estimation with the optimal reliable data selection threshold and without threshold ($\eta = 0$) are compared under Channel II. One iteration and three iterations are simulated in Fig. 5.7. Since at high SNR, $\eta = 0$ may become the optimal threshold and therefore the SNR range $6 - 15$dB is adopted as the effective range for the proposed IDDCE with reliable data selection. It can be observed that the MSE of the optimal reliable data selection outperforms the one using all hard decision

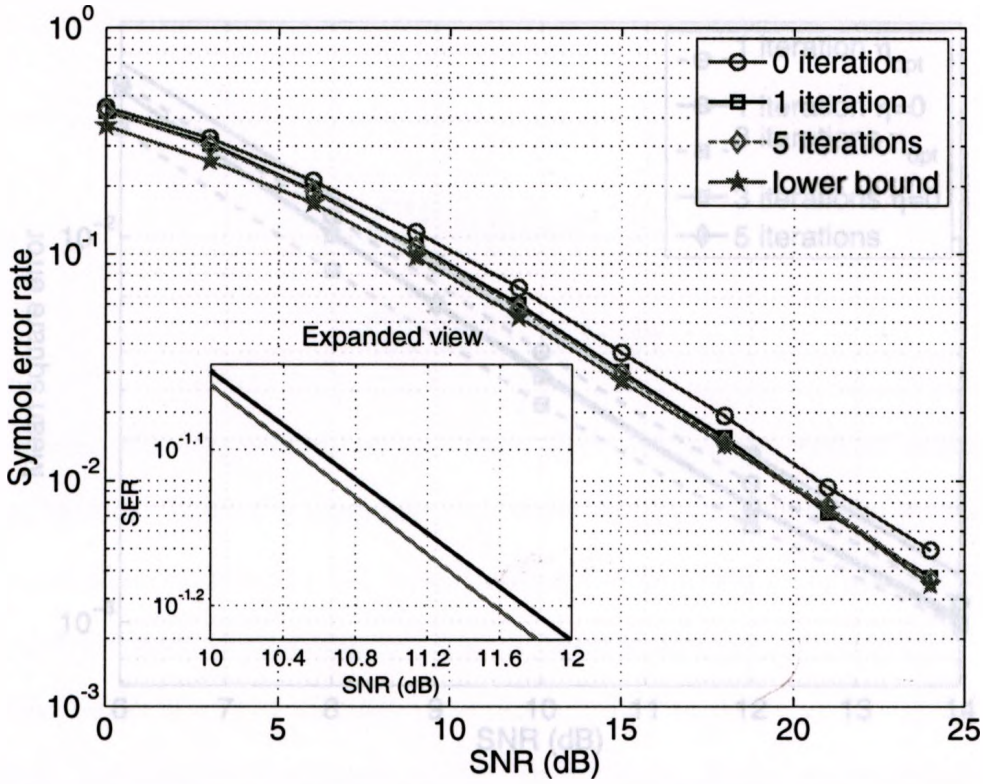

Figure 5.6: Symbol error rate at the receiver using the proposed IDDCE with different iterations under Channel II.

feedback for the corresponding iterations. More than 20% MSE gain can be achieved over the conventional decision feedback scheme when the proposed data feedback selection is adopted in the IDDCE. It is also apparent that the performance of 1 iteration with η_{opt} is approaching that of 3 and 5 iterations with $\eta = 0$. Therefore, it is confirmed that the computational complexity can also be significantly reduced with the proposed optimal threshold in terms of iteration number.

5.6 Summary

A new IDDCE with reliable data decision feedback selection is proposed. The optimal selection threshold is derived to eliminate the data feedback on the subcarriers

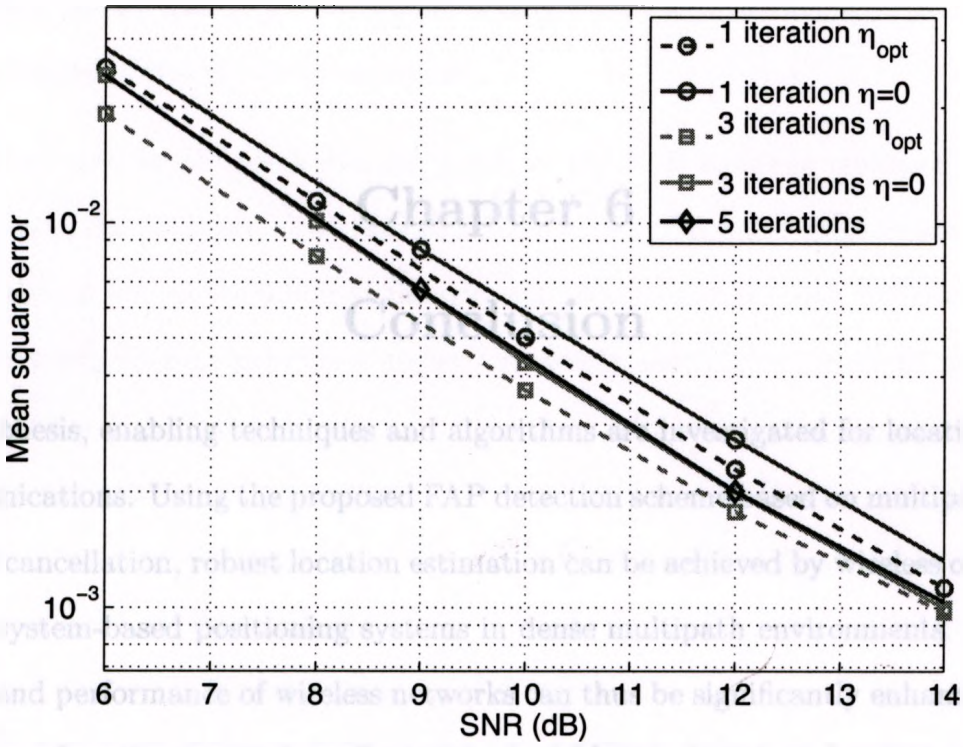

Figure 5.7: Mean square error of channel estimation with and without the optimal reliable data selection under Channel II.

where the noise is enhanced due to the low channel frequency response. The accuracy of channel estimation is significantly improved by using the proposed iterative channel estimation scheme. Theoretical performance analysis is also given in terms of the variance of estimation error for the proposed channel estimation. Simulation results show that the proposed channel estimation scheme with the optimal selection threshold outperforms the conventional one without data feedback selection.

Chapter 6
Conclusion

In this thesis, enabling techniques and algorithms are investigated for location-aware communications. Using the proposed FAP detection scheme based on multipath interference cancellation, robust location estimation can be achieved by wireless communication system-based positioning systems in dense multipath environments. The efficiency and performance of wireless networks can thus be significantly enhanced based on various location-assisted applications. In addition, based on location-awareness capability, efficient strategy of multicell cooperation can be designed to improve the throughput and coverage of traditional wireless networks. Therefore, a robust, efficient and flexible platform based on the proposed ML-OFDM is investigated for multicell cooperative communications. Finally, an enhanced IDDCE is proposed to improve the performance of OFDM receiver such that it can be utilized to further enhance the performance of proposed FAP detection. The major contributions of this thesis are summarized as follows:

- A robust FAP detection scheme using multipath interference cancellation is proposed for TOA-based positioning system in dense multipath environments. An iterative estimator is proposed to provide LAPs and data estimation with high accuracy. The complexity of iterative estimator is effectively reduced by the proposed automatic stopping criterion. Based on the estimated LAPs and

data, the interference components of LAPs can be accurately reconstructed and mitigated from the received signal.

- Motivated by the weak average power of the FAP in dense multipath environments, the proposed detection algorithm constructs a new *augmented preamble* which is the combination of the original preamble signal and the demodulated data sequence to provide a higher correlation gain. The new FAP detector is based on the cross-correlation between the LAPs interference-suppressed signal and the *augmented preamble* and hence a significant SINR gain can be achieved with the proposed algorithm. The accuracy of location estimation based on the proposed FAP detection algorithm is substantially increased, which is particularly important for location-assisted applications.

- A reliable, efficient and flexible ML-OFDM system is proposed to support multicell cooperation network. Motivated by the technical challenges of multicell cooperation including BS backhaul issues, synchronization problem and potential network latency, the proposed ML-OFDM utilizes some dedicated signaling links, referred to as *Enhanced Layers*, which are superimposed onto data-carrying information in both frequency and time domains. BS coordination can be concurrently achieved including the sharing of channel and data information, transmission parameters, users' location information and synchronization with the transmission of data-carry signals. Traditional control channels can be eliminated to reduced the radio resource overhead and thus enhance the network efficiency.

- An *iterative decision-directed channel estimation* is proposed in this thesis for accurate channel estimation with limited training overhead. Different from traditional decision-directed channel estimation, an optimal threshold is derived to

select the reliable data decision feedback and eliminate the unreliable ones on the subcarriers suffering from the noise enhancement effects due to the frequency selective channel. Utilizing the proposed IDDCE, the accuracy of channel estimation is maximized in this case and therefore, the performance of OFDM receiver is significantly enhanced with a short training sequence. Furthermore, this technique is suitable or cooperation network since the sharing of channel information for multicell cooperation requires large training overhead and it helps to overcome the contradiction between the large overhead and limited performance caused by the short training.

6.1 Future Work

There are still several topics related to the presented research worthwhile for further studies. Some of them are listed as follows:

- In Chapter 3, the optimal threshold to select the dominant LAPs is derived with the assumption that the variance of the significant LAPs is known to the receiver. In future work, a suboptimal threshold independent of channel statistic information needs to be derived for real applications.
- In Chapter 4, the *Enhanced Layers* uses the modified Code Shift Keying as their modulation schemes. The ELs will have some negative impact on the performance of the *Base Layer* although most of the mutual layer interference can be removed. Therefore, alternative modulation and coding schemes will be investigated for the ELs which can completely eliminate the impact to the BL.

References

[1] E. D. Kaplan, *Understanding GPS: Principles and Applications*, Artech House, Norwood, Mass, USA, 1996.

[2] J. A. Farrel and M. Barth, *The Global Positioning System & Interial Navigation*, McGraw-Hill, London, UK, 1999.

[3] M. S. Grewal, L. R. Weill, and A. P. Andrews, *Global Positioning Systems, Intertial Navigation, and Integration*, John Wiley & Sons, Hoboken, NJ, USA, 2001.

[4] European Commission, "European transport policy for 2010: Time to decide," Tech. Rep., 2001.

[5] FCC, "Revision of the commission's rules to ensure compatibility with enhanced 911 emergency calling system," Et docket no. 94–102, Jul. 1996.

[6] L. Cong and W. Zhuang, "Hybrid TDOA/AOA mobile user location for wideband CDMA cellular systems," *IEEE Trans. Wireless Commun.*, vol. 1, no. 3, pp. 439–447, Jul. 2002.

[7] J. J. Caffery and G. L. Stüber, "Subscriber location in CDMA cellular networks," *IEEE Trans. Veh. Technol.*, vol. 47, no. 2, pp. 406–416, May 1998.

[8] S. Bartelmaos, K. Abed-Meraim, and E. Grosicki, "General selection criteria for mobile location in NLOS situations," *IEEE Trans. Wireless Commun.*, vol. 7, no. 11, pp. 4393–4403, Nov. 2008.

[9] P. Prasithsangaree, P. Krishnamurthy, and P. K. Chrysanthis, "On indoor position location with wireless LANs," in *Proc. 13th IEEE Int. Symp. Pers., Indoor Mobile Radio Commun. (PIMRC '02)*, Lisboa, Sep. 2002, vol. 2, pp. 720–724.

[10] X. Wang, Y. Wu, and J.-Y. Chouinard, "A new position location system using DTV transmitter identification watermark signals," *EURASIP Journal on Applied Signal Processing*, , no. Article ID 42737, pp. 1–11, 2006.

[11] X. Li, "RSS-based location estimation with unknown pathloss model," *IEEE Trans. Wireless Commun.*, vol. 5, no. 12, pp. 3623–3633, Dec. 2006.

[12] J. Yin, Q. Yang, and L. M. Ni, "Learning adaptive temporal radio maps for signal-strength-based location estimation," *IEEE Trans. Mobile Comput.*, vol. 7, no. 7, pp. 869–883, Jul. 2008.

[13] K. Yu, "3-D localization error analysis in wireless networks," *IEEE Trans. Wireless Commun.*, vol. 6, no. 10, pp. 3472–3481, Oct. 2007.

[14] P. Stoica, O. Besson, and A. B. Gershman, "Direction-of-arrival estimation of an amplitude-distorted wavefront," *IEEE Trans. Signal Process.*, vol. 49, no. 2, pp. 269–276, 2001.

[15] R. Zhang and X. Dong, "A new time of arrival estimation method using UWB dual pulse signals," *IEEE Trans. Wireless Commun.*, vol. 7, no. 6, pp. 2057–2062, Jun. 2008.

[16] A. A. D'Amico, U. Mengali, and L. Taponecco, "TOA estimation with the IEEE 802.15.4a standard," *IEEE Trans. Wireless Commun.*, vol. 9, no. 7, pp. 2238–2247, Jul. 2010.

[17] J. Yang, X. Wang, S. I. Park, and H. M. Kim, "A novel first arriving path detection algorithm using multipath interference cancellation in indoor environments," in *Proc. IEEE 72nd Veh. Technol. Conf. (VTC '10-Fall)*, Ottawa, Sep. 2010, pp. 1–5.

[18] R. K. Martin, C. Yan, H. H. Fan, and C. Rondeau, "Algorithms and bounds of distributed TDOA-based positioning using OFDM signals," *IEEE Trans. Signal Process.*, vol. 59, no. 3, pp. 1255–1268, 2011.

[19] E. Xu, Z. Ding, and S. Dasgupta, "Source localization in wireless sensor networks from signal time-of-arrival measurements," *IEEE Trans. Signal Process.*, vol. PP, no. 99, pp. 1–11, 2011.

[20] K. W. Cheung, H. C. So, W.-K. Ma, and Y. T. Chan, "Least squares algorithms for time-of-arrival-based mobile location," *IEEE Trans. Signal Process.*, vol. 52, no. 4, pp. 1121–1130, 2004.

[21] S. Gezici and H. V. Poor, "Position estimation via ultra-wide-band signals," *Proc. of the IEEE*, vol. 97, no. 2, pp. 386–403, Feb. 2009.

[22] I. Guvenc and Z. Sahinoglu, "TOA estimation with different IR-UWB transceiver types," in *Proc. IEEE Int. Conf. Ultra-Wideband, 2005 (ICU '05)*, Zurich,, Sep. 2005, pp. 426–431.

[23] I. Guvenc and Z. Sahinoglu, "Threshold-based TOA estimation for impulse radio UWB systems," in *Proc. IEEE Int. Conf. Ultra-Wideband, 2005 (ICU '05)*, Zurich,, Sep. 2005, pp. 420–425.

[24] W. Ciccognani, A. Durantini, and D. Cassioli, "Time-domain propagation measurements of the UWB indoor channel using PN-sequence in the FCC-compliant band 3.6-6GHz," *IEEE Trans. Antennas and Propagat.*, vol. 53, no. 4, pp. 1542–1549, Apr. 2005.

[25] P. L. Kafle, A. Intarapanich, A. B. Sesay, J. McRoory, and R. J. Davies, "Spatial correlation and capacity measurments for wideband MIMO channels in indoor office environment," *IEEE Trans. Wireless Commun.*, vol. 7, no. 5, pp. 1560–1571, May 2008.

[26] X. Li and K. Pahlavan, "Super-resolution TOA estimation with diversity for indoor geolocation," *IEEE Trans. Wireless Commun.*, vol. 3, no. 1, pp. 224–234, Jan. 2004.

[27] T. Manabe and H. Takai, "Superresolution of multipath delay profiles measured by PN correlation method," *IEEE Trans. Antennas and Propagat.*, vol. 40, no. 5, pp. 500–509, May 1992.

[28] F. Bouchereau, D. Brady, and C. Lanzl, "Multipath delay estimation using a superresolution PN-correlation method," *IEEE Trans. Signal Process.*, vol. 49, no. 5, pp. 938–949, May 2001.

[29] J. Andrews, "Interference cancellation for cellular systems: A contemporary overview," *IEEE Wireless Commun.*, vol. 12, no. 2, pp. 19–29, Apr. 2005.

[30] D. Gesbert, S. Hanly, H. Huang, S. Shamai, O. Simeone, and W. Yu, "Multi-cell MIMO cooperative netwokrs: A new look at interference," *IEEE J. Sel. Area Commun.*, vol. 28, no. 9, pp. 1380–1408, Dec. 2010.

[31] S. Shamai and B. Zaidel, "Enhancing the cellular downlink capacity via co-processing at the transmitter end," in *Proc. IEEE 53rd Veh. Technol. Conf, (VTC '01 Spring)*, Rhodes, Greece, May 2001, vol. 3, pp. 1745–1749.

[32] M. Karakayali, G. Foschini, and R. Vlenzuela, "Network coordination for spectrally efficient communications in cellular systems," *IEEE Wireless Commun.*, vol. 13, no. 4, pp. 56–61, Aug. 2006.

[33] H. Zhang and H. Dai, "Cochannel interference mitigation and cooperative processing in downlink multicell multiuser MIMO networks," *EURASIP J. Wireless Commun. Netw.*, vol. 2004, no. 2, pp. 222–235, Feb. 2004.

[34] B. Clerckx, A. Lozano, S. Sesia, C. V. Rensburg, and C. B. Papadias, "3GPP LTE and LTE Advanced," *EURASIP J. Wireless Commun. Netw.*, vol. 2009, Article ID 472124, pp. 1–3, Sep. 2009.

[35] H. Weingarten, Y. Steinberg, and S. Shamai, "The capacity region of the Gaussian multiple-input-multiple-output broadcast channel," *IEEE Trans. Inf. Theory*, vol. 52, no. 9, pp. 3936–3964, Sep. 2006.

[36] O. Somekh, B. Zaidel, and S. Shamai, "Sum rate characterization of joint multiple cell-site processing," *IEEE Trans. Inf. Theory*, vol. 53, no. 12, pp. 4473–4497, Dec. 2007.

[37] O. Somekh and S. Shamai, "Shannon-theoretic approach to a Gaussian cellular multiple access channel with fading," *IEEE Trans. Inf. Theory*, vol. 46, no. 4, pp. 1401–1425, Jul. 2000.

[38] N. Levy, O. Zeitouni, and S. Shamai, "Information theoretic aspects of users' activity in a Wyner-like cellular model," *IEEE Trans. Inf. Theory*, vol. 56, no. 5, pp. 2241–2248, May 2010.

[39] Y. Liang and A. Goldsmith, ," in *Proc. IEEE Globe Telecommun. Conf., 2006 (GLOBECOM '06)*, San Francisco, USA, Dec. 2006, pp. 1–5.

[40] M. Bacha, J. Evans, and S. Hanly, "On the capacity of cellular networks with mimo links," in *Proc. IEEE Int. Conf. Commun., 2006 (ICC '06)*, June 2006, vol. 3, pp. 1337–1342.

[41] G. Caire and S. Shamai, "On the achievable throughput of a multi-antenna Gaussian broadcast channel," *IEEE Trans. Inf. Theory*, vol. 49, no. 7, pp. 1691–1706, Jul. 2003.

[42] O. Simeone, O. Somekh, H. V. Poor, and S. Shamai, "Downlink multicell processing with limited backhaul capacity," *EURASIP J. Adv. Signal Process.*, vol. 2009, Article ID 840814, pp. 1–10, Feb. 2009.

[43] O. Simeone, O. Somekh, Y. Bar-Ness, and U. Spagnolini, "Throughput of low-power cellular systems with collaborative base stations and relaying," *IEEE Trans. Inf. Theory*, vol. 54, no. 1, pp. 459–467, Jan. 2008.

[44] S. Jing, D. N. C. Tse, J. B. Soriaga, J. Hou, J. E. Smee, and R. Padovani, "Multicell downlink capacity with coordinated processing," *EURASIP J. Wireless Commun. Netw.*, vol. 2008, Article ID 586878, pp. 1–19, 2008.

[45] O. Simeone, O. Somekh, G. Kramer, H. V. Poor, and S. Shamai, "Throughput of cellular systems with conferencing mobiles and cooperative base stations," *EURASIP J. Wireless Commun. Netw.*, vol. 2008, Article ID 652325, pp. 1–14, 2008.

[46] P. Marsch and G. Fettweis, "On base station coopearation schemes for downlind network MIMO under a constrained backhaul," in *Proc. IEEE Global Telecommun. Conf., 2008 (Globecom '08)*, Dec. 2008, pp. 1–6.

[47] P. Marsch and G. Fettweis, "On uplink network MIMO under a constrained backhaul and imperfect channel knowledge," in *Proc. IEEE Int. Conf. Commun., 2009 (ICC' 09)*, Jun. 2009, pp. 1–6.

[48] H. Skjevling, D. Gesbert, and A. Hjorungners, "Low-complexity distributed multibase transmission and scheduling," *EURASIP J. Adv. Signal Process.*, vol. 2008, Article ID 741593, pp. 1–9, 2008.

[49] W. Choi and J. Andrews, "The capacity gain from base station cooperative scheduling in a MIMO DPC cellular system," in *Proc. IEEE Int. Symp. Inf. Theory*, Jul. 2006, pp. 1224–1228.

[50] W. Yu, T. Kwon, and C. Shin, "Multicell coordination via joint scheduling, beamforming and power spectrum adaptation," in *Proc. IEEE INFOCOM, 2011*, Jun. 2011, pp. 2570–2578.

[51] S. G. Kiani and D. Gesbert, "Optimal and distributed scheduling for multicell capacity maximization," *IEEE Trans. Wireless Commun.*, vol. 7, no. 1, pp. 288–297, Jan. 2008.

[52] T. Hwang, C. Yang, G. Wu, S. Li, and G. Y. Li, "OFDM and its wireless applications: A survey," *IEEE Trans. Veh. Technol.*, vol. 58, no. 4, pp. 1673–1694, May 2009.

[53] G. Y. Li and G. Stüber, *Orthogonal Frequency Divison Multiplexing for Wireless Communications*, Springer-Verlag, Boston, MA, Jan. 2006.

[54] S. Coleri, M. Ergen, A. Puri, and A. Bahai, "Channel estimation techniques based on pilot arrangement in OFDM systems," *IEEE Trans. Broadcast.*, vol. 48, no. 3, pp. 223–229, Sep. 2002.

[55] M. Morelli and U. Mengali, "A comparison of pilot-aided channel estimation methods for OFDM systems," *IEEE Trans. Signal Process.*, vol. 49, no. 12, pp. 3065–3073, Dec. 2001.

[56] G. Y. Li, "Pilot-symbol-aided channel estimation for OFDM in wireless systems," *IEEE Trans. Veh. Technol.*, vol. 49, no. 4, pp. 1205–1215, Jul. 2000.

[57] P. Hoeher, S. Kaiser, and P. Robertson, "Two-dimensional pilot symbol-aided channel estimation by Wiener filtering," in *Proc. IEEE Int. Conf. Acoust. Speech Signal Process., 1997 (ICASSP '97)*, Munich, Apr. 1997, pp. 1845–1848.

[58] R. Negi and J. Cioffi, "Pilot tone selection for channel estimation in a mobile OFDM system," *IEEE Trans. Consum. Electron.*, vol. 44, no. 3, pp. 1122–1128, Aug. 1998.

[59] J. K. Cavers, "An analysis of pilot symbol assisted modulation for Rayleigh fading channels," *IEEE Trans. Veh. Technol.*, vol. 40, no. 4, pp. 686–693, Nov. 1991.

[60] S. Adireddy and L. Tong, "Optimal placement of training for frequency-selective block-fading channels," *IEEE Trans. Inf. Theory*, vol. 48, no. 44, pp. 2338–2353, Aug. 2002.

[61] S. Ohno and G. B. Giannakis, "Capacity maximizing MMSE-optimal pilots for wireless OFDM over frequency-selective block Rayleigh-fading channels," *IEEE Trans. Inf. Theory*, vol. 50, no. 9, pp. 2138–2145, Sep. 2004.

[62] X. Ma, G. B. Giannakis, and S. Ohno, "Optimal training for block transmission over doubly selective wireless fading channels," *IEEE Trans. Signal Process.*, vol. 51, no. 5, pp. 1351–1366, May 2003.

[63] M. Dong and L. Tong, "Optimal design and placement of pilot symbols for channel estimation," *IEEE Trans. Signal Process.*, vol. 50, no. 12, pp. 3055–3069, Dec. 2002.

[64] X. Cai and G. B. Giannakis, "Error probability minimization pilots for OFDM with M-PSK modulation over Rayleigh-fading channels," *IEEE Trans. Veh. Technol.*, vol. 53, no. 1, pp. 146–155, Jan. 2004.

[65] L. Tong, B. M. Sadler, and M. Dong, "Pilot-assisted wireless transmission: General model, design criteria and signal processing," *IEEE Signal Process. Mag.*, vol. 21, no. 6, pp. 12–25, Nov. 2004.

[66] L. J. Cimini, "Analysis and simulation of a digital mobile channel using orthogonal frequency domain division multiplexing," *IEEE Trans. Commun.*, vol. COM-33, no. 7, pp. 665–675, Jul. 1985.

[67] H. Zhang and Y. G. Li, "Cluster OFDM with adaptive antenna array for interference suppression," *IEEE Trans. Wireless Commun.*, vol. 3, no. 6, pp. 2189–2197, Nov. 2004.

[68] P. Hoeher and F. Tufvesson, "Channel estimation with superimposed pilot sequence," in *Proc. IEEE Globe Telecommun. Conf., 1999 (GLOBECOM '99)*, Rio de Janeireo, Sep. 1999, vol. 4, pp. 2162–2166.

[69] J. K. Tugnait and W. Luo, "On channel estimation usng superimposed training and first-order statistic," *IEEE Commun. Lett.*, vol. 7, no. 9, pp. 413–415, Sep. 2003.

[70] B. Farhang-Boroujeny, "Pilot-based channel identification: Proposal for semi-blind identification of communication channels," *Electron. Lett.*, vol. 31, no. 13, pp. 1044–1046, Jun. 1995.

[71] F. Mazzenga, "Channel estimation and equalization for M-QAM transmission with a hidden pilot sequence," *IEEE Trans. Broadcast.*, vol. 46, no. 2, pp. 170–176, Jun. 2000.

[72] G. T. Zhou, M. Viberg, and T. McKelvey, "A first-order statistical method for channel estimaiton," *IEEE Signal Process. Lett.*, vol. 10, no. 3, pp. 57–60, Sep. 2003.

[73] C.-T. Lam, D. D. Falconer, and F. Danilo-Lemoine, "Iterative frequency domain channel estimation for DFT-precoded OFDM systems using in-band pilots," *IEEE J. Sel. Areas Commun.*, vol. 26, no. 2, pp. 348–358, Feb. 2008.

[74] O. Edfors, M. Sandelland J. Beek, S. K. Wilson, and P. O. Borjesson, "OFDM channel estimation by singular value decomposition," *IEEE Trans. Commun.*, vol. 46, no. 7, pp. 931–939, Jul. 1998.

[75] V. Mignone and A. Morello, "CD3-OFDM: A novel demoulation scheme for fixed and mobile radio channels," *IEEE Trans. Commun.*, vol. 44, no. 9, pp. 1144–1151, Sep. 1996.

[76] S. T. Brink, F. Sanzi, and J. Speidel, "Two-dimensional APP channel estmiation and decoding for OFDM systems," in *Proc. IEEE Global Telecommun. Conf., 2000 (Globecom '00)*, San Francisco, Nov. 2000, vol. 2, pp. 741–745.

[77] S. Y. Park, Y. G. Kim, C. G. Kang, and D. E. Kang, "Iterative receiver with joint detection and channel estimation for OFDM system with multiple receiver antennas in mobile radio channels," in *Proc. IEEE Globe Telecommun. Conf., 2001 (GLOBECOM '01)*, San Antonio, TX, Nov. 2001, vol. 5, pp. 3085–3089.

[78] L. Jarbot, "Combined decoding and channel estimation of OFDM systems in mobile radio networks," in *Proc. IEEE 47th Veh. Technol. Conf. (VTC '97)*, Phoenix, AZ, May 1997, vol. 3, pp. 1601–1604.

[79] T. Kella, "Decision-directed channel estimation for supporting higher terminal velocities in OFDM based WLANs," in *Proc. IEEE Globe Telecommun. Conf., 2003 (GLOBECOM '03)*, San Francisco, CA, Dec. 2003, vol. 3, pp. 1306–1310.

[80] F. Yang, K. Peng, J. Wang, J. Song, and Z. Yang, "Simplified decision-directed channel estimation method for OFDM system with transmit diversity," in *Proc. IEEE 69th Veh. Technol. Conf. (VTC '09 Spring)*, Barcelona, Apr. 2009, pp. 1–5.

[81] I. Guvenc, C.-C. Chong, and F. Watanabe, "NLOS identification and mitigation for UWB localization systems," in *Proc. IEEE Wireless Commun. Netw. Conf., 2007 (WCNC '07)*, Kowloon, Mar. 2007, pp. 1573–1578.

[82] M. Heidari, F. O. Akgul, and K. Pahlavan, "Identification of the absence of direct path in indoor localization systems," in *Proc. 18th IEEE Int. Symp. Pers., Indoor Mobile Radio Commun. (PIMRC '07)*, Athens, Sep. 2007, pp. 1–6.

[83] L. Mucchi and P. Marcocci, "A new UWB indoor channel identification method," in *Proc. 2nd Int. Conf. Cognit. Radio Oriented Wireless Netw. Commun. (CrownCom '07)*, Orlando, FL, Aug. 2007, pp. 58–62.

[84] H. Minn, V. K. Bhargava, and K. B. Letaif, "A robust timing and frequency synchronization and channel estimation for OFDM," *IEEE Trans. Commun.*, vol. 2, no. 4, pp. 822–839, Jul. 2003.

[85] Y. G. Li, "Simplified channel estimation for OFDM systems with multiple transmit antennas," *IEEE Trans. Wireless Commun.*, vol. 1, pp. 67–75, Jan. 2005.

[86] H. Minn, V. K. Bhargava, and K. B. Letaief, "A robust timing and frequency synchronization and channel estimation for OFDM," *IEEE Trans. Wireless Commun.*, vol. 2, no. 4, pp. 822–839, Jul. 2003.

[87] Y. Kang, K. Kim, and H. Park, "Efficient DFT-based channel estimation for OFDM systems on multipath channels," *IET Commun.*, vol. 1, no. 2, pp. 197–202, Apr. 2007.

[88] "Evolved universal terrestrial radio access (E-UTRA); user equipment (UE) radio tranmission and reception (Release 8), *Technical Specification*," Sophia antipolis, france, 3GPP (TR 36.803), 2007.

[89] D. Molkdar, "Review on radio propagation into and within buildings," *IEE Proceedings H: Microwaves, Antennas and Propagation*, vol. 138, no. 1, pp. 61–73, Feb. 1991.

[90] U. Horn, R. Keller, and N. Niebert, "Iterative mobile streaming services-convergence of broadcast and mobile communication," *EBU Technical Rev.*, pp. 14–19, 1999.

[91] R. Keller, T. Lohman, R. Tonjes, and J. Thielecke, "Covergence of cellular and broadcast networks from a multi-radio perspective," *IEEE Pers. Commun.*, vol. 8, no. 2, pp. 51–56, Apr. 2001.

[92] O. Benali, K. E.-Khazen, D. Garrec, M. Guiraudou, and G. Martinez, "A framework for an evolutionary path toward 4G by means of cooperation of networks," *IEEE Commun. Mag.*, vol. 42, no. 5, pp. 82–89, May 2004.

[93] F. Allamandri, S. Campion, A. Centonza, A. Chernilov, J. P. Cosmas, A. Duffy, D. Garrec, M. Guiraudou, K. Krishnapillai, T. Levesque, B. Mazieres, R. Mies, T. Owens, M. Re, E. Tsekleves, and L. Zheng, "Service platform for converged interactive broadband broadcast and cellular wireless," *IEEE Trans. Broadcast.*, vol. 53, no. 1, pp. 200–211, Mar. 2007.

[94] G. M. Dillard, M. Reuter, J. Zeidler, and B. Zeidler, "Cyclic code shift keying: a low probability of intercept communication technique," *IEEE Trans. Aero. Electron. Syst.*, vol. 39, no. 3, pp. 786–798, Jul. 2003.

[95] S. Erkucuk, D. I. Kim, and K. S. Kwak, "Code shift keying impulse modulation for UWB communications," *IEEE Trans. Wireless Commun.*, vol. 7, no. 9, pp. 3285–3291, Sep. 2008.

[96] Y.-R. Tsai and X.-S. Li, "Kasami code-shift-keying modulation for ultra wide-band communication systems," *IEEE Trans. Commun.*, vol. 55, no. 6, pp. 1242–1252, Jun. 2007.

[97] R. Bhagavatula and R. Heath, "Adaptive bit partitioning for multicell inter-cell interference nulling with delayed limited feedback," *IEEE Trans. Signal Process.*, vol. PP, no. 99, pp. 1–16, Apr. 2011.

[98] Y. Liang, R. Schober, and W. Gerstacker, "Time-domain transmit beamforming for MIMO-OFDM system with finite rate feedback," *IEEE Trans. Commun.*, vol. 57, no. 9, pp. 2828–2838, Sep. 2009.

[99] J. G. Proakis, *Digital Communications*, McGraw-Hill, New York, 1995.

[100] M. Medard, "The effect upon channel capacity in wireless communications of perfect and imperfect knowledge of the channel," *IEEE Trans. Inf. Theory*, vol. 46, no. 3, pp. 933–946, May 2000.

[101] S. Boyd and L. Vandenberghe, *Convex Optimization*, Cambridge University Press, Cambridge, UK, 2004.

[102] C. S. Park and K. B. Lee, "Transmit power allocation for BER performance improvement in multicarrier systems," *IEEE Trans. Commun.*, vol. 52, no. 10, pp. 1658–1663, Oct. 2004.